Manuscript title: Molecular Diversity of Intrinsically Photosensitive Ganglion Cells

Authors:

Daniel Berg[1,2], Katherine Kartheiser[2], Megan Leyrer[2], Alexandra Saali[2], David Berson[2]

1. Molecular Biology Program

2. Department of Neuroscience

Brown University, Providence, RI 02912

Correspondence to: David Berson (david_berson@brown.edu)

WORD COUNT: **Abstract** (148 words); **Intro** (784 words); **Results** (5159); **Discussion** (2657)

Abstract

Intrinsically photosensitive retinal ganglion cells (ipRGCs) are rare mammalian photoreceptors essential for non-image-forming vision functions, such as circadian photoentrainment and the pupillary light reflex. They comprise multiple subtypes distinguishable by morphology, physiology, projections, and levels of expression of melanopsin (Opn4), their photopigment. The molecular programs that differentiate ipRGCs from other ganglion cells and ipRGC subtypes from one another remain elusive. Here, we present comprehensive gene expression profiles of early postnatal and adult mouse ipRGCs purified from two lines of reporter mice marking different sets of ipRGC subtypes. We find dozens of novel genes highly enriched in ipRGCs. We reveal that Rasgrp1 and Tbx20 are selectively expressed in subsets of ipRGCs, though these molecularly defined groups imperfectly match established ipRGC subtypes. We demonstrate that the ipRGCs regulating circadian photoentrainment are unexpectedly diverse at the molecular level. Our

findings reveal unexpected complexity in gene expression patterns across mammalian ipRGC subtypes.

Introduction

Many unique attributes distinguish intrinsically photosensitive RGCs from conventional RGCs. Only ipRGCs express the blue-light sensitive photopigment melanopsin (OPN4), which renders them autonomously light-sensitive. They violate the usual stratification rule in which ON-type RGCs deploy their dendrites only in the inner (proximal) half of the inner plexiform layer; their inputs from ON bipolar cells are atypical (Dumitrescu et al., 2009; Hoshi et al., 2009; Kim et al., 2010). Whereas most RGCs direct their entire output through the optic nerve, some ipRGCs modulate intraretinal processing, through dopaminergic (Zhang et al., 2008; Xue et al., 2011) and other amacrine cells (Reifler et al., 2015; Sabbah et al., 2017) and spontaneous retinal waves during the early postnatal period (Renna et al., 2011). Additionally, ipRGCs appear more resistant than RGCs overall to various sorts of insults, including intraocular hypertension, optic nerve injury, glutamate-induced excitotoxicity, and glaucoma (Cui et al., 2015). Functionally, ipRGCs are unique among RGCs in their ability to encode overall light intensity for extended periods (Wong, 2012). This tonic luminance signal is transmitted to specific brain targets for a variety of functions. Projections to the hypothalamus mediate photoentrainment of circadian rhythms, while those to the midbrain to drive pupillary constriction. These outputs derive from molecularly distinct ipRGC subtypes.

The distinctive structural and functional properties of ipRGCs must ultimately be traceable to different patterns of gene expression. However, there is very little information on what these differences might be. For example, the basic molecular framework of the melanopsin phototransduction cascade, a major defining feature of ipRGCs, has only begun to be identified (Hughes et al., 2012) and the precise phototransduction mechanisms remain poorly characterized. More generally, very little is known about the developmental molecular

mechanisms that direct certain immature RGCs to an ipRGC fate, or that maintain the distinctive features of ipRGCs throughout maturity. Thus, there is ample motivation for comparing the transcriptional profiles of ipRGCs as compared to those of conventional RGCs.

The ipRGCs consist of at least six anatomically distinct retinal subtypes, termed M1-M6. These which differ in their level of melanopsin expression, visual response properties, dendritic stratification, axonal projections, and contributions to light-modulated behavioral responses (Schmidt et al., 2011). Little is known about the gene regulatory programs that differentiate and maintain the specialized properties of individual ipRGC subtypes. M1 ipRGCs have been further subdivided based on their expression of the transcription factor Pou4f2 (Brn3b) (Chen et al., 2011; Jain et al., 2012). M1 ipRGCs that innervate the suprachiasmatic nucleus (SCN) do not express Brn3b, while those that project to other M1-cell targets, such as the olivary pretectal nucleus (OPN), do express this transcription factor (Chen et al., 2011). Indeed, ablation of Brn3b-positive ipRGCs severely impairs the pupillary light reflex, but leaves circadian photoentrainment intact (Chen et al., 2011). There is surely additional molecular diversity among ipRGCs, both within and between established ipRGC subtypes, and this further motivates the present study.

Previous attempts to develop a “molecular parts list” for ipRGCs through gene expression profiling of adult ipRGCs have been limited by the extreme heterogeneity of retinal tissue, and the fragility of mature retinal neurons, and the minuscule amount of genetic material from ipRGCs, which comprise far fewer than 1% of all retinal neurons (Lobo et al., 2006; Heiman et al., 2008; Sanes and Masland, 2015). Some progress has been made by purifying ipRGCs from enzymatically dissociated retinas using either anti-melanopsin immuno-panning or fluorescence-activated cell sorting (FACS) of genetically-labeled fluorescent ipRGCs. However, prior efforts have been limited by low yield and inclusion of contaminating cell populations such as rods (Hartwick et al., 2007; Peirson et al., 2007; Siegert et al., 2012).

Here we conducted a thorough unbiased transcriptomic analysis of ipRGCs by purifying GFP-tagged ipRGCs through a combination of FACS and immunoaffinity and comparing this the

transcriptional profile of GFP-negative RGCs. We did this in two different mouse lines, marking partially overlapping subsets of ipRGCs. One was a BAC transgenic reporter (*Opn4-GFP*), which fluorescently labels M1-M3 ipRGCs (see Methods) and the other was a *Opn4-Cre;Z/EG* reporter system, which labels all ipRGC subtypes, M1-M6 (Schmidt et al., 2008; Ecker et al., 2010; Quattrochi et al., 2018; Stabio et al., 2018). The specificity and purity achieved by our approach is validated by the substantial enrichment in the ipRGC samples of known molecular markers of ipRGCs and by the fact that transcripts selectively expressed in potential contaminating cell types are generally absent. We identified more than 75 new gene candidates expressed much more highly in adult ipRGCs than in other RGCs. We validate two of the new molecular markers at the protein level: the Ras GEF Rasgrp1 and the T-box transcription factor Tbx20 and relate these to established ipRGC subtypes and patterns of central projection.

Results

We enzymatically dissociated retinas from melanopsin-reporter mice, selected for RGCs by anti-Thy1 immunoaffinity, and sorted these into presumptive ipRGC and conventional ganglion-cell (cRGC) pools by FACS based on the fluorescent labeling of ipRGCs (see Methods, Figure 1A). We then compared gene expression in these ipRGC-enriched and cRGC-enriched cell samples to identify genes differentially expressed in ipRGCs as compared to other ganglion cells. We used two strains of melanopsin-reporter mice (see Methods). One of these was a BAC transgenic mouse (here termed *Opn4-GFP*) in which retinal GFP expression is apparently restricted to ipRGCs of subtypes M1, M2 and M3 (see Methods; personal communication R. Maloney and L. Quattrochi). This is presumably because expression of the reporter is coupled to expression of melanopsin, which is highest in this subset of ipRGCs. The other melanopsin reporter mouse was obtained by crossing a knock-in mouse in which *Cre* replaces *Opn4* ($Opn4^{cre/cre}$) with a Cre reporter strain (Z/EG). The resulting Cre-driven labeling of melanopsin-expressing cells is more sensitive than in the other strain of reporter mice, and labels all known

104 types of ipRGCs, M1-M6, while labeling few if any conventional RGCs (cRGCs) (Ecker et al.,
105 2010; Estevez et al., 2012; Quattrochi et al., 2018; Stabio et al., 2018) (Figure 1A; see Methods).
106
107 **Cell composition and purity of isolated ipRGCs and conventional RGCs**
108 The relationship among the transcriptional profiles of ipRGC and cRGC samples across
109 replicates are illustrated in the multidimensional scaling (MDS) plots of Fig. 1B. These show the
110 relationship between all pairs of samples (one of ipRGCs, the other of cRGCs) based on a count-
111 specific pairwise distance measure (Anders et al., 2013) (Figure 1B). These sample pairs were
112 clearly separated along the first dimension, indicating pronounced differences in overall gene-
113 expression patterns between ipRGC and cRGC samples. Samples of ipRGCs and cRGCs derived
114 from the same retina and processed in parallel tended to be closely spaced along the second
115 dimension, indicating greater similarity within than across replicates. This may reflect slight
116 differences in overall genetic makeup of mice contributing to each pool, since both strains used
117 were on a mixed genetic background, or to slight technical differences in the acquisition and
118 processing of RNA from one run to the next.
119 Transcriptional data offer broad internal evidence for the efficacy of purification of cell
120 samples. As expected, the *Opn4* (melanopsin) gene was among the genes much more highly
121 expressed in ipRGCs than in cRGCs. For example, *Opn4* was enriched 40-fold in adult ipRGCs
122 purified from *Opn4-GFP* mice, and this was highly significant, at $q<1x10^{-55}$ false discovery rate
123 (FDR). Though *Opn4* expression was detected in cRGCs at modest levels (Figure S1), this was
124 expected, because some ipRGCs lack GFP expression in both melanopsin reporter lines (Opn4-
125 GFP and Opn4-cre/GFP), and these would have been pooled with cRGCs during the FACS
126 procedure.
127 Transcripts of other genes known to be expressed in ipRGCs were also enriched in the
128 ipRGC pool relative to the cRGC pool (FDR < 0.05, significantly expressed in ipRGC samples,
129 and absent or weakly expressed in cRGC samples). Among these genes were *Adcyap1* (pituitary

adenylate-cyclase activating polypeptide; PACAP), *Tbr2*, (*Eomesodermin*), *Trpc7* and, to a lesser extent, *Trpc6* (Hannibal et al., 2004; Xue et al., 2011; Sand et al., 2012; Mao et al., 2014; Sweeney et al., 2014). Taken together, these results demonstrate that mRNA isolated from purified ipRGC samples were enriched as expected for transcripts for genes that are known to be differentially expressed in ipRGCs.

In the purified ipRGC samples, we found little or no evidence of contamination by transcripts from other retinal cell types. For example, transcript levels were very low for rod and cone opsins, for the amacrine-specific marker ChAT, for several bipolar markers (Otx2; Vsx2; Grm6; Trpm1), and for markers of astrocytes, microglial and vascular cells (Figure S1). Several transcripts suitable for assessing potential contamination from Müller glia (*Glul, Vim)* were present at surprisingly high levels in the purified ipRGC samples, suggesting that these glial cells may contaminate the transcriptional picture to some degree.

In general, the cRGC samples were relatively less pure than the ipRGCs samples by this measure. A particularly informative transcript for assessing such contamination is that for the rhodopsin gene (*Rho*), because rods are by far the most common neuronal type in the mouse retina and express *Rho at* very high levels. Rhodopsin transcripts were significantly (150-fold) more abundant in the cRGC samples than in ipRGC samples (Figure Supplement 1), whether isolated from *Opn4-GFP* or *Opn4-Cre/GFP* adult reporter mice (FDR < 6×10^{-9}). Evidently, the second isolation step in which GFP+ positive cells were isolated by FACS from the purified RGC pool was a key factor in the greater purity of the ipRGC sample. Similarly, transcripts associated with bipolar cells and Müller glial cells were generally more abundant in cRGC than ipRGC samples. For example, the cRGCs had relatively high expression of the known Müller glia markers *Glul*, *Apoe*, *Aqp4*, and *Vim*, generally higher than in the ipRGC pool (Figure S1). Contamination of adult cRGC samples by other cell types may explain why most RGC markers, such as *Rbpms* and *Sncg* (Soto et al., 2008; Rodriguez et al., 2014), were less abundant in the cRGC cell pool than in the ipRGC pool. However, the data suggest that contamination in the cRGC pool was not

uniform across retinal cell types. Amacrine-specific transcripts were no more abundant overall in cRGCs than in ipRGCs, and microglial and vascular markers were essentially absent, as in ipRGCs.

In immature mice (P5; *Opn4-GFP*), contamination of cRGC samples by non-RGC transcripts appeared more modest than in adults. The major sources of contamination (rods and Müller glia) are still being born and undergoing early-stage differentiation at this age, and this would presumably depress the abundance of their cell-type-specific transcripts (Young, 1985; Morrow et al., 1998; Matsushima et al., 2011).

To summarize, this analysis suggests that all samples were relatively free of contamination by most other retinal cell types, and that the ipRGC samples were particular pure. Contamination of the cRGC samples appears to derive mainly from Müller cells and strongly expressed genes in rods. Though this must be factored into the analysis, our primary focus was on genes more strongly expressed in ipRGCs than in cRGCs, and this difference seems unlikely to be affected by the modest contamination of the cRGC pool.

Genes differentially expressed in ipRGCs

Comparing the abundance of transcripts in the ipRGC and cRGC pools, we identified over 75 genes that were differentially elevated expression in ipRGCs (as marked by one or both melanopsin-reporter lines) relative to cRGCs. Briefly, identification of differentially expressed genes in ipRGCs relied on the following stringent criteria: 1) low false discovery rate with high fold-change, 2) corroboration of differential expression across both ipRGC reporters, and 3) absence of gene expression in cRGC samples (see Methods). The identified differentially expressed genes are diverse, and most have not been previously identified as ipRGC-enriched (Figure 2; see Methods). Here, we survey some of these genes, grouped by their functional features (Figure 2).

1. *Transcription factors*

Transcription factors, by regulating other genes, help to generate and maintain ipRGC identity. We noted above that the T-box transcription factor *Tbr2* was much more strongly expressed in adult ipRGCs than in cRGCs, as expected (Sweeney et al., 2014). *Tbr2* is best known for its key role in early retinal development. Its expression in adult retina is far more restricted, but it remains expressed in the majority of ipRGCs. A second T-box transcription factor, *Tbx20*, was similarly enriched (Figure 2). *Tbx20* has not been previously linked to adult retinal function, but we will show that it too is quite selectively expressed in ipRGCs. Additionally, four other transcription factors, *Irx6*, *Dmrtb1*, *Nr4a3*, and *Pou6f2,* were differentially expressed in adult ipRGCs. Most of these genes serve as broad lineage determinants in early retinal development (Zhou et al., 1996; Star et al., 2012). Other highly expressed genes included the neuron-derived orphan receptor 1 *Nor1* (*Nr4a3*), which codes for a nuclear receptor, and *Elavl2* gene, which codes for a RNA-binding protein important for mRNA metabolism and neuronal differentiation (Fornaro et al., 2007; Hinman and Lou, 2008). Pathway analysis (DAVID) of differentially expressed genes in ipRGCs suggested specialization in heparan sulfate biosynthesis, including *Hs3st4*, *Hs3st2*, *Hs6st2*, *Ndst4*, and *Gpc5* (Figure 2).

2. *Synaptic transmission*

Some of the genes differentially expressed in ipRGCs have known roles in regulating synaptic function, especially at presynaptic sites. Among others, these genes include *Sh3gl3*, *Entpd1*, *Rab3b*, *Baiap3*, *Chl1*, *Sh3gl3*, and *Adra2a* (Figure 2).

3. *Growth factors and neuropeptides*

Multiple growth factors and neuropeptides were also differentially expressed in adult ipRGCs. These include *Bmp7*, *Fgf1*, *Gal*, *Gdf6*, *Grem1*, *Nmb* and *Nppb*) (Figure 2).

4. ***Receptors and channels***

Multiple genes encoding diverse surface receptors were differentially expressed in ipRGCs (Figure 2—figure supplement 2). For example, expression data suggest that ionotropic nicotinic acetylcholine receptors in ipRGCs may be composed of α3, α4, α6, β2 and β3 subunits (Figure 2—figure supplement 2), although the α3 and α4 transcripts were borderline for differential expression in ipRGCs. In agreement with previous studies, we found that ipRGCs expressed the Drd1 dopamine receptor, but had low levels of Drd2 expression (Van Hook et al., 2012). Several serotonin receptor genes (Htr1b, Htr1d, and Htr5a) were modestly enriched in ipRGCs. The ipRGCs were also found to express many glutamate receptors subunits, but only one of these - the NMDA receptor subunit 3A (GRIN3A) - was differentially expressed relative to other adult RGCs. The mu opioid receptor gene *Oprm1* is differentially expressed in ipRGCs; it could regulate their light responses interacting with L-type calcium channels, which carry the majority of light-evoked inward calcium current in ipRGCs (Moises et al., 1994; Diaz et al., 1995; Doğrul et al., 2001; Hartwick et al., 2007). Our data appear at odds with earlier reports that M1 and M4 ipRGCs express the melatonin receptor genes Mtnr1a and Mtnr1b (Sengupta et al., 2011; Pack et al., 2015; Sheng et al., 2015). Additionally, *Kcnh1*, also known as ether-a-go-go (*Eag1*), was differentially expressed in ipRGCs (Figure 2). Kcnh1 is a voltage-gated K+ channel that has been shown to be crucial for the generation of dark current in the inner segment of rods (Frings et al., 1998), but may normally regulate other neuronal functions in ipRGCs (Martin et al., 2008).

5. ***Cell adhesion***

Genes encoding for several cell adhesion molecules were differentially expressed in ipRGCs (Figure 2—figure supplement 3B). For example, the cell adhesion molecule *DscamL1* was relatively low in ipRGCs during postnatal development, but the closely related genes encoding the immunoglobulin superfamily (IgSF) adhesion molecules *Sidekick-1* and *Sidekick-2* were enriched in developing ipRGCs. *Unc5a* and *Unc5d* were significantly differentially expressed

both in early postnatal and adult ipRGCs. In contrast, expression of *Unc5b* and *Unc5C* in ipRGCs was low relative to that in cRGCs. As suggested previously, expression of the repulsive ligand *Sema6a* was significantly lower in ipRGCs than cRGCs during postnatal development (Matsuoka et al., 2011). However, its receptor *PlxnA4* was enriched in P5 ipRGCs. Another semaphorin, *Sema5a*, was also significantly enriched in developing ipRGCs. Other differentially expressed cell-adhesion molecules *Salm5* (*Lrfn5*), *Clstn2*, *Thbs1*, *Lrrtm2*, *Pcdh19*, *Ptprm*, and *Lrrc4c (Ngl1)* could play significant roles in the formation of ipRGC synapses (Burden-Gulley and Brady-Kalnay, 1999; Lin et al., 2003; de Wit et al., 2009; Xu et al., 2010; Lipina et al., 2016; Pederick et al., 2016; Lin et al., 2018). The cell surface glycoprotein *Mdga1* was also differentially expressed in developing ipRGCs, and is known to influence the formation and maintenance of inhibitory synapses (Pettem et al., 2013).

6. ***Tolerance to stress***

There is increasing evidence that ipRGCs are resistant to stress and able to survive under circumstances that are fatal for other retinal neurons (Li et al., 2008; de Sevilla Müller et al., 2014; Cui et al., 2015; Duan et al., 2015). The harsh dissociation and FACS processing has the potential of generating stress-induced gene expression changes (Figure 1 and 2, see methods). We attempted to identify potential survival molecular programs that are specific to ipRGCs compared to generic RGCs. The genes *Adcyap1* (PACAP), *Igf1*, and *Spp1* (*osteopontin*), all of which have previously described roles in promoting ipRGC survival (Atlasz et al., 2010; Duan et al., 2015) were differentially expressed in ipRGCs. We also identified a number of genes related to glial function differentially expressed in ipRGCs, including *Gldn*, *Cntn2*, *Lama4*, and *Astn2*, and *Thbs1* (Figure 2).

7. ***Phototransduction***

Photoactivation of melanopsin photopigment typically triggers a phosphoinositide signaling cascade resembling that in rhabdomeric (invertebrate) photoreceptors, involving G proteins in the Gq family, phospholipase C, and canonical TRP channels. In ipRGCs, the phototransduction cascade typically signals through Gq-family proteins and phospholipase C beta 4 (PLCB4) to open canonical TRP channels (Trpc7 and Trpc6) (Graham et al., 2008; Xue et al., 2011; Hu et al., 2013; Emanuel and Do, 2015; Emanuel et al., 2017) (Figure 2—figure supplement 4A). We determined that the genes in this signaling cascade (*Opn4*, *Trpc7*, *Trpc6*, *Plcb4*, and several Gq genes) were expressed at relatively high levels in all three ipRGC pools (i.e., selective-postnatal; selective-adult; or pan-subtype adult). Moreover, two key genes - *Opn4* and *Trpc7* - were more highly expressed in ipRGCs than in cRGCs in all three ipRGC pools. *Trpc6* was also significantly overexpressed in ipRGCs in younger animals, with a trend in this direction also in adult ipRGCs, but *Trpc7* was expressed at much higher levels than *Trpc6*. Plcb4 appears essential for melanopsin phototransduction in some cells, and it was expressed at much higher levels than Plcb1, 2 or 3. However, except in young mice, it was not more highly expressed in ipRGCs than cRGCs.

Only recently has the precise identity of the Gα subunits combination in ipRGCs been identified as redundantly expressing and signaling through the Gnaq, Gna11, or Gna14 subunits (Hughes et al., 2015). Our studies suggest a similar expression pattern, including a lack of Gna15 expression (Figure 2—figure supplement 4A). Further, we determined that Gna14 was differentially expressed in our P5 ipRGC samples, but it did not reach a statistical significant difference in adult Opn4-GFP ipRGCs. Gnaq appears to be among the highest expressing Gq/11 subunits in our study, in contrast to the lack of Gnaq gene expression detected by Siegert and colleagues (2012). To date, the Gβγ complex remains unknown. Our studies determined that the beta subunit Gnb1 is by far the highest expressing, having a 15-fold higher expression than the other subunits Gnb2, Gnb4, or Gnb5; while Gnb3 showed no expression in adult ipRGCs (Figure

2—figure supplement 4C). Additionally, we found that the gamma subunit Gng4 is differentially expressed in ipRGCs.

Also differentially expressed in ipRGCs were two factors with known roles in diacylglycerol (DAG) signaling, *Rasgrp1* and *Dgkg* (Figure 2—figure supplement 4B). Ras guanyl nucleotide-releasing protein 1 (*Rasgrp1*) is a guanine nucleotide exchange factor (GEF) that activates *Ras* by facilitating its GTP binding (Bivona et al., 2003). Rasgrp1 binds DAG and Ca^{2+}, both of which are elevated by melanopsin phototransduction. This provides a possible basis for intrinsic photoresponses of ipRGCs to modulate Ras signaling and thus genes governing cell growth, differentiation and survival. We will return to a more detailed consideration of Rasgrp1 later in this report. Diacylglycerol kinase gamma (*Dgkg*) (Bivona et al., 2003; Shulga et al., 2011) converts DAG to phosphatidic acid, thus acting as a terminator of DAG signaling. Because DAG appears to be a key link between early steps in phototransduction and gating of the light-activated channels, Dgkg may regulate the kinetics of the photoresponse in ipRGCs. The protein products of the two overexpressed genes may interact. Diacylglycerol kinases are also known to bind to Rasgrp and modulate its activity (Topham and Prescott, 2001). Diacylglycerol and calcium are also known to activate the protein kinase C (PKC) family members Prkcd and Prkcq (Oancea and Meyer, 1998), which we determined to be differentially expressed in ipRGCs. Protein kinase C (PKC) activity has been suggested to be important for deactivating TRPC activity in the invertebrate photoreceptors and potentially also for the Opn4 phototransduction cascade (Graham et al., 2008). Peirson and colleagues (2007) previously identified another PKC member, Prkcz, as being important for ipRGC-mediated photoentrainment of circadian rhythms (Peirson et al., 2007). However, Prkcz is only moderately expressed and similar to control samples in our study.

In other photoreceptors, RGS (Regulator of G protein signaling) proteins play a key role in terminating the photoresponse by accelerating the intrinsic GTPase activity of the cognate G-protein (e.g., transducin in rods). Two RGS genes were overexpressed in all three ipRGC pools:

Rgs4 and *Rgs17*. At least one of these (Rgs17) regulates Gq signaling (Mao et al., 2004; Ji et al., 2011) (Figure 2—figure supplement 4B).

The arrestins also contribute to response termination by binding to phosphorylated opsin. ipRGCs exhibited strong expression of both beta arrestin genes (Arrb1, Arrb2) but low expression of rod (*Sag*) and cone (*Arr3*) arrestin genes. This is consistent with earlier evidence that beta arrestins rather than conventional retinal arrestins bind photoactivated melanopsin in ipRGCs (Cameron and Robinson, 2014). Still, these beta arrestin transcripts are both at similarly high levels in cRGCs as in ipRGCs, presumably because these arrestins regulate diverse GPCRs (Figure 2—figure supplement 4B).

Many of the genes involved in rod and cone phototransduction had low expression (scarce or no read alignment) and/or were present at much lower levels in ipRGCs than cRGCs. These include the genes for opsins, transducin alpha, and arrestin in rods (*Rho*, *Gnat1, Sag*) and cones (*Opn1mw, Opn1sw, Gnat2,* and *Arr3*; Figure 2—figure supplement 4C). Although Cngb1 was differentially expressed in ipRGCs, the total reads aligning to the Cngb1 locus were low and derived mainly from a limited region of the gene, and the obligatory alpha subunits were not detected, so this could be a false positive (Figure 2—figure supplement 4C).

Genes differentially repressed in ipRGCs

The lack of contamination by non-RGC retinal neurons in the postnatal day 5 (P5) samples allowed us to identify genes that were differentially repressed in ipRGCs compared to cRGCs in early postnatal development. Our data suggested that the transcription factor *Jun* (Jun Proto-Oncogene) and *Irx4* are differentially repressed in P5 ipRGCs samples (Figure 2—figure supplement 3). Other genes that were differentially repressed in the P5 ipRGC samples included *Satb1*, *Satb2*, and *Foxp2* showed, all of which are known to have restricted expression in the abundant F-RGC type that is likely included in the cRGC samples (Rousso et al., 2016). The *Pou4f1* (*Brn3a)* and *Pou4f3* (*Brn3c*) transcription factors were both differentially repressed in P5

ipRGCs, consistent with their known lack of expression in ipRGCs (Jain et al., 2012) (Figure 2—figure supplement 3). The transcriptional repressors *Bcl11b (CTIP2)*, *Irx4*, and *Tbr1* were all found to be differentially repressed in ipRGC compared to cRGCs samples. Furthermore, the *Cdkn1c* (*p57KIP2),* a gene known to be transcriptionally repressed by Bcl11b (Topark-Ngarm et al., 2006), had relatively increased expression in ipRGCs (Figure 2—figure supplement 3).

Expression differences between the *Opn4-GFP* and *Opn4-Cre/GFP* reporter systems

To study gene expression differences across the different ipRGC subtypes, we compared the expression patterns of *Opn4-Cre/GFP* (labels all M1-M5 subtypes) and *Opn4-GFP* (labels only the M1-M3 subtypes) (Figure 2—figure supplement 1). In general, genes differentially expressed in ipRGCs identified in the two reporter systems were both supportive and cross-correlated. However, we identified 24 genes that were differentially expressed in the adult *Opn4-Cre/GFP* reporter but had low or no apparent expression in the *Opn4-GFP* reporter, suggesting selective expression in one or more of the M4-M6 ipRGC subtypes. The *Opn4-Cre/GFP* specific genes included *Anxa2*, *Gem*, *Sema3d*, *Rbp4*, and *Rxrg*. Recently, an Rpb4 reporter (Rbp4-Cre) was demonstrated to mark amacrine cells coupled to ipRGCs, although there was an apparent lack of labeling in ipRGCs (Sabbah et al., 2017). The Kcnk4/TRAAK, another gene that was differentially expressed in the *Opn4-Cre/GFP* reporter, encodes a two-pore potassium channel subunit (Fink et al., 1998). Additionally, our data suggest that the Kcns3 electrically silent voltage-gated potassium channel subunit has its expression restricted to the ipRGCs labeled by *Opn4-Cre/GFP*, but this difference did not reach statistical significance (FDR 0.13). However, close inspection of reads aligning to Kcns3 using the integrated genome viewer (IGV) confirmed weak expression in ipRGCs and absent expression in cRGCs for *Opn4-Cre/GFP* samples (data not shown). Lastly, the neurexophilins Nxph1 and Nxph3 were differentially expressed in the *Opn4-GFP* and *Opn4-Cre/GFP* reporters, respectively (Figure 2—figure supplement 1). These proteins

361 are known to bind α-neurexins in mice and have restricted expression patterns (Missler et al.,
362 1998; Beglopoulos et al., 2005; Craig and Kang, 2007).
363
364 **Rasgrp1 is selectively expressed in ipRGCs**
365 We sought to test our transcript-level differential expression analysis at the protein level
366 and to determine whether their expression is selective for particular adult ipRGC subtypes.
367 Transcriptional profiling suggested that Rasgrp1 is expressed differentially, possibly even
368 selectively, in ipRGCs. However, differential mRNA expression does not guarantee a
369 correspondence with protein product (Koussounadis et al., 2015). Therefore, we used
370 immunofluorescence against Rasgrp1 (Puente et al., 2000) to label the Rasgrp1 protein in whole-
371 mount retinas from adult wild type mice. Rasgrp1-immunopositive somata were present in the
372 ganglion cell layer (GCL) and in the inner nuclear layer (INL). The latter likely represent amacrine
373 cells or displaced ganglion cells, judging by their close proximity to the inner plexiform layer (IPL)
374 (Figure 3). Immunolabeling marked the cytoplasm as well as the somatic plasma membrane of
375 these cells. Occasionally, particularly strongly Rasgrp1-labeled cells had some dendritic labeling.
376 Rasgrp1 immunostaining was also observed in a subset of photoreceptors in the outer retina (data
377 not shown).
378 To test whether the Rasgrp1-positive cells in the ganglion-cell layer were RGCs, we
379 carried out double immunofluorescence for both Rasgrp1 (antibody m199) and the RNA-binding
380 protein Rbpms, which selectively labels all and only RGCs (Rodriguez et al., 2014). About half of
381 Rasgrp1-immunopositive cells in the GCL were RGCs, as determined by co-labeling for Rbpms
382 (56%, n = 708 across three retinas, Figure 3A,B). The remainder can be assumed to be displaced
383 amacrine cells.
384 Most of these Rasgrp1-expressing RGCs were ipRGCs, as revealed by their
385 immunoreactivity for melanopsin (95.9±1.1%, n = 412, Figure 3A,B). In contrast, only a fraction of

386 Opn4-immunopositive ipRGCs were Rasgrp1 immunopositive (34%, *n* = 1169). Thus, Rasgrp1
387 expression in the GCL is apparently restricted to a subpopulation of ipRGCs.

388 We next tested whether the immunolabeling of RGCs represented endogenous Rasgrp1
389 protein expression. The antibody used in this study has been previously shown to specifically
390 label Rasgrp1 protein expression in hippocampal neurons (Pierret et al., 2000). As a further test
391 for the specificity of the antibody, we compared immunofluorescence labelling of whole mount
392 retinas from normal and Rasgrp1-knockout mice generated by inserting *LacZ* and a *Neo* cassette
393 into the Rasgrp1 gene to disrupt its expression (Dower et al., 2000). Our control experiments
394 showed that the GCL and INL cellular immunolabeling is absent in the Rasgrp1 knockout (Figure
395 3C). However, vasculature and photoreceptor cell labeling persisted in Rasgrp1-knockout mouse
396 retinas, suggesting cross-reactivity of antibody with other proteins.

397

398 **Rasgrp1 expression is restricted to diverse ipRGC subtypes**

399 We next determined which of the established morphological subtypes of ipRGCs express
400 Rasgrp1 into adulthood (Figure 3D). For this purpose, we used key characteristics such as relative
401 Opn4 expression, soma size, and dendritic morphology (see Methods). In the GCL, the majority
402 of M1/3 cells (71.6±3.9%, *n* = 300 across three retinas) but only a fraction of M2 cells (23.4±5.4%,
403 *n* = 389) and M5/6 cells (31.4±6.13%, *n* = 138) expressed Rasgrp1 (Figure 3D). In the INL,
404 displaced M1 cells express Rasgrp1 at a similar percentage as conventionally placed M1 cells
405 (70.7±8.0%, *n* = 3 retinas). We found no examples of Rasgrp1 immunoreactivity in M4 cells (0%,
406 *n* = 172, Figure 3D). Of the Rasgrp1-expressing ipRGCs, half were M1/3 cells (52.8±3.8%), nearly
407 a quarter were M2 cells (21.1±2.7%) and a small percent (10.4±1.8%) were M5/6 cells (*n* = 396
408 Rasgrp1^{+}/Opn4^{+} cells across three retinas). Therefore, Rasgrp1 is selectively expressed in a
409 diverse set of ipRGC subtypes.

410

411 **Spatial Distribution of Rasgrp1-expressing ipRGCs and amacrine cells**

412 Our data show neither a ventral-dorsal nor a naso-temporal density gradient of Rasgrp1-
413 expressing M1-M3 ipRGC across the retina (Figure 3—figure supplement 1C). However, we did
414 observe a minor ventral-dorsal gradient of Rasgrp1-expressing RGCs, with a higher density in
415 the ventral (65%) compared to the dorsal (35%) retina (Figure 3—figure supplement 1E). As
416 shown above, Rasgrp1-expressing RGCs are almost exclusively ipRGCs (96%).

417

418 **Tbx20 is expressed in a diverse subset of ipRGCs**

419 The T-box transcription factor Tbx20 was suggested from our gene expression analysis
420 to be differentially expressed in ipRGCs. Immunofluorescence co-loclalization analysis of Tbx20
421 and Opn4 expression confirmed its high expression in a subset of ipRGCs (Figure 4D). Tbx20
422 was expressed in most M1 cells (82.6±1.8%, n=514 across four retinas), but only in a minority of
423 M2/3 cells (30.2±6.5%, n=1305) and M5/6 cells (12.4±3.4%, *n* = 603). Half of the displaced M1
424 (dM1) cells expressed Tbx20 (46.0±7.1%, *n* = 153). Strikingly, however, Tbx20 was not expressed
425 in M4 cells (0%, *n* = 283). These results demonstrate that Tbx20 is expressed in a diverse subset
426 of ipRGCs.

427 Many Tbx20 cells were not detectably immunopositive for Opn4. Only 41% of Tbx20
428 immunopositive were also Opn4-immunoreactive (18.5±2.6% were M1 cells; 16.0±2.0% were
429 M2/3 cells; and only 3.6±0.9% were M5/6 cells; *n* = 2184 across four retinas; Figure 4—figure
430 supplement 1). The remaining Tbx20-immunopositive cells were RGCs, as confirmed by Rbpms-
431 immunoreactivity (data not shown). Additionally, Tbx20-immunopositive RGCs that were also
432 Opn4-immunonegative were topographically enriched in the ventral retina, with most Tbx20-
433 positive cells in the dorsal retina being accounted for by Opn4-immunoreactivity.

434

435 **Tbx20 expression in M5-M6 ipRGCs**

436 To investigate whether some or all of the Tbx20-immunopositive RGCs that were Opn4-
437 immunonegative might be ipRGCs of the M5 and M6 subtypes that exhibit weak Opn4
438 immunostaining, we examined the co-localization of Tbx20-immunopositive cells, Opn4-
439 immunopositive cells, and all GFP-labeled cells in the *Opn4-Cre;Z/EG* mouse reporter, which
440 among other ipRGCs, labels M5 and M6 cells. We observed examples of Tbx20-immunopositive
441 cells that were GFP-positive (M1-M6 ipRGCs), but not Opn4-immunopositive (M1-M4),
442 suggesting that Tbx20 is expressed in at least a subset of M5 or M6 ipRGCs (Figure 4—figure
443 supplement 1A,B).

444 To test the implication that many Tbx20 cells were M5 or M6, we turned to Cdh3-GFP
445 mice. Recently, our group determined that essentially all GFP+ RGCs in the Cdh3-GFP reporter
446 mouse you used in your studies are either M6 cells (the great majority) or M5 cells (minority)
447 (Quattrochi et al., 2018). We tested Tbx20 immunoreactivity in the context of Opn4
448 immunofluorescence and *Cdh3-GFP* labeling (Figure 4B,C). For the purpose of this study, we
449 focused on GFP cells in the GCL that are Opn4-immunonegative (to distinguish from Opn4-
450 immunopositive M2 types). We found that at three weeks after birth, most *Cdh3-GFP* cells express
451 the Tbx20 protein (82.1±4.3%, *n* = 439 across four retinas, Figure 4C). Many, but not all, of the
452 Opn4-immunonegative Tbx20-positive cells were GFP^+ (27%, n=1277 $Tbx20^+$;$Opn4^-$ cells; 4
453 retinas). The dorsal-ventral gradient of Tbx20-positive cells that are Opn4-immunonegative was
454 broadly similar to the retinal labeling of the *Cdh3-GFP* reporter. A large portion of Tbx20-
455 immunopositive cells remained unclassified (43.3±3.8%, n=2184; Figure 4—figure supplement
456 1D).

457 Further, we determined whether Tbx20 expression correlates with the related T-box
458 transcription factor Tbr2, a gene previously described to be enriched in adult ipRGCs (Mao et al.,
459 2014; Sweeney et al., 2014). All Tbx20-expressing cells were strongly Tbr2-immunopositive (*n* =
460 328; 4 regions distributed across a single adult *Opn4-Cre/GFP* retina; Figure 4—figure

supplement 1C). Therefore, whereas Tbr2 is expressed in a broad range of types that includes the entire ipRGC family, Tbx20 expression is confined to a diverse subset of ipRGC subtypes.

Molecular diversity of Rasgrp1 and Tbx20 expression in ipRGCs

Our expression studies revealed that Rasgrp1 and Tbx20 have a strikingly similar pattern of expression among ipRGC subtypes. Both genes were expressed in the majority of M1 cells, a minority of M2 cells, and a small population of M5/6 cells, but not in M4 cells (Figures 4 and 5). To directly test for co-expression, we compared and contrasted the expression patterns of Tbx20- and Rasgrp1-immunoreactivity in the context of the M1-M4 subtypes revealed by Opn4-immunoreactivity (Figure 5). Rasgrp1 co-expression with Tbx20 was only observed in a fraction of M1/3 cells (26.0±1.8%; *n* = 241 across two retinas; Figure 5). Further, M1 cells expressing either Rasgrp1 or Tbx20 alone accounted for roughly similar fractions of M1 cells (37.3±4.0% and 31.1±3.5%, respectively). Only a small fraction of M1 cells were immunonegative for both Rasgrp1 and Tbx20 (5.3±0.7%). In contrast, half of M2 cells lacked Rasgrp1 and Tbx20 immunoreactivity (57.7±3.3%; *n* = 388 across two retinas). Approximately a third of M2 cells expressed Tbx20 (31.0±0.7%), while only 11.3±5.1% expressed Rasgrp1. We did not observe any example of an M2 cell expressing both Rasgrp1 and Tbx20.

Molecular diversity of SCN-projecting ipRGCs

We further examined the Rasgrp1- and Tbx20-expressing ipRGC subtypes to seek intersectional expression patterns that would divide ipRGCs by their downstream visual pathways. Earlier studies showed that M1 cells could be subdivided based on their level of expression of Brn3b (Chen et al., 2011). We used quadruple immunolabeling to simultaneously test Brn3b expression with Rasgrp1- and Tbx20-immunoreactivity in the context of Opn4-immunolabeled ipRGCs (25 regions, three wild type retinas; Figure 5A,B). We determined that a minority of M1/3

cells express Brn3b (7.9±6.0%, n=241), which is similar to previous studies (Jain et al., 2012). The Brn3b$^+$ M1/3 cells expressed either Tbx20 or Rasgrp1 (91.0 and 9.0±10.1%, respectively; n=30) (Figure 5C).

Further, we determined that most M2 cells expressed Brn3b (90.8±6.9, n=168). In contrast to M1/3 ipRGCs, the majority of Brn3b$^+$ M2 ipRGCs did not express either Rasgrp1 or Tbx20 (67.4.6±13.8, n=222). Most M2 cells expressing Tbx20 were also Brn3b immunopositive (84.5±25.1, n=118). The small subset of M2 cells that express Rasgrp1 could be further divided by Brn3b presence or absence (5.0±6.0% and 4.5±1.4%, respectively; n=168). Generally, we found no cells co-expressing all three genes (n=729).

Our immunostaining study in the retina suggested that SCN-projecting M1 cells (Brn3b-negative) might represent molecularly diverse cell populations (Figure 5C). We correlated gene expression of Rasgrp1 and Tbx20 in the retina with retrograde labeling from the SCN (Figure 6A). We injected rhodamine-conjugated retrobeads in the SCN, followed by immunofluorescence labeling for Opn4, Rasgrp1, and Tbx20 (Figure 6A-C). All injection sites clearly involved the SCN, as revealed by DAPI labeling, but did not spread to the optic chiasm or tract (Figure 6B). Quantitative co-expression analysis (18 confocal images collected across the contralateral and ipsilateral retinas) revealed that nearly all retrolabeled cells were Opn4-immunopositive (95%). These cells exhibited variable patterns of staining for the other proteins. Most cells expressed both Rasgrp1 and Tbx20 (76%), but equal minorities expressed either Rasgrp1 (12%) or Tbx20 (12%, Figure 6D). This expression pattern was consistent across the ipsi- and contralateral retina (Figure 6D), as suggested by a bilateral input to the SCN (Hattar et al., 2006; Fernandez et al., 2016). Therefore, we show that SCN-projecting ipRGCs have a complex pattern of Rasgrp1 and Tbx20 gene expression. Together, these results provide evidence for previously unrecognized molecular diversity in adult ipRGCs.

Discussion (2657 words)

Prior efforts to assess the distinctive genetic composition of ipRGCs have been complicated by their rarity among diverse retinal cell types and the inherent difficulties of maintaining viability of dissociated mature neurons (Lobo et al., 2006). Our approach was first to isolate RGCs by immunoaffinity, then to further purify ipRGCs from these based on genetic labeling and FACS, and to finally to compare the transcriptional profiles of the purified ipRGCs to those of the residual cell pool, consisting mainly of conventional RGCs. The relative purity of our ipRGC sample is supported by enrichment for transcripts of genes known to be differentially expressed in ipRGCs and the low levels of transcripts selectively expressed in potentially contaminating populations, including the abundant rod photoreceptors. Our isolation method and differential expression analysis allowed us to identify more than 75 differentially expressed genes in ipRGCs relative to conventional RGCs.

Genes differentially expressed in adult ipRGCs

There is limited knowledge of specific gene expression in ipRGCs generally and within particular ipRGC subtypes, especially non-M1 ipRGCs. Many diverse genes appeared more highly expressed in ipRGCs than in conventional RGCs. We confirmed differential protein expression in ipRGCs immunohistochemically for two of these genes: Tbx20, a transcription factor implicated in visual development; and Rasgrp1, a G-protein exchange factor that may interact with the melanopsin phototransduction cascade. However, only a subset of ipRGCs appeared to express detectable levels of these proteins, and such variable expression was apparent even among ipRGCs of the same subtype. Some ipRGCs expressed both proteins, but many did not. This diversity even extended to the M1 cells projecting to the SCN, which had been thought to share the distinctive molecular feature of little or no expression of the transcription factor Brn3b. These novel markers of molecularly distinctive ipRGC varieties open the way for cell-type-specific manipulations through intersectional strategies.

What type(s) of adult ipRGCs express Rasgrp1?

Rasgrp1 expression has previously been detected in the hippocampus, striatum and olfactory regions of the brain (Ebinu et al., 1998; Toki et al., 2001), but our study appears to be the first to explore Rasgrp1 expression in the eye. Rasgrp1-like immunoreactivity marked a diverse subpopulation of ipRGC subtypes, including the M1-M3 ipRGC subtypes but not the M4-type. Either M5 or M6 ipRGCs, or both, also appear likely to express Rasgrp1, because some Rasgrp1 immunoreactive cells had weak Opn4-immunoreactivity without the characteristic dendritic labeling of M1-M3 ipRGCs and with somas too small to be M4 cells (Ecker et al., 2010; Quattrochi et al., 2018; Stabio et al., 2018).

What is the function of Rasgrp1 in adult ipRGCs?

The function of Rasgrp1 in ipRGCs is unknown, but it could interact with the melanopsin phototransduction cascade. The direct photoresponse of ipRGCs appears to increase levels of both DAG and calcium. Both of these signaling molecules bind to and activate Rasgrp1, and trigger its translocation to the Golgi apparatus (Bivona et al., 2003; Graham et al., 2008; Zhang et al., 2010). However, ipRGC phototransduction Rasgrp1 signaling does not appear to be essential for ipRGC phototransduction because more than a quarter of M1 ipRGCs and the great majority of M2 cells are immunonegative for Rasgrp1. Even in ipRGCs, Rasgrp1 may be activated by DAG and calcium signals unrelated to Opn4 phototransduction, and such signals are presumably also responsible for modulating Rasgrp1 in cells (such as certain amacrine cells) which express Rasgrp1 but not melanopsin.

Rasgrp1 has the potential to affect any number of neuronal signaling pathways. Ras signaling pathways are enormously complex and the cross talk between pathways makes it even harder to identify specific effects. One basic mechanism for specificity in Ras signaling is the distinct subcellular targeting of downstream components of the signaling pathway. In

563 lymphocytes, localized Ras signaling of Rasgrp1 occurs preferentially on the Golgi apparatus,
564 which is a rare form of compartmentalized Ras signaling (Bivona et al., 2003; Zhang et al., 2010).
565 The Golgi apparatus in neurons provides the posttranslational protein modifications required for
566 organizing protein and organelle trafficking throughout the cell. Rasgrp1 could play a crucial role
567 in orchestrating a specific set of post-translational modifications at the Golgi.

568 An important survival mechanism in M1 ipRGCs is the maintenance of mTOR expression
569 by melanopsin phototransduction (Duan et al., 2015; Li et al., 2016). The DAG-activated Rasgrp1-
570 Ras-Mek1/2-Erk1/2 pathway contributes to mTOR activation in thymocytes (Gorentla et al., 2011).
571 The percentage of M1 cells expressing Rasgrp1 (72%) in this study is similar to the percentage
572 of M1 cells that survive optic nerve crush (~70%, Li et al., 2016). It would be interesting to test
573 whether Rasgrp1 is required for the maintained mTOR levels in these surviving M1 ipRGCs.
574 Recent studies have also clarified different mechanisms responsible for M1 survival and the
575 regeneration potential of alpha-RGCs such as M4 ipRGCs (Duan et al., 2015; Li et al., 2016).
576 Despite surviving well, M1 ipRGCs were not capable of regenerate their axons (Li et al., 2016).
577 In contrast, alpha-RGCs had a unique capability to regenerate their axons that was promoted by
578 their high levels of mTOR expression as well as osteopontin/Spp1 expression coupled with the
579 growth factor IGF-1(Duan et al., 2015). Whereas M1 ipRGCs were found to maintain mTOR
580 expression after axon injury, M4 ipRGCs and other alpha RGC types were demonstrated to have
581 diminished mTOR expression levels (Li et al., 2016). The absence of detectable Rasgrp1
582 expression in M4 ipRGCs may help to account for their failure to maintain mTOR expression after
583 injury.

584

585 **Central brain targets of Rasgrp1-expressing ipRGCs**

586 At the circuit level, Rasgrp1 is not anticipated to be an essential regulator of circadian
587 photoentrainment. The majority of M1 ipRGCs are known to provide the primary retinal input to
588 the SCN, while a subset of M1 ipRGCs send input to the OPN to regulate the pupillary reflex. Our

studies found that Rasgrp1 was expressed in the majority of M1 ipRGCs, which suggested to us that it might correlate directly and completely with the SCN-projecting M1s. However, retrograde tracing experiments from the SCN revealed that some SCN-projecting M1 cells were Rasgrp1-immunonegative. Accumulating research suggests that the SCN is more compartmentalized than previously recognized (Bedont and Blackshaw, 2015). The question of whether Rasgrp1 is expressed in a subset of M1 ipRGCs that targets a specific compartment of the SCN remains to be determined.

We find Rasgrp1 to be expressed not only in SCN-projecting M1 ipRGCs, but also in other ipRGC subtypes, especially M2 cells and apparently M5 and/or M6 cells. Collectively, these types project to various non-image-forming visual centers, including the olivary pretectal nucleus, intergeniculate leaflet, and dorsal lateral geniculate nucleus (Quattrochi et al., 2018; Stabio et al., 2018).

Tbx20 is expressed in a diverse set of ipRGC subtypes

The T-box transcription factor Tbx20 exhibited enriched expression relative to conventional RGCs in postnatal and adult retinas. Double immunolabeling revealed that many ganglion cells that expressed this protein also expressed melanopsin. As was true for Rasgrp1, Tbx20 was determined to be expressed in most M1 ipRGCs (75%), a substantial minority of M2 cells (40%) and an additional population of RGCs whose identity was not immediately obvious. We decided to then compare Tbx20 against other known molecular patterns in ipRGCs. Whereas most RGCs follow a Brn3b-dependent developmental program, the M1 ipRGCs that project to the SCN do not express Brn3b while OPN-projecting M1 ipRGCs express Brn3b. We found that Brn3b-expressing M1 cells are also Tbx20-immunopositive. The Brn3b-negative M1 cells are split between cells that express Tbx20 and those that do not. This finding suggests that ipRGCs are more molecularly diverse than originally anticipated: Tbx20 is expressed in ipRGCs with differing brain targets, Tbx20 is expressed across multiple morphologically defined subtypes, and Tbx20

615 is not expressed in all of any one type. The exploration of Tbx20 coexpression with Rasgrp1
616 revealed a complex coexpression pattern among M1-M3 ipRGCs.
617
618 **What is the function of Tbx20 in adult ipRGCs?**
619 Tbx20 has well-established roles in embryonic development and is continuously required
620 in mature neurons and other cell types to maintain their identities and functional properties during
621 adulthood (Naiche et al., 2005). Tbx20 functions as a repressor in early embryonic ocular
622 development (Carson et al., 2000; Pocock et al., 2008) and is required for the expansion of the
623 small pool of precursor cells in the optic vesicle (Carson et al., 2004). However, little is known
624 about the function of Tbx20 in the adult retina.
625 Tbx20 can function as a transcriptional activator in parallel with its repressor activity, with
626 these two roles impinging on distinct biological processes (Sakabe et al., 2012). In addition to its
627 key developmental roles, Tbx20 appears vital for maintaining the structure and function of cardiac
628 muscle cells in the adult mouse heart (Stennard et al., 2003; Shen et al., 2011). In adult
629 cardiomyocytes, Tbx20 is responsible for directly activating genes critical for normal adult cardiac
630 function such as those required for ion transport and heart contraction (Shen et al., 2011; Sakabe
631 et al., 2012). In contrast, genes directly repressed by Tbx20 have known roles in non-heart
632 developmental programs, cell cycle, proliferation, and immune response (Sakabe et al., 2012).
633 The transcriptional effects of Tbx20 shift during cardiac development, from early mediation of
634 proliferation of cardiac progenitors, to implementation of an anti-proliferative program in the adult
635 heart (Cai et al., 2005; Takeuchi et al., 2005). Therefore, Tbx20 cooperates with distinct cohorts
636 of transcription factors to either promote or repress distinct molecular programs in a context-
637 dependent manner (Sakabe et al., 2012). Similarly, binary cell fate specification in the retina is
638 driven by complex genetic programs that require the simultaneous activation and repression of
639 genes by transcription factors. Tbx20 may prove to have a similar reversal in its transcriptional
640 activity in the retina when transitioning from broad embryonic development program to regulating

641 adult neuron identity of a subset of ipRGCs. Further, Tbr2 is another Tbox family member that is
642 known to have a critical role in the development of retinal ganglion cells (Mao et al., 2008), which
643 later becomes essential to a restricted set of ipRGCs that participate in NIF visual circuits (Mao
644 et al., 2014; Sweeney et al., 2014). Our studies determined that Tbx20 and Tbr2 are coexpressed
645 in adult ipRGCs. They may work cooperatively to specify ipRGC subtype identity by regulating
646 cell-specific transcriptional programs and repressing alternate fates.
647
648 **Characterization of ipRGC subtypes**
649 Retinal cell types are generally classified using a combination of morphology, gene
650 expression, mosaic organization, light responses and synaptic connectivity (Sanes and Masland,
651 2015). By these criteria, intrinsically photosensitive RGCs comprise at least 6 distinct cell types
652 (Figure 7). Though all express melanopsin, they differ from one another in the strength of the
653 intrinsic response, their morphology, pattern of light responses, and projections to the brain.
654 However, the further subdivision may be in order. The M1 type appears subdivisible into at least
655 two subtypes, one expressing the transcription factor Brn3b and innervating the OPN and
656 geniculate complex, while the other lacks Brn3b expression and innervates the SCN (Chen et al.,
657 2011). Our study shows further diversity in the M1 and M2 types based on the expression of
658 Rasgrp1 and Tbx20. For example, we find molecular diversity among in the SCN-projecting
659 ipRGC subtypes (Figure 7). It is unclear to us whether this should be used to propose a further
660 formal subdivision of M1 and M2 cells. For example, the expression of these proteins could
661 fluctuate over time in individual cells and be uncorrelated across cells of the same type. One
662 would like to know that these patterns of expression are stable over time and correlated with other
663 cell features before proposing such further subdivision. The extensive overlap among dendritic
664 fields of M1 (and of M2) cells (Berson et al., 2010) means that either type could be subdivided
665 into two or perhaps three subtypes while still maintaining full retinal coverage (i.e., tiling), but it
666 seems likely that we will either have to accept that there is substantial molecular diversity with

667 single types (as there is substantial functional diversity among M1 cells (Emanuel et al., 2017))
668 or that the dogma of complete retinal tiling by single types must be abandoned.

669 In addition to Tbx20 expression in a subset of SCN-projecting M1s, Tbx20 may also
670 regulate the molecular program of ipRGCs projecting to the OPN and control the pupillary light
671 reflex. The Brn3b-expressing M1 ipRGCs, a subset of M2 ipRGCs and *Cdh3-GFP* labeled M6
672 ipRGCs are all known to project to the OPN, and all express Tbx20. However, this is not a direct
673 association and further retrograde or Tbx20 conditional knockout studies are required, especially
674 to determine the function of Tbx20-expressing M2s.

675

676 **Comparison with other ipRGC gene expression profiles**

677 Siegert and colleagues (2012) surveyed gene expression in many different sets of mouse
678 retinal neurons, using specific mouse reporters strains (including the *Opn4-Cre* reporter system
679 for ipRGCs), FACS isolation of labeled cells, and microarray analysis. Many of the genes they
680 found strongly expressed in ipRGCs were also among the genes we found differentially expressed
681 in ipRGCs. However, dozens of additional genes differentially expressed in ipRGCs emerged
682 from our analysis that were not detected in theirs (Siegert et al., 2012). Discrepancies between
683 their findings and ours may stem from technical factors such as differing degrees of contamination
684 of the starting material with rod photoreceptor transcripts, the use of internal control cell
685 populations for relative gene expression comparison in our study but not theirs, and differences
686 between microarray and RNA-sequencing methodologies.

687 Another recent studied used single-cell transcriptomic analysis of the mouse retina and
688 were able to identify ipRGCs from their cell suspensions (Macosko et al., 2015). Single cell
689 technology is ideal, in principle, for the precise identification of an individual neuron's molecular
690 identity despite the extreme heterogeneity of the nervous system. Macosko et al., 2015 could
691 definitively distinguish the main broad class of RGCs, but they required *post hoc* supervised
692 analysis to distinguish a limited number of genes attributed to Opn4-positive cell clusters. They

identified nine genes with a two-fold increase in expression compared to Opn4-negative cells. Three genes (Tbr2, Igf1, and Tbx20) were also found to be enriched in our ipRGC samples. In contrast, Tbx20 did not reach above threshold for Siegert et al., (2012), but it is among the highest expressing ipRGC-enriched genes in our study. Single-cell gene expression profiling methods such as Drop-Seq hold great promise and will certainly continue to be pursued more in future studies of neuron subtype gene expression. Recently, single-cell studies of pre-enriched bipolar cells were able to distinguish molecular markers for all previously recognized bipolar cell types (Shekhar et al., 2016). Similarly, ipRGCs subtype-specific gene expression may become deciphered in the future using single-cell analysis that incorporates a pre-enrichment step for ganglion cells.

Conclusion

In conclusion, our results demonstrate a method to purify ipRGCs and identify an extensive list of more than 75 genes that are differentially expressed compared to generic RGCs. Of course, our identified differentially expressed genes in ipRGCs should not be considered a complete account of all genes relevant to ipRGC function. Instead, we hope that it will provide a beneficial resource that will generate hypothesis that lead to key insights into ipRGC function in non-image forming vision. The more than 75 genes suggested to be differentially expressed in ipRGCs will be useful for the identification of marker genes for ipRGC subtypes, comparison of gene expression across types, understanding the intracellular gene networks underlying ipRGC phenotypes, and the testing for conservation of ipRGC molecular programs across mammalian species.

We are encouraged that our gene expression profiling data of ipRGCs lead us to the identification of Tbx20 and Rasgrp1 as novel, selectively expressed genes in ipRGCs. These results serve as a good proof of principal for the validity of our gene expression profiling results. In addition, the stable, specific expression in adult ipRGCs suggests that the differential gene

719 expression of Rasgrp1 and Tbx20 were not simply due to transient, stress-induced molecular
720 program resulting from the harsh processing steps prior to sequencing. We determined that Tbx20
721 and Rasgrp1 are expressed across ipRGCs that belong to multiple morphological types, have
722 diverse molecular expression, differing physiology, and are involved with multiple visual brain
723 circuits.
724

725 **Methods**

726 *Animals:*

727 All experiments were conducted in accordance with NIH guidelines under protocols approved by
728 the Brown University (Providence, RI) Animal Care and Use Committee. Both male and female
729 adult mice (P30 to P90) were used unless otherwise stated. *Opn4*$^{cre/cre}$ mice (Ecker et al. 2010)
730 crossed with floxed-stop reporter mice: "*Z/EG*" (*Jax#003920*); the offspring express GFP in *cre*-
731 expressing cells (M1-M6), as described by Ecker et al., 2010. *Opn4-GFP(ND100Gsat)* is a BAC
732 transgenic originated from the GENSAT project at Rockefeller University. Rasgrp1-KO
733 (Rasgrp1^{tm1Jstn}, Dower et al., 2000) was initially provided generously by Robert Barrington, U. of
734 Alabama for initial testing. A colony was created inhouse from stock at Jackson labs (Jax 022353).
735 *Rasgrp1-Cre*(PO1 founder line) was rederived from Jackson Labs (#34811-UCD). *Cdh3-GFP*
736 reporter is a BAC transgenic originally generated by the Gensat project (MMRRC,
737 BK102Gsat/MMNC) and has been used previously (Quattrochi et al., 2018). This mouse line has
738 been backcrossed in wild type background for at least 10 generations. *Cdh3-GFP* mice were three
739 weeks old or younger unless otherwise stated.
740

741 *Gene expression analysis of purified mouse ipRGCs*

742 For our transcriptomics studies, we used two ipRGC reporters available in the lab to
743 identify selective gene expression in ipRGCs compared to RGCs as a whole: 1) BAC transgenic
744 *Opn4-EGFP* Gensat mice from MMRRC (#033064-UCD) and 2) knock-in *Opn4-Cre* mice

(obtained from S. Hattar; Ecker et al., 2010) with Cre-dependent GFP reporter (Z/EG obtained from Jackson labs; (Novak et al., 2000). The *Opn4-GFP* mice were maintained as heterozygotes on *C57/BL6* background while *Opn4*$^{Cre/+}$*;Z/EG* mice were generated by breeding homozygous *Opn4-Cre* mice with heterozygous *Z/EG* mice and maintained on mixed background. Although *Opn4-GFP* reporter labeling in ipRGCs has not been reported previously, a similar BAC transgenic strategy has been demonstrated to label M1-M3 ipRGCs (Schmidt et al., 2008). We tested the correlation of the *Opn4-GFP* reporter expression and endogenous melanopsin in RGCs. We used anti-melanopsin immunoreactivity label M1-M3 ipRGCs (Berson et al., 2010) and anti-EGFP antibodies in a whole-mount retina from an adult *Opn4-EGFP* mouse. Importantly, all *Opn4-GFP*$^{+}$ cells were Opn4-immunopositive (n=60 GFP^{+} cells across seven regions of one retina, Figure 8A). Unexpectedly, more than half of the Opn4-immunopositive M1-M3 ipRGCs were not labeled by the reporter (55%, n=133). Therefore, the coexpression of EGFP expression by the *Opn4-GFP* reporter is strongly correlated with M1-M3 ipRGCs, but only accounts for about half of the population. The other reporter system used in this study, *Opn4*$^{Cre/+}$ *; Z/EG* mice, has been previously demonstrated to label with EGFP all six known morphological types of ipRGCs), named M1–M6 (Ecker et al., 2010; Quattrochi et al., 2018; Stabio et al., 2018). However, Opn4-immunofluorescence studies of four regions across an *Opn4-Cre/GFP* retina revealed that more than one-fourth of M1, displaced M1, and M2 cells lacked discernable GFP-labeling (28%, n=81; 27%, n=15; 33%, n=132, respectively) (Figure 8C). There were many additional GFP^{+} cells that were Opn4-immunonegative, with large soma cells being designated as M4 ipRGCs (54%, n=67 M4 cells). The remaining identified M4 cells had somas with weak, but present, Opn4-immunoreactivity and were only partially accounted for by GFP-labeling (27% Opn4^{+};GFP$^{neg.}$, n=67 M4 cells). Additionally, small soma GFP^{+} cells with absent Opn4-immunoreactivity were designated as M5/6 cells, since the lack of dendritic labeling made it impossible to distinguish between the M5 and M6 types (72%, n=202 M5/6 cells). We observed small cell bodies with weakly Opn4-immunlabeling that did not extend to the dendrites, which were also designated as

771 M5/6 types (28%).

772 Two ages were chosen for retina tissue collection for purification of ipRGC neurons:
773 Postnatal day 5 (+/- 1day) and young adult (P30 +/- 3 days). Three or more biological replicates
774 were used for each dataset (three for postnatal day 4-6 (P4-6) Gensat *Opn4::GFP*, six replicates
775 for Gensat *Opn4::GFP*, four replicates for *Opn4::Cre/GFP* reporter). Each adult replicate required
776 the pooled retinas from 15-20 transgenic mice to acquire suitable numbers of cells for the
777 transcriptomics. These steps are outlined in much more depth and detail in the following sections.

778 The choice of transcriptomics preparation strategies and final readout of processed
779 samples are interrelated and subject to a number of technical concerns vital to the success of
780 transcriptomics analysis. Seven steps in the development and completion of the cell type-specific
781 transcriptomics procedure of cells isolated from early postnatal and adult mouse retinas (Figure
782 1). **First**, dissociation of retinal tissue to a cell suspension; **Second**, purification of RGCs; **Third**,
783 FACS analysis and sorting; **Fourth**, extraction of RNA; **Fifth,** cDNA amplification because the
784 resulting RNA is typically low in abundance; **Sixth**, shear cDNA into sequenceable fragments that
785 are then sequenced with Illumina deep-sequencing; and **Finally**, the raw reads must be analyzed
786 to identify differential expression of genes in ipRGCs.

787

788 *Retina dissociation*

789 The intertwined nature and tight cell–cell adhesions of neural cells make it difficult to
790 separate cells without causing cellular damage and activating stress or cell death pathways.
791 Therefore, vigorous dissociation of tissues can lead to activation of stress or cell death pathways
792 and distort the resulting expression profile. However, poor dissociation can lead to a severe
793 decrease in isolated cells and make downstream expression studies an impossibility. As a first
794 step, we dissected retinal tissue, which we then digested in a protease solution to loosen and
795 disrupt the intertwined neural cells into single cell suspensions for subsequent cell-type isolation.
796 The essential components for proper dissociation included: the proteolytic enzyme papain L-

797 cysteine to promote enzymatic activity, DNase for destroying the extremely sticky free DNA
798 strands released by damaged cells, and an absence of calcium from solutions to promote
799 disruption of cell-cell adhesions (Barres et al., 1988). We further optimized cell viability and
800 recovery by replacing dPBS with HibernateA and including B27 throughout the cell-isolation
801 procedure (Brewer et al., 1993; Brewer, 1997; Brewer and Torricelli, 2007). The use of survival-
802 promoting media such as Hibernate-A and supplements such as B27 was particularly relevant for
803 adult neural dissociation since adult neurons have been demonstrated to be especially prone to
804 cell death (Eide et al., 2005; Brewer and Torricelli, 2007). We incubated the dissected retinas in
805 pre-activated protease solution and completed the cell dissociation by triturating the cells with a
806 1mL pipette tip.
807
808 *RGC Pre-Enrichment*
809 Pre-enrichment of ganglion cells prior to isolation of ipRGCs is necessary due to their
810 extraordinary rarity in the retina. Ganglion cells only make up 1% of mouse retinal cells and only
811 1-5% of ganglion cells are ipRGCs (0.01-0.05% of retina cells) (Hattar et al., 2002; Ecker et al.,
812 2010; Berson et al., 2010). In contrast, the classic photoreceptors rods and cones account for 75-
813 80% of all mouse retinal cells (Jeon et al., 1998). Therefore, we pre-enriched for ganglion cells
814 prior to positively selecting fluorescently labeled ipRGCs using fluorescence activated cell sorting.
815 We incorporated an immunopanning system that has proven effective at isolating a homogeneous
816 population of RGCs (Barres et al., 1988; Cahoy et al., 2008). Immunopanning takes advantage
817 of the cell surface protein Thy1 which is shared among retinal ganglion cells (Barres et al., 1988).
818 The classic immunopanning process uses antibodies raised against Thy1 to select the RGCs
819 from the heterogeneous retinal cell suspension. We improved upon viability and reproducibility of
820 the immunopanning procedure by adapting it to use a magnetic-activated cell sorting procedure
821 (MACS, Miltenyi Biotec), eliminating the need for using harsh lysis treatment (data not shown).
822 We incubated the dissociated retinal cell solution with Thy1.2-conjugated magnetic nanoparticles

which are retained in a magnetized column and the isolated RGCs can then be acquired (Haeryfar and Hoskin, 2004). In preparation for FACS, the DNA intercalating dye, 7-AAD, was added to the solution to discriminate dying cells that consequently had compromised cell membranes.

Fluoresence-Activated Cell Sorting (FACS)

We used a FACS Aria (BD Biosciences) electrostatic sorter to isolate a homogeneous GFP-labeled cell population from the dissociated RGC-enriched cell suspension of the transgenic melanopsin reporter mice (Figure 1). FACS has been successfully used previously to profile gene expression in cell subtypes of the nervous system (Lobo et al., 2006; Cahoy et al., 2008; Siegert et al., 2012). Live cell gating was achieved by excluding 7-AAD labeled cells (high fluorescence signal in far red emission) (Figure 9). Fluorescently labeled ipRGCs were positively selected from the solution of enriched ganglion cells by their relatively high level of GFP fluorescence (FITC gating). In parallel, cells with relatively low GFP-fluorescence (low FITC) were also isolated and designated as a “generic RGC” control population for direct comparison with correlated ipRGC samples. The parallel isolation of generic RGCs was designed as an internal negative control for comparison with isolated ipRGCs. Accordingly, the generic RGC populations were treated with the same reagents, cytometer settings, centrifugation forces, and temperatures throughout the procedure. This is especially important for isolating adult RGC populations, since they are particularly susceptible to the stresses of FACS sorting(Lobo et al., 2006; Cahoy et al., 2008; Heiman et al., 2008). The large amount of small cellular debris generated during the dissociation process made it a challenge to keep the number of collected generic RGCs consistent with the rare ipRGCs (Figure 9). Cellular debris registers as being essentially non-fluorescent, is smaller and less complex than the generic RGC population that is of the same relative size and complexity as the isolated GFP-positive cells. Therefore, we limited cell debris by acquiring the ipRGC (GFP+) and generic RGC (GFP-negative) populations with the same relative cell complexity

(indicator of cell health) and cell size selection to exclude the relatively small cellular debris or doublets.

RNA Extraction

The small volumes allowed by the electrostatic FACSAria sorter allowed us to lyse sorted cells directly into Qiagen RLT buffer and directly proceed to RNA extraction using Minelute columns (Qiagen). The enriched RNA was treated on-column with DNase to remove any residual genomic DNA from the sample. RNA-processing was done in an enclosed RNase-free environment to limit degradation of RNA throughout the extraction process. Additionally, RNA integrity was analyzed using the Agilent 2100 Bioanalyzer and the PicoChip, which is able to qualitatively test the low RNA recovery samples (Figure 10A). Initially, we proceeded immediately with cDNA processing after RNA extraction. However, freezing at -80 degrees did not seem to effect RNA integrity since the frozen RNA samples still received RIN score of 9.0 or greater (Figure 10A). Therefore, most of the cDNA libraries were prepared after storage of extracted RNA at -80 degrees Celsius.

cDNA Preparation

RNA-seq transcriptome analysis requires large amounts of RNA material using TruSeq, ranging on the order of 100-1000ng of total RNA. However, our improved method for isolating ipRGCs was able to isolate 12,000 GFP+ ipRGCs from nine postnatal day 5 (P5) transgenic reporter mice. This was only expected to provide about 12ng of extracted total RNA by qualitative estimates considering that a single cell holds 5-10pg of total RNA. Further, twice as many adult mice of the same genotype were required to provide only 1,000 cells due the the relative fragility of adult retinal ganglion cells described above. Therefore, we decided that some form of amplification was necessary to study the molecular programs used by adult ipRGCs. The Nugen Ovation RNA amplification system was successfully used in microarray studies with as little as

500pg of total RNA input (Caretti et al., 2008; Clément-Ziza et al., 2009; Morse et al., 2010) (Figure 10B). Sequencing analysis using the Ovation system has previously been reported to generate cDNA containing negligible rRNA reads (<4%), while providing a representative transcriptome with sufficient biological replicates(Tariq et al., 2011).

RNA-seq library preparation

We determined that the Truseq system was the necessary platform for my cDNA samples to produce the 10nM sequencing library concentration required at the on-site Genomics Core facility in preparation for 50bp single-end Illumina sequencing. Before preparing the library, we first sheared cDNA to the appropriate size, (200-300bp median) using the Covaris system (Figure 10C). Each sample was subsequently processed using a unique barcode adapter to allow for multiplexing multiple samples on the HiSeq (commonly 200million 50bp reads divided among sequencing samples). Excess adapter sequences was removed using Ampure bead isolation, which removes all DNA fragments less than 200bp. Finally, the Genomics Core completed the final quality control of the DNA library prior to sequencing: testing the library fragment size distribution (High Sensitivity Bioanalyzer) and qPCR analysis using primers that match the library adapters (Quail et al., 2008) (Figure 10D).

Initially, we processed a large number of samples at once with multiplexed sequencing using HiSeq (8 samples per lane) to minimize high costs of sequencing at the expense of sequencing depth. We later reran many of the sequencing libraries with less multiplexing, enabling increased sequencing depth. The corresponding technical replicates were merged together for differential expression analysis (Figure 10E). The final read counts of each sample is shown in Figure 10F.

Differential gene and transcript expression analysis

The completion of sequencing generated tens of millions of reads that are used to

compare gene expression levels between isolated ipRGCs (GFP+) and generic RGCs (GFP-). Well-established, powerful RNA-seq differential expression analysis pipelines have been developed such as Cuffdiff, EdgeR, and DESeq (Anders and Huber, 2010; Trapnell et al., 2012; Anders et al., 2013). The Cuffdiff pipeline prioritizes isoform quantification and diversity (Trapnell et al., 2012). However, the short 50bp single-end reads that are generated in our study are not well-suited for prioritizing isoform discovery and analysis. Further, Cuffdiff does not fully take advantage of our purposeful pairwise-comparison between groups. In contrast, the EdgeR package is better suited for our purpose; it is designed to count the number of reads that align to an annotated gene (mouse reference genome, in our case) and subsequently performs statistical analysis on a generated table of counts to identify quantitative changes in expression levels between the two experimental samples. EdgeR compares and retains the relationship between all pairs of experimental samples when calculating differential expression likelihood (Anders et al., 2013). Our analysis filtered out genes with very low counts, less than 1 count per million (cpm), in more than half of the samples used in the differential expression analysis. This is a common cutoff and considers 1) that a gene must be expressed at a minimum threshold in order to become biologically important and 2) that the inclusion of genes with very low counts may negatively affect the statistical approximations used by the EdgeR pipeline.

To identify the set of differentially expressed genes in the ipRGC populations, we used the following strict criteria. First, we identified genes with low false discovery rate (FDR < 0.05) and high fold-change (greater than 2-fold) suggesting differential expression between ipRGCs and generic RGCs. Second, we considered whether the differentially gene expression was corroborated across both reporters (*Opn4::GFP* labeling M1-M3 cells and the *Opn4::Cre/GFP* system that labels M1-M6 ipRGCs) and both ages (P5 and adult). Third, we identified whether the differentially expressed genes have nearly absent gene expression in generic RGC samples to distinguish potential for selective gene expression in ipRGCs. This was distinguished both at the level of count-values and manual inspection of aligned raw reads using the Integrated

Genome Viewer (IGV) (Thorvaldsdóttir and Robinson, 2013). Using IGV, we verified that the reads align with reference gene model for full-length coverage across multiple ipRGC replicates and that there were absent or partial reads aligned across the generic RGC replicates.

Determining differentially *repressed* genes in adult ipRGCs was confounded by the high amount of contaminants in generic RGC populations. We could not decipher whether a gene with relatively low expression in ipRGCs was the result of non-RGC populations contaminating the generic RGC control population. In contrast, the P5 generic RGC samples from the *Opn4-GFP* reporter were determined to have greatly reduced levels of contamination and similar levels of RGC marker expression (Figure 1—figure supplement 1). This made it possible to identify genes more weakly expressed in ipRGCs than in generic RGCs in early postnatal development (Figure 2—figure supplement 1).

Count-based differential expression pipeline for RNA-seq data using edgeR and/or DESeq.

```
# 1) Assess sequence quality control with FastQC)
# 2) remove adapters
$ fastx_clipper -Q33 -a adapter_sequence -l 15 -v -i DJB0005.fastq -o ad_DJB0005.fastq

# 3) remove low quality reads
$ fastq_quality_filter -v -Q33 -q 30 -p 90 -i ad_DJB0005.fastq -o adq_DJB0005.fastq

#####################################################################

#  Align the reads (using tophat2) to the reference genome
$  tophat2 --no-coverage-search -o DJB05_th2out genome DJB05_merged.fastq

#####################################################################

#  Sort by name, convert to SAM for htseq-count
$ samtools sort -n DJB05_th2out/accepted_hits.bam -o DJB05_sortname.bam
$ samtools view -o DJB05_sortname.sam DJB05_sortname.bam

#####################################################################

# COUNT READS USING HTSEQ-COUNT
$ htseq-count -s no -a 10 DJB05_sortname.sam genes.gtf > DJB05.count

#####################################################################
```

```
# Count-based differential analysis with edgeR
$ module load R
$ cd ~/data/2016_rerun_myrnaseq/
$ Rscript edgeR_filter1cpm_updated.R GSad_2016.filelist

#####################################################################

#Below is script within “edgeR_filter1cpm_updated.R”
#!/usr/bin/Rscript
#structure of file:1 col of batch names, 2 columns of sample names, with label at top of each
column, tab separated
#label1label2
#b1     samp1 samp4
#b2     samp2 samp5
#b3     samp3 samp6
#samples in same row are assumed to be in same batch
args <- commandArgs(TRUE)
filename=args[1]
bampath="~/data/2016_rerun_myrnaseq"
annotation="~/data/2016_rerun_myrnaseq/genes.gtf"
baseoutdir="~/data/2016_rerun_myrnaseq/"

library(edgeR)

x=read.table(filename,header=T)
label1=colnames(x[1])
label2=colnames(x[2])
samplelist=c(as.vector(x[,1]),as.vector(x[,2]))
conditions=c(rep(label1,nrow(x)),rep(label2,nrow(x)))
batch=rep(row.names(x),2)
names(conditions)=samplelist

#convert condition and batch to factors--prob not necessary for DESeq but edgeR likes it
condition=factor(conditions)
batch=factor(batch)

#set up output directory for this experiment, create if it doesn't exist
outdir=sprintf("%s/%s-%s",baseoutdir,label1,label2)
dir.create(outdir)

#read in count table
count.table=read.table(sprintf("%s/%s-%s-rawcounts.txt",outdir,label1,label2),header=T)

# filtering--keep only reads with > 1cpm in at least half the samples
keep_cpm <- rowSums(cpm(count.table)>1) >=nrow(x)
keep_quantile <- rowSums(count.table)>quantile(rowSums(count.table), probs=.5)

#save output of cpm vs quantile filters to log file
sink(sprintf("%s/edgeR.log",outdir),append=T,split=T)
cat("Comparison table of cpm vs quantile filters. CPM>2 in half of samples, quantile at 50%.\n")
addmargins(table(keep_cpm, keep_quantile))
```

```
sink()
count.table <- count.table[keep_cpm, ]

edesign=model.matrix(~batch+condition)
e <- DGEList(counts=count.table)
e <- calcNormFactors(e)
e <- estimateGLMCommonDisp(e, edesign)
e <- estimateGLMTrendedDisp(e, edesign)
e <- estimateGLMTagwiseDisp(e, edesign)

#print size factors to log file
sink(sprintf("%s/edgeR.log",outdir),append=T,split=T)
cat("Normalization factors:\n")
e$samples
sink()
#print dispersion and PCA plots to pdf
pdf(sprintf("%s/%s-%s-edgeRdispersion.pdf",outdir,label1,label2))
plotBCV(e, cex=0.4, main="edgeR: Biological coefficient of variation (BCV) vs abundance")
dev.off()
pdf(sprintf("%s/%s-%s-edgeRPCA.pdf",outdir,label1,label2))
plotMDS(e, main="edgeR MDS Plot")
dev.off()

#Fit curves to GLM
efit <- glmFit(e, edesign)
efit <- glmLRT(efit, coef=sprintf("condition%s",label1))
#make results table and save
stats <- topTags(efit, n=nrow(e))$table
cpms <- cpm(e,)[rownames(stats),normalized.lib.sizes=T]
etable=data.frame(stats,cpms)
etable <- etable[order(etable$FDR), ]
write.table(etable,file=sprintf("%s/%s-%s-edgeR-
filtered.txt",outdir,label1,label2),quote=F,sep="\t")
#copy sample file (argument) to outdir
file.copy(filename,sprintf("%s/%s-%s-samplelist",outdir,label1,label2))

#####################################################################

#Below is script within “GSad_2016.filelist”
GSadPos       GSadNeg
b1      DJB07 DJB08
b2      DJB30 DJB31
b3      DJB28 DJB29
b4      DJB16 DJB21
b5      DJB36 DJB37
b6      DJB38 DJB39

#####################################################################
```

Antibodies for i*mmunohistochemistry:*

For these studies, the following primary antibodies were used: rabbit anti-melanopsin (Advanced Targeting Systems; 1:10,000), guinea pig anti-RBPMS (PhosphoSolutions 1832-RBPMS), rabbit anti-green fluorescent protein (GFP; Invitrogen); Goat anti-Brn3b antibody (Santa Cruz #sc-6026); mouse anti-Rasgrp1 (Santa Cruz sc-8430); guinea pig anti-Tbx20[1:8500] (Song et al., 2006)Rabbit anti-Giantin (Abcam ab24586). Secondary antibodies consisted of Alexa Fluor 350, 488, 594 or 647 donkey anti-goat, Alexa Fluor 594 donkey anti-rabbit and Alexa Fluor 594 goat anti-guinea pig.

Retina Tissue Preparations and Solutions

Mice were euthanized by inhalation of CO2. Prior to removing the eye, the dorsal margin of the cornea was marked with a cautery and this was used to guide the placement of a large relieving cut in the dorsal retina as a subsequent guide to retinal orientation. Eyes were removed immediately after death and placed in Hibernate-A solution preheated to 37 °C. To keep track of retinal orientation, the right and left eye were identified and processed separately.

Immunohistochemistry

After the retina was removed from the eye, it was placed on Millipore nitrocellulose paper. The retinas were fixed for 30 minutes at room temperature using 4% paraformaldehyde freshly prepared in 0.1M phosphate buffered saline (PBS; pH 7.4). The tissue was then washed for 15 minutes in PBS three times. The tissue was then incubated in a blocking solution of 0.5% Triton-X and 5% Goat Serum in PBS for two hours at room temperature. The tissue was incubated for two nights at 4 °C while on a shaker in the primary antibodies diluted in this same blocking solution. The following day, the samples were washed six times for 20 minutes in 0.1% Tween-20 in PBS. The tissue was then incubated for two hours in the appropriate Invitrogen or Jackson labs secondary antibodies diluted 1:1000 in the blocking solution at room temperature. The tissue

was then washed six times for 10 minutes in 0.1% Tween-20 in PBS. The retinas were then mounted in Aquamount, coverslipped, and sealed with fingernail polish.

For Rasgrp1 immunofluorescence studies, an additional antigen retrieval step was included. antigen retrieval the tissue was then placed in Tris-EDTA (pH 8.0) for 30 minutes at 80 °C. The samples were then allowed to return to room temperatures (about 15-30 minutes) before they were removed from the Tris-EDTA solution and washed three times for 15 minutes in PBS.

Image Acquisition

Immunofluorescent images were captured on a Zeiss Confocal (LSM 510) and Nikon Eclipse microscope (Micro Video Instruments, Inc. E614, Avon, MA) with a built in Spot Camera (Diagnostic Instruments, Inc. HRD 100-NIK Sterling Heights, MI). Confocal images were taken with a 20x objective (Plan Apochromat, WD 0.55 mm) at a resolution of 2048 pixels. To enhance clarity, image files were pseudocolored and the brightness and contrast was adjusted using ImageJ 1.47 (National Insistute of Heath, Bethesda, MD). All final images were constructed using ImageJ and Powerpoint (Microsoft Corporation, Redmond, WA).

Analysis of Rasgrp1 expression in ipRGC subtypes.

Because M1 and M2 cells have the highest levels of melanopsin expression of the ipRGC population, their dendrites were clearly visible and decipherable with immunostaining. M1 cells were identified by their dendritic projections to the OFF layer of the inner plexiform layer (IPL). M2 cells were identified by their dendrites which monostratify the ON sublamina of the IPL (Berson et al. 2010; Schmidt and Kofuji 2009). M3 cells bistratify the ON and OFF sublamina of the IPL (Schmidt and Kofuji 2011) and because these cells have similar levels of melanopsin expression and soma size as M2 cells, it is likely that M3 cells were included in the M2 population quantified in this study.

M4-M6 cells have the lowest levels of melanopsin-expression of the ipRGC population and their dendrites were not visible or decipherable with immunostaining. However, at least some members of the M4/M5/M6 population had lightly immunoreactive somas (Ecker et al., 2010; Quattrochi et al., 2018; Stabio et al., 2018). M4 cells were identified by their large soma size, low melanopsin immunodetectability and the lack of dendritic labeling (Estevez et al., 2012). The M5 and M6 cells we observed were identified by their low levels of melanopsin labeling and M2-sized somas (Ecker et al., 2010; Quattrochi et al., 2018; Stabio et al., 2018).

Analysis of Tbx20 expression in Cdh3-GFP mice.

ipRGC subtypes were identified using a combination of morphological clues and process of elimination. In the case of M1 and M2 cells, which express the highest levels of melanopsin, confocal images of their immunofluorescence reveal dendritic information. As a result, unique dendritic features distinguish M1 and M2 cells. Cells with dendrites stratifying in the OFF layer of the IPL were identified as M1 cells, whereas cells stratifying in the ON layer were identified as M2 cells (Berson et al. 2010; Schmidt and Kofuji 2009). Using this method, M3 cells, which stratify in the ON and OFF sublamina of the IPL, were included in the M1 cell population unless otherwise noted (Schmidt and Kofuji 2011). As a result of their low levels of melanopsin, M4 and M5/6 cells are weakly labeled using anti-melanopsin immunohistochemistry with only some of their somata, but no dendrites, visible (Ecker et al., 2010; Estevez et al., 2012; Quattrochi et al., 2018; Stabio et al., 2018). Therefore, the method employed for deciphering M1 and M2 cells cannot be used to identify M4 and M5/6 cells. Instead, M4 cells were categorized by their lack of dendritic labeling, and their large soma size (Estevez et al., 2012). M5/6 cells were characterized by their lack of dendritic labeling, M2-sized somata, and process of elimination (Ecker et al., 2010; Estevez et al., 2012; Quattrochi et al., 2018; Stabio et al., 2018). In other words, cells that were not stained by the melanopsin antibody (which would detect M1-M3), but were labeled by GFP (labeling M1-M6), and had small somata, fell into the M5/6 category.

Brain injection of retrobeads into suprachiasmatic nucleus

Adult wild type mice (P30-P60) were anaesthetized with isofluorance and fluorescently labelled rhodamine latex microspheres (RetroBeads, Lumafluor) were injected into the ipsilateral suprachiasmatic nucleus to retrogradely label RGCs with axon terminals at the injections site. Three to five days later, the brain was removed and immediately fixed overnight. The following day, the brain was rinsed in 0.1M PBS and sectioned at 50um in the coronal plane. The slices were incubated with DAPI staining for 10 minutes was done in order to provide a reference for SCN location as indicated by concentrated cellular staining at the SCN. The slices were imaged for DAPI in UV channel and overlayed with rhodamine channel to identify the injection site in relation to SCN location. Special attention was paid to ensure that the injection did not extend into optic nerve and confound results by introducing off-target RGC labeling of fibers of passage.

Brain histology

Animals were sacrificed via transcardial perfusion, and brains were removed and incubated in 4% paraformaldehyde overnight. Brains were sectioned at 50µm in the coronal plane. To reveal individual processes in viral tracing experiments, virallyexpressed EYFP was enhanced using rabbit-anti-gfp (1:1000) and goat-anti-rabbit alexa 488 (1:500). To observe parvalbumin expression in OPN neurons, parvalbumin immunohistochemistry was performed using mouse-anti-parvalbumin (1:1000) followed by goat-anti-mouse alexa 488.

Stained and sliced brain slices were mounted on glass cover slides and imaged using a SPOT RT Slider digital microscope camera mounted to a Nikon (Diagnostic Instruments) as described previously (Berson et al., 2010; Estevez et al., 2012). Images were assembled in Adobe Photoshop CS3.

Figure legends (see attached PDF for figure images)

Figure 1. Experimental design of gene expression profiling from purified ipRGCs and comparison with generic RGCs.

A. Two transgenic reporters were used for gene expression profiling of ipRGCs. The BAC transgenic Opn4-GFP labels M1-M3 ipRGCs while the Opn4-Cre crossed with a cre-dependent GFP reporter labels M1-M6 ipRGCs. B. Schematic of the gene expression profiling procedure. 1) Isolation of cell populations from enzymatically dissociated retinas. 2) The surface protein Thy-1 is enriched in RGCs, this high affinity of Thy1-conjugated magnetic beads to RGCs was used to enrich the extracted cell populations with RGCs. 3) Fluorescence-activated cell sorting (FACS) was used to isolate GFP-positive cells (ipRGCs) from GFP-negative cells (cRGCs). These two populations were isolated in parallel to provide direct internal testing of ipRGCs versus cRGCs under the same treatments, conditions, and genetic backgrounds. 4) The RNA of these two main populations was subjected to mRNA extraction. 5) The RNA was converted to cDNA and amplified using Nugen Ovation RNA amplification system. 6) Illumina Truseq sequencing libraries were prepared by ligating adapters to the cDNA. Single-end 50 base pair sequencing was completed using the Illumina HiSeq system. 7) Differentially expressed genes were determined using EdgeR bioinformatics pipeline. See Methods for details.

B. EdgeR multi-dimensional scaling (MDS) plot illustrates the overall similarity between expression profiles of different samples. Each sample is denoted by a letter (“i” for ipRGCs; c for cRGCs) and a number, corresponding to particular replicate, comprising one pool of purified RGCs then divided into the two pools. Numbering scheme represents paired ipRGCs (GFP+) and

cRGCs (GFP-) replicates (i.e., ipRGC sample 'i1' was processed in parallel with cRGC sample 'c1', sample 'i2' with 'c2', etc.). Distances are approximately the log2 fold changes between samples. Green and gray ovals represent ipRGC (GFP+) and cRGC (GFP-) samples, respectively. Adapted from EdgeR simple graphical output of individual samples in 2D space.

Figure 1—figure supplement 1. Purity and cell composition assessment of ipRGC and generic RGC samples.

Heat map of known cell type marker gene expression in the retina to assess purity and cell composition of ipRGC and generic RGC samples. Shown are biological replicates tested for *Opn4-GFP* (P5 and adult) and *Opn4-Cre/GFP* reporters. Relative expression levels, fold change, and false discovery rate (FDR) are color-coded as indicated in the figure. White boxes indicate high gene expression, while blue represents little or no detected expression. FDR is not available ("NA") in cases that our analysis filtered out genes with very low counts, less than 1 count per million (cpm), in more than half of the samples used in the differential expression analysis.

Figure 2. The expression pattern of candidate ipRGC-specific genes.

Heat map of 83 genes differentially expressed in ipRGCs that have functional links to GPCR signaling, regulation and maintenance of molecular programs, neuron communication and organization, neuron survival, and neuron-glia interactions. Relative expression levels, fold change, and FDR are color-coded as indicated in the figure.

Figure 2—figure supplement 1.

Heat map of genes differentially expressed in adult ipRGCs labeled by the *Opn4-Cre/GFP* reporter (M1-M6 ipRGCs) compared to *Opn4-GFP* (M1-M3 ipRGCs). Relative expression levels, fold change, and FDR are color-coded as indicated in the figure.

Figure 2—figure supplement 2.

Heat map of genes encoding for nicotinic acetylcholine, dopamine, serotonin, glycine, glutamate, and melatonin receptors. Relative expression levels, fold change, and FDR are color-coded as indicated in the figure.

Figure 2—figure supplement 3. The expression pattern of developmentally regulated genes in ipRGCs.

A. Heat map of genes encoding transcription factors that have a particular temporal pattern of differential expression in ipRGCs (e.g., high gene expression in P5 ipRGCs relative to adult expression). Relative expression levels, fold change, and FDR are color-coded as indicated in the figure.

B. Heat map of genes relevant for development of ipRGCs. Relative expression levels, fold change, and FDR are color-coded as indicated in the figure.

Figure 2—figure supplement 4.

A. Distinct from rod and cone photoreceptors, the light-activation of Opn4 triggers a membrane-bound signaling cascade including $G_{q/11}$ type G-proteins, the generation of 1,2-diacylglycerol (DAG) by PLCβ4, the opening of downstream TRPC6 and TRPC7 channels, and ultimately leads to the influx of calcium through L-type voltage-gated calcium channels.

B. Heat map of genes that are potentially relevant to the Opn4-mediated phototransduction signaling cascade. Relative expression levels, fold change, and FDR are color-coded as indicated in the figure.

C. Heat map of genes previously described to play a role in the light response, dark adaptation, and chromophore regeneration of rod and cone photoreceptors. Relative expression levels, fold change, and FDR are color-coded as indicated in the figure.

Figure 3. Rasgrp1 is selectively expressed in ipRGCs.

A. Whole mount retina immunostained for Opn4, Rasgrp1, and the pan-RGC marker Rbpms (gray-scale). Focal plane is at the ganglion cell layer (GCL). We quantified co-localization of the three markers in confocal images of 49 regions that were topographically dispersed across three whole-mount adult retinas.

B. Co-localization of Rasgrp1 (green), Rbpms (red), and Opn4 (magenta). Rasgrp1 is expressed in a subpopulation of amacrine cells and RGCs (Rbpms-negative and -positive, respectively). Scale bar, 20 μm.

C. Rasgrp1 immunolabeling (antibody sc-8430) of cell bodies in GCL of Rasgrp1$^{+/-}$ heterozygous mice (left, yellow arrows). Absence of cell body immunolabeling in Rasgrp1$^{-/-}$ knockout mice (right) suggests a lack of cellular off-target antibody staining.

D. Quantification of Rasgrp1-expression across Opn4-immunopositive ipRGC subtypes. 70% of M1 cells were Rasgrp1 immunopositive while only 20-30% of either M2, M5 or M6 cells were Rasgrp1 immunopositive. None of the identified M4 cells were Rasgrp1 immunopositive. M1 and M3 types were combined during the process of co-expression analysis (designated “M1/M3”). Error bars represent standard error of the mean.

Figure 3—figure supplement 1.

A. Distribution of all Rasgrp1-expressing RGCs (Rasgrp1^{+};Rbpms^{+}) that belong to specific RGC types, to the extent that could be determined, including Opn4-immunoreactive ipRGC subtypes. No examples of M4 cells were observed to express Rasgrp1. The vast majority (96%) of Rasgrp1-RGCs are Opn4-immunopositive and therefore ipRGCs. The remaining “unknown” RGC types expressing Rasgrp1 (Rasgrp1^{+} ; Rbpms^{+} ; Opn4$^{neg.}$) could be a low-expressing ipRGC type or conventional RGCs. Error bars represent standard error of the mean.

B. Areas sampled for two wholemount wild type retinas immunostained for Rasgrp1, Opn4 and RBPMS. Yellow squares represent the locations of confocal images used for cell quantification.

C. Analysis of the M1-M3 ipRGC population did not suggest a gradient of ipRGC spatial distribution across the retina. Seven frames were used to represent each area of the retina to maintain equal spatial contribution. Total M1-M3 represented in the dorsal-ventral and nasal-temporal columns is 217.

E. Analysis of the M1 cell population revealed a slight naso-temporal gradient of M1 spatial distribution across the retina. Seven frames were used to represent each area of the retina to maintain equal spatial contribution. Total M1s represented in the dorsal-ventral column and nasal-temporal columns is 113 and 110, respectively.

F. Analysis of the Rasgrp1-positive RGC population suggests a slight ventral-dorsal gradient of Rasgrp1-positive RGCs spatial distribution across the retina. Seven frames were used to represent each area of the retina to maintain equal spatial contribution. Total Rasgrp1-positive RGCs represented in the dorsal-ventral column and nasal-temporal column is 117 and 118, respectively.

F. The amacrine cells (presumed) expressing Rasgrp1 exhibited a dramatic center-peripheral gradient of Rasgrp1-positive non-RGC spatial distribution across the retina. Four frames were used to represent each area of the retina to maintain equal spatial contribution. The total Rasgrp1-positive non-RGCs represented in the periphery and center was 314.

Figure 4. Colocalization study of Tbx20-expression in ipRGC subtypes.

A. Triple immunofluorescence of Opn4, Tbx20, and *Cdh3-GFP* (gray scale).

B. Tbx20-expression in subset of M1-M3 ipRGCs as well as an additional population of Opn4-immunonegative cells.

B,C. Tbx20 is concentrated in the nucleus of most *Cdh3-GFP*-cells.

D. Quantification of Tbx20-expression across Opn4-immunopositive ipRGC subtypes. Tbx20 immunofluorescence labels multiple ipRGC subtypes, including M1s, M2 cells and small soma, low Opn4 expression cells (presumptive M5/6 ipRGCs), and Cdh3-GFP cells (M6-type enriched).

M2 and M3 types were combined during the process of co-expression analysis (designated "M2/M3"). Error bars represent standard error of the mean.

Figure 4—figure supplement 1. Coexpression study of Tbx20 with Opn4-Cre/GFP and Tbr2, including distribution of Tbx20-expression across ipRGC subtypes.

A-C. Quadruple immunofluorescence of Opn4, Tbx20, Opn4-Cre/GFP, and Tbr2. Scale bar, 20 μm.

A. Gray scale of Opn4, Opn4-Cre/GFP, and Tbx20 immunofluorescence.

B. Co-expression study of Tbx20 (green) in the context of Opn4 (magenta) and *Opn4-Cre/GFP* (red) labeling. GFP cells that are Opn4-immunonegative are inferred M4-M6 types.

C. Co-expression analysis of Tbr2 (magenta) with Tbx20 (green).

D. Distribution of Tbx20 expressing cells that belong to specific RGC types, to the extent that could be determined, including Opn4-immunoreactive ipRGC subtypes and RGCs labeled by the *Cdh3-GFP* transgenic reporter. Unaccounted Tbx20-expressing cells are designated as "unknown" RGC types. Error bars represent standard error of the mean.

Figure 5. Complex pattern of Rasgrp1-Tbx20-Brn3b co-expression suggests further diversity in ipRGC family.

A. Quadruple immunofluorescence study of Tbx20, Brn3b, Opn4, and Rasgrp1 (gray-scale).

B. Rasgrp1 and Opn4 (left panel) were initially quantified for ipRGC subtype expression prior to comparison with Tbx20 (middle panel) and Brn3b (right panel) expression. Rasgrp1, Brn3b, and Tbx20 expression are partially overlapping.

C. Integrated co-expression patterns of Brn3b, Rasgrp1, and Tbx20 with M1 and M2 ipRGC subtypes. The M1 group includes displaced M1 and M3 types.

Figure 5—figure supplement 1. Topographic distribution and ipRGC subtype-specific quantification of Rasgrp1-Tbx20-Brn3b expression.

A. Comparison of co-expression patterns of Brn3b, Rasgrp1, and Tbx20 within group of combined M1-M3 (M1+M2+M3) ipRGCs, the M1/3 ipRGCs (M1+M3), displaced M1s, and M2 ipRGCs.

B. Lack of major topographic variations in the fraction of M1/M3 ipRGCs immunoreactive for Rasgrp1, Tbx20, and Brn3b.

C. Comparison of Rasgrp1-Tbx20-Brn3b expression pattern in M2 ipRGCs across dorsal, center, and ventral regions of the retina.

D. Distribution of Tbx20-expression in M1-M3 ipRGCs compared to Opn4-immunonegative cells in the context of topgraphic regions across the retina.

Figure 6. The ipRGCs projecting to the suprachiasmatic nucleus (SCN) have a molecularly diverse pattern of Rasgrp1 and Tbx20 expression.

A. Experimental design of fluorescent bead injection to SCN, followed by examination of Rasgrp1 and Tbx20 expression in retrograde labeled RGCs.

B. Neuroannatomical study to verify that retrograde injection is within the SCN, but not the optic nerve.

B. Triple immunofluorescence of Opn4, Rasgrp1, and Tbx20 in combination with fluorescent Retrobeads. Retrobeads were mostly observed in Opn4-immunopositive RGCs (M1-M3 ipRGCs). Quantification of Rasgrp1 and Tbx20 in retrolabeled cells.

D. SCN-projecting ipRGCs in the ipsilateral and contralateral retina are molecularly diverse for Tbx20 and Rasgrp1 expression.

Figure 7. Current model of ipRGC family members integrating molecular, physiology, brain circuitry, and morphology (see text for details).

Figure 8. Coexpression of BAC transgenic Opn4-GFP reporter with Opn4 immunoreactivity.

A. Immunofluorescence of anti-Opn4 staining of whole mount retina from transgenic *Opn4-GFP* mice with fluorescent protein expression in ipRGCs. Red, Opn4-immunolabeling; green, fluorescently labeled cells; yellow, merged co-localized labeling pattern. Scale bar, 20 µm.

B. Co-expression of *Opn4-Cre/GFP* labeling with immunofluorescence of anti-Opn4 staining of whole mount retina. Red, Opn4-immunolabeling; green, fluorescently labeled cells; yellow, merged co-localized labeling pattern. Scale bar, 20 µm.

C. Quantification of labeling efficiency of Opn4-immunolabeled M1-M3 ipRGCs by *Opn4-Cre/GFP*. Additional comparison of GFP-labeling in low Opn4-expressing ipRGC subtypes M4 (large soma) and M5/6 (small soma).

Figure 9. Fluorescence activated cell sorting (FACS) gating strategy for isolating ipRGCs (GFP+) in parallel with GFP-negative cells that are enriched for RGCs.

A-C. Healthy cells were selected against death marker 7-AAD (not G1). The ipRGCs (GFP^+) and generic RGCs (GFP^-) cells were selected based on intensity and similar relative cell size ultimately using gates G2A and G3A, respectively.

A. Example sort from retina of postnatal day 4 (P4) *Opn4-GFP* mouse.

C. Example sort from retina of young adult *Opn4-GFP* mouse, with noticeably higher debri and cell death.

D. Microscopy testing of accurate sorting of GFP+ cells isolated from P4 *Opn4-Cre/GFP* mouse.

Figure 10. Steps involved with processing mRNA extracted from purified cell populations and preparing for RNA-sequencing (see Methods for details).

References

1377 Anders S, Huber W (2010) Differential expression analysis for sequence count data. Genome
1378 Biology 2010 11:10 11:R106.

1379 Anders S, McCarthy DJ, Chen Y, Okoniewski M, Smyth GK, Huber W, Robinson MD (2013)
1380 Count-based differential expression analysis of RNA sequencing data using R and
1381 Bioconductor. Nature Protocols 8:1765–1786.

1382 Atlasz T, Szabadfi K, Kiss P, Racz B, Gallyas F, Tamas A, Gaal V, Marton Z, Gabriel R, Reglodi
1383 D (2010) Pituitary adenylate cyclase activating polypeptide in the retina: focus on the
1384 retinoprotective effects. Ann N Y Acad Sci 1200:128–139.

1385 Barres BA, Silverstein BE, Corey DP, Chun LLY (1988) Immunological, morphological, and
1386 electrophysiological variation among retinal ganglion cells purified by panning. Neuron
1387 1:791–803.

1388 Bedont JL, Blackshaw S (2015) Constructing the suprachiasmatic nucleus: a watchmaker's
1389 perspective on the central clockworks. Front Syst Neurosci 9:74.

1390 Beglopoulos V, Montag-Sallaz M, Rohlmann A, Piechotta K, Ahmad M, Montag D, Missler M
1391 (2005) Neurexophilin 3 is highly localized in cortical and cerebellar regions and is
1392 functionally important for sensorimotor gating and motor coordination. Mol Cell Biol
1393 25:7278–7288.

1394 Berson DM, Castrucci AM, Provencio I (2010) Morphology and mosaics of melanopsin-
1395 expressing retinal ganglion cell types in mice. Journal of Comparative Neurology 518:2405–
1396 2422.

1397 Bivona TG, Pérez De Castro I, Ahearn IM, Grana TM, Chiu VK, Lockyer PJ, Cullen PJ, Pellicer
1398 A, Cox AD, Philips MR (2003) Phospholipase Cgamma activates Ras on the Golgi
1399 apparatus by means of RasGRP1. Nature 424:694–698.

1400 Brewer GJ (1997) Isolation and culture of adult rat hippocampal neurons. Journal of
1401 Neuroscience Methods 71:143–155.

1402 Brewer GJ, Torricelli JR (2007) Isolation and culture of adult neurons and neurospheres. Nature
1403 Protocols 2:1490–1498.

1404 Brewer GJ, Torricelli JR, Evege EK, Price PJ (1993) Optimized survival of hippocampal neurons
1405 in B27-supplemented neurobasal™, a new serum-free medium combination. Journal of
1406 Neuroscience Research 35:567–576.

1407 Burden-Gulley SM, Brady-Kalnay SM (1999) PTPmu regulates N-cadherin-dependent neurite
1408 outgrowth. J Cell Biol 144:1323–1336.

1409 Cahoy JD, Emery B, Kaushal A, Foo LC, Zamanian JL, Christopherson KS, Xing Y, Lubischer
1410 JL, Krieg PA, Krupenko SA, Thompson WJ, Barres BA (2008) A transcriptome database for
1411 astrocytes, neurons, and oligodendrocytes: a new resource for understanding brain
1412 development and function. J Neurosci 28:264–278.

1413 Cai C-L, Zhou W, Yang L, Bu L, Qyang Y, Zhang X, Li X, Rosenfeld MG, Chen J, Evans S
1414 (2005) T-box genes coordinate regional rates of proliferation and regional specification
1415 during cardiogenesis. Development 132:2475–2487.

1416 Cameron EG, Robinson PR (2014) β-Arrestin-Dependent Deactivation of Mouse Melanopsin
1417 Craft CM, ed. PLoS ONE 9:e113138.

1418 Caretti E, Devarajan K, Coudry R, Ross E, Clapper ML, Cooper HS, Bellacosa A (2008)
1419 Comparison of RNA amplification methods and chip platforms for microarray analysis of
1420 samples processed by laser capture microdissection. Journal of Cellular Biochemistry
1421 103:556–563.

1422 Carson CT, Kinzler ER, Parr BA (2000) Tbx12, a novel T-box gene, is expressed during early
1423 stages of heart and retinal development. Mechanisms of Development 96:137–140.

1424 Carson CT, Pagratis M, Parr BA (2004) Tbx12 regulates eye development in Xenopus embryos.
1425 Biochemical and Biophysical Research Communications 318:485–489.

1426 Chen SK, Badea TC, Hattar S (2011) Photoentrainment and pupillary light reflex are mediated
1427 by distinct populations of ipRGCs. Nature 476:92–95.

1428 Clément-Ziza M, Gentien D, Lyonnet S, Thiery J-P, Besmond C, Decraene C (2009) Evaluation
1429 of methods for amplification of picogram amounts of total RNA for whole genome
1430 expression profiling. BMC Genomics 10:246.

1431 Craig AM, Kang Y (2007) Neurexin-neuroligin signaling in synapse development. Current
1432 Opinion in Neurobiology 17:43–52.

1433 Cui Q, Ren C, Sollars PJ, Pickard GE, So KF (2015) The injury resistant ability of melanopsin-
1434 expressing intrinsically photosensitive retinal ganglion cells. Neuroscience 284:845–853.

1435 de Sevilla Müller LP, Sargoy A, Rodriguez AR, Brecha NC (2014) Melanopsin Ganglion Cells
1436 Are the Most Resistant Retinal Ganglion Cell Type to Axonal Injury in the Rat Retina Tosini
1437 G, ed. PLoS ONE 9:e93274.

1438 de Wit J, Sylwestrak E, O'Sullivan ML, Otto S, Tiglio K, Savas JN, Yates JR, Comoletti D, Taylor
1439 P, Ghosh A (2009) LRRTM2 interacts with Neurexin1 and regulates excitatory synapse
1440 formation. Neuron 64:799–806.

1441 Diaz A, Ruiz F, Flórez J, Hurlé MA, Pazos A (1995) Mu-opioid receptor regulation during opioid
1442 tolerance and supersensitivity in rat central nervous system. J Pharmacol Exp Ther
1443 274:1545–1551.

1444 Doğrul A, Yeşilyurt O, Işimer A, Güzeldemir ME (2001) L-type and T-type calcium channel
1445 blockade potentiate the analgesic effects of morphine and selective mu opioid agonist, but
1446 not to selective delta and kappa agonist at the level of the spinal cord in mice. Pain 93:61–
1447 68.

1448 Dower NA, Stang SL, Bottorff DA, Ebinu JO, Dickie P, Ostergaard HL, Stone JC (2000)
1449 RasGRP is essential for mouse thymocyte differentiation and TCR signaling. Nat Immunol
1450 1:317–321.

1451 Duan X, Qiao M, Bei F, Kim I-J, He Z, Sanes JR (2015) Subtype-Specific Regeneration of
1452 Retinal Ganglion Cells following Axotomy: Effects of Osteopontin and mTOR Signaling.
1453 Neuron 85:1244–1256.

1454 Dumitrescu ON, Pucci FG, Wong KY, Berson DM (2009) Ectopic retinal ON bipolar cell
1455 synapses in the OFF inner plexiform layer: Contacts with dopaminergic amacrine cells and
1456 melanopsin ganglion cells. Journal of Comparative Neurology 517:226–244.

1457 Ebinu JO, Bottorff DA, Chan EY, Stang SL, Dunn RJ, Stone JC (1998) RasGRP, a Ras guanyl
1458 nucleotide- releasing protein with calcium- and diacylglycerol-binding motifs. Science
1459 280:1082–1086.

1460 Ecker JL, Dumitrescu ON, Wong KY, Alam NM, Chen S-K, LeGates T, Renna JM, Prusky GT,
1461 Berson DM, Hattar S (2010) Melanopsin-Expressing Retinal Ganglion-Cell Photoreceptors:
1462 Cellular Diversity and Role in Pattern Vision. Neuron 67:49–60.

1463 Eide EJ, Woolf MF, Kang H, Woolf P, Hurst W, Camacho F, Vielhaber EL, Giovanni A, Virshup
1464 DM (2005) Control of mammalian circadian rhythm by CKIepsilon-regulated proteasome-
1465 mediated PER2 degradation. Mol Cell Biol 25:2795–2807.

1466 Emanuel AJ, Do MTH (2015) Melanopsin Tristability for Sustained and Broadband
1467 Phototransduction. Neuron 85:1043–1055.

1468 Emanuel AJ, Kapur K, Do MTH (2017) Biophysical Variation within the M1 Type of Ganglion
1469 Cell Photoreceptor. Cell Rep 21:1048–1062.

1470 Estevez ME, Fogerson PM, Ilardi MC, Borghuis BG, Chan E, Weng S, Auferkorte ON, Demb
1471 JB, Berson DM (2012) Form and function of the M4 cell, an intrinsically photosensitive
1472 retinal ganglion cell type contributing to geniculocortical vision. J Neurosci 32:13608–13620.

1473 Fernandez DC, Chang Y-T, Hattar S, Chen S-K (2016) Architecture of retinal projections to the
1474 central circadian pacemaker. Proc Natl Acad Sci USA 113:6047–6052.

1475 Fink M, Lesage F, Duprat F, Heurteaux C, Reyes R, Fosset M, Lazdunski M (1998) A neuronal
1476 two P domain K+ channel stimulated by arachidonic acid and polyunsaturated fatty acids.
1477 EMBO J 17:3297–3308.

1478 Fornaro M, Raimondo S, Lee JM, Giuseppina Giacobini-Robecchi M (2007) Neuron-specific Hu
1479 proteins sub-cellular localization in primary sensory neurons. Annals of Anatomy -
1480 Anatomischer Anzeiger 189:223–228.

1481 Frings S, Brüll N, Dzeja C, Angele A, Hagen V, Kaupp UB, Baumann A (1998) Characterization
1482 of ether-à-go-go channels present in photoreceptors reveals similarity to IKx, a K+ current in
1483 rod inner segments. J Gen Physiol 111:583–599.

1484 Gorentla BK, Wan C-K, Zhong X-P (2011) Negative regulation of mTOR activation by
1485 diacylglycerol kinases. Blood 117:4022–4031.

1486 Graham DM, Wong KY, Shapiro P, Frederick C, Pattabiraman K, Berson DM (2008) Melanopsin
1487 Ganglion Cells Use a Membrane-Associated Rhabdomeric Phototransduction Cascade.
1488 Journal of Neurophysiology 99:2522–2532.

1489 Haeryfar SMM, Hoskin DW (2004) Thy-1: More than a Mouse Pan-T Cell Marker. The Journal of
1490 Immunology 173:3581–3588.

1491 Hannibal J, Hindersson P, Østergaard J, Georg B, Heegaard S, Larsen PJ, Fahrenkrug J (2004)
1492 Melanopsin Is Expressed in PACAP-Containing Retinal Ganglion Cells of the Human
1493 Retinohypothalamic Tract. Invest Ophthalmol Vis Sci 45:4202–4209.

1494 Hartwick ATE, Bramley JR, Yu J, Stevens KT, Allen CN, Baldridge WH, Sollars PJ, Pickard GE
1495 (2007) Light-evoked calcium responses of isolated melanopsin-expressing retinal ganglion
1496 cells. J Neurosci 27:13468–13480.

1497 Hattar S, Kumar M, Park A, Tong P, Tung J, Yau K-W, Berson DM (2006) Central projections of
1498 melanopsin-expressing retinal ganglion cells in the mouse. J Comp Neurol 497:326–349.

1499 Heiman M, Schaefer A, Gong S, Peterson JD, Day M, Ramsey KE, Suárez-Fariñas M, Schwarz
1500 C, Stephan DA, Surmeier DJ, Greengard P, Heintz N (2008) A Translational Profiling
1501 Approach for the Molecular Characterization of CNS Cell Types. Cell 135:738–748.

1502 Hinman MN, Lou H (2008) Diverse molecular functions of Hu proteins. Cell Mol Life Sci
1503 65:3168–3181.

1504 Hoshi H, Liu W-L, Massey SC, Mills SL (2009) ON inputs to the OFF layer: bipolar cells that
1505 break the stratification rules of the retina. J Neurosci 29:8875–8883.

1506 Hu C, Hill DD, Wong KY (2013) Intrinsic physiological properties of the five types of mouse
1507 ganglion-cell photoreceptors. Journal of Neurophysiology 109:1876–1889.

1508 Hughes S, Hankins MW, Foster RG, Peirson SN (2012) Melanopsin phototransduction: slowly
1509 emerging from the dark. Prog Brain Res 199:19–40.

1510 Hughes S, Jagannath A, Hickey D, Gatti S, Wood M, Peirson SN, Foster RG, Hankins MW
1511 (2015) Using siRNA to define functional interactions between melanopsin and multiple G
1512 Protein partners. Cell Mol Life Sci 72:165–179.

1513 Jain V, Ravindran E, Dhingra NK (2012) Differential expression of Brn3 transcription factors in
1514 intrinsically photosensitive retinal ganglion cells in mouse. Journal of Comparative
1515 Neurology 520:742–755.

1516 Jeon C-J, Strettoi E, Masland RH (1998) The Major Cell Populations of the Mouse Retina. J
1517 Neurosci 18:8936–8946.

1518 Ji M, Zhao W-J, Dong L-D, Miao Y, Yang X-L, Sun X-H, Wang Z (2011) RGS2 and RGS4
1519 modulate melatonin-induced potentiation of glycine currents in rat retinal ganglion cells.
1520 Brain Research 1411:1–8.

1521 Kim I-J, Zhang Y, Meister M, Sanes JR (2010) Laminar restriction of retinal ganglion cell
1522 dendrites and axons: subtype-specific developmental patterns revealed with transgenic
1523 markers. J Neurosci 30:1452–1462.

1524 Koussounadis A, Langdon SP, Um IH, Harrison DJ, Smith VA (2015) Relationship between
1525 differentially expressed mRNA and mRNA-protein correlations in a xenograft model system.
1526 Sci Rep 5:10775.

1527 Li S, Yang C, Zhang L, Gao X, Wang X, Liu W, Wang Y, Jiang S, Wong YH, Zhang Y, Liu K
1528 (2016) Promoting axon regeneration in the adult CNS by modulation of the
1529 melanopsin/GPCR signaling. Proc Natl Acad Sci USA 113:1937–1942.

1530 Li S-Y, Yau S-Y, Chen B-Y, Tay DK, Lee VWH, Pu M-L, Chan HHL, So K-F (2008) Enhanced
1531 Survival of Melanopsin-expressing Retinal Ganglion Cells After Injury is Associated with the
1532 PI3 K/Akt Pathway. Cell Mol Neurobiol 28:1095–1107.

1533 Lin JC, Ho W-H, Gurney A, Rosenthal A (2003) The netrin-G1 ligand NGL-1 promotes the
1534 outgrowth of thalamocortical axons. Nature Neuroscience 6:1270–1276.

1535 Lin Z, Liu J, Ding H, Xu F, Liu H (2018) Structural basis of SALM5-induced PTPδ dimerization
1536 for synaptic differentiation. Nature Communications 9:268.

1537 Lipina TV, Prasad T, Yokomaku D, Luo L, Connor SA, Kawabe H, Wang YT, Brose N, Roder
1538 JC, Craig AM (2016) Cognitive Deficits in Calsyntenin-2-deficient Mice Associated with
1539 Reduced GABAergic Transmission. Neuropsychopharmacology 41:802–810.

1540 Lobo MK, Karsten SL, Gray M, Geschwind DH, Yang XW (2006) FACS-array profiling of striatal
1541 projection neuron subtypes in juvenile and adult mouse brains. Nature Neuroscience 9:443–
1542 452.

1543 Macosko EZ, Basu A, Satija R, Nemesh J, Shekhar K, Goldman M, Tirosh I, Bialas AR,
1544 Kamitaki N, Martersteck EM, Trombetta JJ, Weitz DA, Sanes JR, Shalek AK, Regev A,
1545 McCarroll SA (2015) Highly Parallel Genome-wide Expression Profiling of Individual Cells
1546 Using Nanoliter Droplets. Cell 161:1202–1214.

1547 Mao C-A, Kiyama T, Pan P, Furuta Y, Hadjantonakis A-K, Klein WH (2008) Eomesodermin, a
1548 target gene of Pou4f2, is required for retinal ganglion cell and optic nerve development in
1549 the mouse. Development 135:271–280.

1550 Mao C-A, Li H, Zhang Z, Kiyama T, Panda S, Hattar S, Ribelayga CP, Mills SL, Wang SW
1551 (2014) T-box transcription regulator Tbr2 is essential for the formation and maintenance of
1552 Opn4/melanopsin-expressing intrinsically photosensitive retinal ganglion cells. J Neurosci
1553 34:13083–13095.

1554 Mao H, Zhao Q, Daigle M, Ghahremani MH, Chidiac P, Albert PR (2004) RGS17/RGSZ2, a
1555 novel regulator of Gi/o, Gz, and Gq signaling. J Biol Chem 279:26314–26322.

1556 Martin S, Lino de Oliveira C, Mello de Queiroz F, Pardo LA, Stühmer W, Del Bel E (2008) Eag1
1557 potassium channel immunohistochemistry in the CNS of adult rat and selected regions of
1558 human brain. Neuroscience 155:833–844.

1559 Matsuoka RL, Nguyen-Ba-Charvet KT, Parray A, Badea TC, Chédotal A, Kolodkin AL (2011)
1560 Transmembrane semaphorin signalling controls laminar stratification in the mammalian
1561 retina. Nature 470:259–263.

1562 Matsushima D, Heavner W, Pevny LH (2011) Combinatorial regulation of optic cup progenitor
1563 cell fate by SOX2 and PAX6. Development 138:443–454.

1564 Missler M, Hammer RE, Südhof TC (1998) Neurexophilin binding to alpha-neurexins. A single
1565 LNS domain functions as an independently folding ligand-binding unit. J Biol Chem
1566 273:34716–34723.

1567 Moises HC, Rusin KI, Macdonald RL (1994) Mu- and kappa-opioid receptors selectively reduce
1568 the same transient components of high-threshold calcium current in rat dorsal root ganglion
1569 sensory neurons. J Neurosci 14:5903–5916.

1570 Morrow EM, Belliveau MJ, Cepko CL (1998) Two Phases of Rod Photoreceptor Differentiation
1571 during Rat Retinal Development. J Neurosci 18:3738–3748.

1572 Morse AM, Carballo V, Baldwin DA, Taylor CG, McIntyre LM (2010) Comparison between
1573 NuGEN's WT-Ovation Pico and one-direct amplification systems. J Biomol Tech 21:141–
1574 147.

1575 Naiche LA, Harrelson Z, Kelly RG, Papaioannou VE (2005) T-box genes in vertebrate
1576 development. Annu Rev Genet 39:219–239.

1577 Novak A, Guo C, Yang W, Nagy A, Lobe CG (2000) Z/EG, a double reporter mouse line that
1578 expresses enhanced green fluorescent protein upon Cre-mediated excision. Genesis.

1579 Oancea E, Meyer T (1998) Protein kinase C as a molecular machine for decoding calcium and
1580 diacylglycerol signals. Cell 95:307–318.

1581 Pack W, Hill DD, Wong KY (2015) Melatonin modulates M4-type ganglion-cell photoreceptors.
1582 Neuroscience 303:178–188.

1583 Pederick DT, Homan CC, Jaehne EJ, Piltz SG, Haines BP, Baune BT, Jolly LA, Hughes JN,
1584 Gecz J, Thomas PQ (2016) Pcdh19 Loss-of-Function Increases Neuronal Migration In Vitro
1585 but is Dispensable for Brain Development in Mice. Sci Rep 6:26765.

1586 Peirson SN, Oster H, Jones SL, Leitges M, Hankins MW, Foster RG (2007) Microarray Analysis
1587 and Functional Genomics Identify Novel Components of Melanopsin Signaling. Current
1588 Biology 17:1363–1372.

1589 Pettem KL, Yokomaku D, Takahashi H, Ge Y, Craig AM (2013) Interaction between autism-
1590 linked MDGAs and neuroligins suppresses inhibitory synapse development. J Cell Biol
1591 200:321–336.

1592 Pierret P, Dunn RJ, Djordjevic B, Stone JC, Richardson PM (2000) Distribution of ras guanyl
1593 releasing protein (RasGRP) mRNA in the adult rat central nervous system. J Neurocytol
1594 29:485–497.

1595 Pocock R, Mione M, Hussain S, Maxwell S, Pontecorvi M, Aslam S, Gerrelli D, Sowden JC,
1596 Woollard A (2008) Neuronal function of Tbx20 conserved from nematodes to vertebrates.
1597 Developmental Biology 317:671–685.

1598 Puente LG, Stone JC, Ostergaard HL (2000) Evidence for protein kinase C-dependent and -
1599 independent activation of mitogen-activated protein kinase in T cells: potential role of
1600 additional diacylglycerol binding proteins. The Journal of Immunology 165:6865–6871.

1601 Quail MA, Kozarewa I, Smith F, Scally A, Stephens PJ, Durbin R, Swerdlow H, Turner DJ
1602 (2008) A large genome center's improvements to the Illumina sequencing system. Nat
1603 Methods 5:1005–1010.

1604 Quattrochi LE, Stabio ME, Kim I, Berson DM (2018) The M6 cell: A small-field bistratified
1605 photosensitive ganglion cell. in press.

1606 Reifler AN, Chervenak AP, Dolikian ME, Benenati BA, Li BY, Wachter RD, Lynch AM,
1607 Demertzis ZD, Meyers BS, Abufarha FS, Jaeckel ER, Flannery MP, Wong KY (2015) All
1608 Spiking, Sustained ON Displaced Amacrine Cells Receive Gap-Junction Input from
1609 Melanopsin Ganglion Cells. Current Biology 25:2763–2773.

1610 Renna JM, Weng S, Berson DM (2011) Light acts through melanopsin to alter retinal waves and
1611 segregation of retinogeniculate afferents. Nature Neuroscience 14:827–829.

1612 Rodriguez AR, Sevilla Müller LP, Brecha NC (2014) The RNA binding protein RBPMS is a
1613 selective marker of ganglion cells in the mammalian retina. Journal of Comparative
1614 Neurology 522:1411–1443.

1615 Rousso DL, Qiao M, Kagan RD, Yamagata M, Palmiter RD, Sanes JR (2016) Two Pairs of ON
1616 and OFF Retinal Ganglion Cells Are Defined by Intersectional Patterns of Transcription
1617 Factor Expression. Cell Rep 15:1930–1944.

1618 Sabbah S, Berg D, Papendorp C, Briggman KL, Berson DM (2017) A Cre Mouse Line for
1619 Probing Irradiance- and Direction-Encoding Retinal Networks. eNeuro 4:ENEURO.0065–
1620 17.2017.

1621 Sakabe NJ, Aneas I, Shen T, Shokri L, Park S-Y, Bulyk ML, Evans SM, Nobrega MA (2012)
1622 Dual transcriptional activator and repressor roles of TBX20 regulate adult cardiac structure
1623 and function. Hum Mol Genet 21:2194–2204.

1624 Sand A, Schmidt TM, Kofuji P (2012) Diverse types of ganglion cell photoreceptors in the
1625 mammalian retina. Progress in Retinal and Eye Research 31:287–302.

1626 Sanes JR, Masland RH (2015) The Types of Retinal Ganglion Cells: Current Status and
1627 Implications for Neuronal Classification. http://dxdoiorg/101146/annurev-neuro-071714-
1628 034120 38:221–246.

1629 Schmidt TM, Do MTH, Dacey D, Lucas R, Hattar S, Matynia A (2011) Melanopsin-positive
1630 intrinsically photosensitive retinal ganglion cells: from form to function. J Neurosci
1631 31:16094–16101.

1632 Schmidt TM, Taniguchi K, Kofuji P (2008) Intrinsic and Extrinsic Light Responses in
1633 Melanopsin-Expressing Ganglion Cells During Mouse Development. Journal of
1634 Neurophysiology 100:371–384.

1635 Sengupta A, Baba K, Mazzoni F, Pozdeyev NV, Strettoi E, Iuvone PM, Tosini G (2011)
1636 Localization of melatonin receptor 1 in mouse retina and its role in the circadian regulation
1637 of the electroretinogram and dopamine levels. Yamazaki S, ed. PLoS ONE 6:e24483.

1638 Shekhar K, Lapan SW, Whitney IE, Tran NM, Macosko EZ, Kowalczyk M, Adiconis X, Levin JZ,
1639 Nemesh J, Goldman M, McCarroll SA, Cepko CL, Regev A, Sanes JR (2016)
1640 Comprehensive Classification of Retinal Bipolar Neurons by Single-Cell Transcriptomics.
1641 Cell 166:1308–1323.e1330.

1642 Shen T, Aneas I, Sakabe N, Dirschinger RJ, Wang G, Smemo S, Westlund JM, Cheng H,
1643 Dalton N, Gu Y, Boogerd CJ, Cai C-L, Peterson K, Chen J, Nobrega MA, Evans SM (2011)
1644 Tbx20 regulates a genetic program essential to adult mouse cardiomyocyte function. J Clin
1645 Invest 121:4640–4654.

1646 Sheng W-L, Chen W-Y, Yang X-L, Zhong Y-M, Weng S-J (2015) Co-expression of two subtypes
1647 of melatonin receptor on rat M1-type intrinsically photosensitive retinal ganglion cells.
1648 Barnes S, ed. PLoS ONE 10:e0117967.

1649 Shulga YV, Topham MK, Epand RM (2011) Regulation and Functions of Diacylglycerol Kinases.
1650 Chemical Reviews 111:6186–6208.

1651 Siegert S, Cabuy E, Scherf BG, Kohler H, Panda S, Le Y-Z, Fehling HJ, Gaidatzis D, Stadler
1652 MB, Roska B (2012) Transcriptional code and disease map for adult retinal cell types.
1653 Nature Neuroscience 15:487–495.

1654 Soto I, Oglesby E, Buckingham BP, Son JL, Roberson EDO, Steele MR, Inman DM, Vetter ML,
1655 Horner PJ, Marsh-Armstrong N (2008) Retinal Ganglion Cells Downregulate Gene
1656 Expression and Lose Their Axons within the Optic Nerve Head in a Mouse Glaucoma
1657 Model. J Neurosci 28:548–561.

1658 Stabio ME, Sabbah S, Quattrochi LE, Ilardi MC, Fogerson PM, Leyrer ML, Kim MT, Kim I, Schiel
1659 M, Renna JM, Briggman KL, Berson DM (2018) The M5 Cell: A Color-Opponent Intrinsically
1660 Photosensitive Retinal Ganglion Cell. Neuron 97:251.

1661 Star EN, Zhu M, Shi Z, Liu H, Pashmforoush M, Sauve Y, Bruneau BG, Chow RL (2012)
1662 Regulation of retinal interneuron subtype identity by the Iroquois homeobox gene Irx6.
1663 Development 139:4644–4655.

1664 Stennard FA, Costa MW, Elliott DA, Rankin S, Haast SJP, Lai D, McDonald LPA, Niederreither
1665 K, Dolle P, Bruneau BG, Zorn AM, Harvey RP (2003) Cardiac T-box factor Tbx20 directly
1666 interacts with Nkx2-5, GATA4, and GATA5 in regulation of gene expression in the
1667 developing heart. Developmental Biology 262:206–224.

1668 Sweeney NT, Tierney H, Feldheim DA (2014) Tbr2 is required to generate a neural circuit
1669 mediating the pupillary light reflex. J Neurosci 34:5447–5453.

1670 Takeuchi JK, Mileikovskaia M, Koshiba-Takeuchi K, Heidt AB, Mori AD, Arruda EP,
1671 Gertsenstein M, Georges R, Davidson L, Mo R, Hui C-C, Henkelman RM, Nemer M, Black
1672 BL, Nagy A, Bruneau BG (2005) Tbx20 dose-dependently regulates transcription factor
1673 networks required for mouse heart and motoneuron development. Development 132:2463–
1674 2474.

1675 Tariq MA, Kim HJ, Jejelowo O, Pourmand N (2011) Whole-transcriptome RNAseq analysis from
1676 minute amount of total RNA. Nucleic Acids Res 39:e120–e120.

1677 Thorvaldsdóttir H, Robinson JT (2013) Integrative Genomics Viewer (IGV): high-performance
1678 genomics data visualization and exploration. Briefings in ….

1679 Toki S, Kawasaki H, Tashiro N, Housman DE, Graybiel AM (2001) Guanine nucleotide
1680 exchange factors CalDAG-GEFI and CalDAG-GEFII are colocalized in striatal projection
1681 neurons. J Comp Neurol 437:398–407.

1682 Topark-Ngarm A, Golonzhka O, Peterson VJ, Barrett B, Martinez B, Crofoot K, Filtz TM, Leid M
1683 (2006) CTIP2 associates with the NuRD complex on the promoter of p57KIP2, a newly
1684 identified CTIP2 target gene. J Biol Chem 281:32272–32283.

1685 Topham MK, Prescott SM (2001) Diacylglycerol kinase zeta regulates Ras activation by a novel
1686 mechanism. J Cell Biol 152:1135–1143.

1687 Trapnell C, Roberts A, Goff L, Pertea G, Kim D, Kelley DR, Pimentel H, Salzberg SL, Rinn JL,
1688 Pachter L (2012) Differential gene and transcript expression analysis of RNA-seq
1689 experiments with TopHat and Cufflinks. Nature Protocols 7:562–578.

1690 Van Hook MJ, Wong KY, Berson DM (2012) Dopaminergic modulation of ganglion-cell
1691 photoreceptors in rat. European Journal of Neuroscience 35:507–518.

1692 Wong KY (2012) A retinal ganglion cell that can signal irradiance continuously for 10 hours. J
1693 Neurosci 32:11478–11485.

1694 Xu J, Xiao N, Xia J (2010) Thrombospondin 1 accelerates synaptogenesis in hippocampal
1695 neurons through neuroligin 1. Nature Neuroscience 13:22–24.

1696 Xue T, Do MTH, Riccio A, Jiang Z, Hsieh J, Wang HC, Merbs SL, Welsbie DS, Yoshioka T,
1697 Weissgerber P, Stolz S, Flockerzi V, Freichel M, Simon MI, Clapham DE, Yau KW (2011)
1698 Melanopsin signalling in mammalian iris and retina. Nature 479:67–73.

1699 Young RW (1985) Cell differentiation in the retina of the mouse. The Anatomical Record
1700 212:199–205.

1701 Zhang M, Xia H, Li X, Wang X, Dong Y, Zhang T, Yu H (2010) C1 domain mediates CalDAGIII
1702 localization to the Golgi. Mol Biol Rep 37:3481–3485.

1703 Zhou H, Yoshioka T, Nathans J (1996) Retina-derived POU-domain factor-1: a complex POU-
1704 domain gene implicated in the development of retinal ganglion and amacrine cells. J
1705 Neurosci 16:2261–2274.

1706

Figure 1.

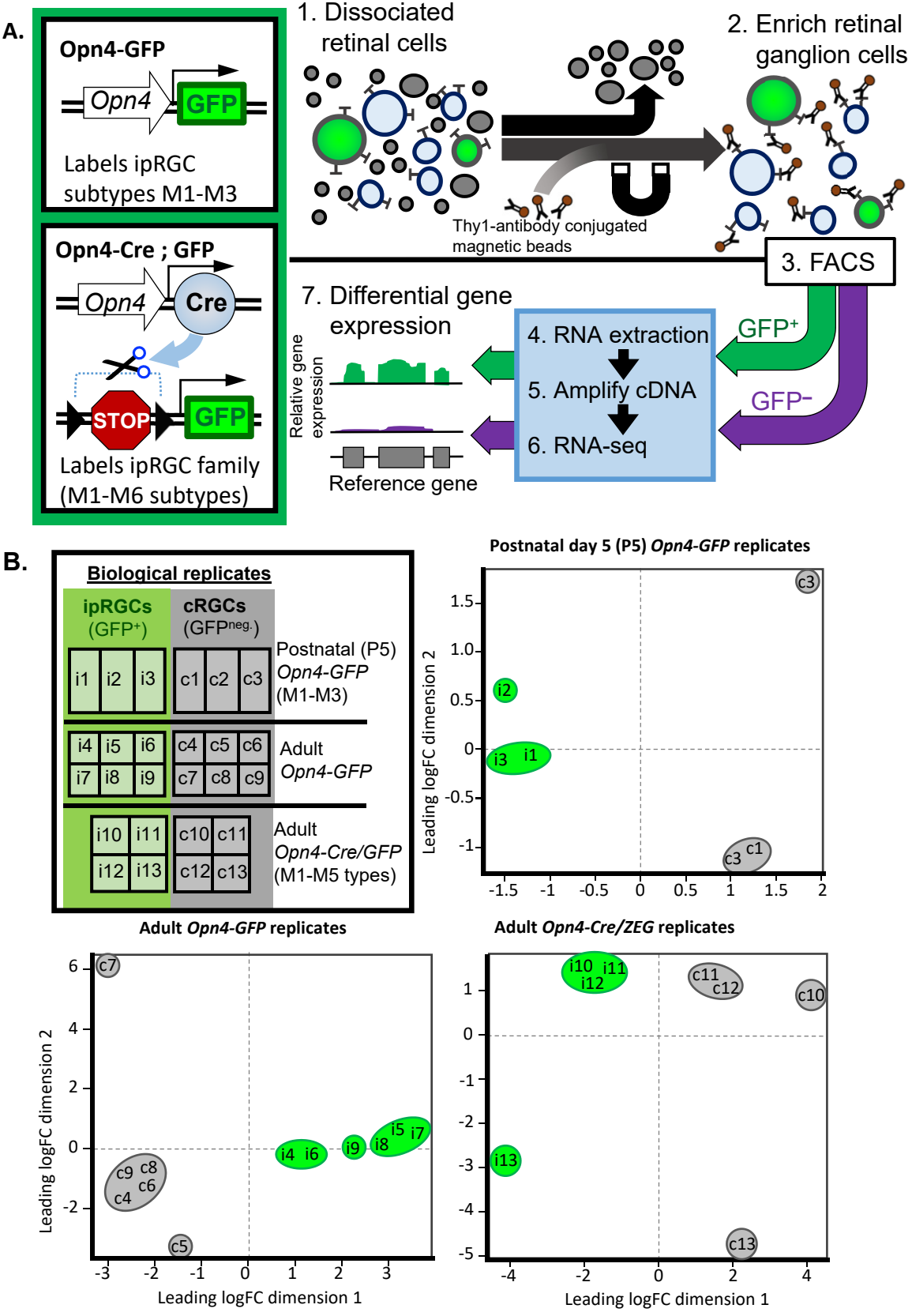
A.
Opn4-GFP
Opn4
GFP
Labels ipRGC subtypes M1-M3
Opn4-Cre ; GFP
Opn4
Cre
STOP
GFP
Labels ipRGC family (M1-M6 subtypes)
1. Dissociated retinal cells
2. Enrich retinal ganglion cells
Thy1-antibody conjugated magnetic beads
3. FACS
7. Differential gene expression
Relative gene expression
Reference gene
4. RNA extraction
5. Amplify cDNA
6. RNA-seq
GFP+
GFP−
B.
Biological replicates
ipRGCs (GFP+)
cRGCs (GFPneg.)
i1 i2 i3
c1 c2 c3
Postnatal (P5) Opn4-GFP (M1-M3)
i4 i5 i6
i7 i8 i9
c4 c5 c6
c7 c8 c9
Adult Opn4-GFP
i10 i11
i12 i13
c10 c11
c12 c13
Adult Opn4-Cre/GFP (M1-M5 types)
Postnatal day 5 (P5) Opn4-GFP replicates
Leading logFC dimension 2
Adult Opn4-GFP replicates
Leading logFC dimension 1
Adult Opn4-Cre/ZEG replicates
Leading logFC dimension 1

Figure 1—figure supplement 1.

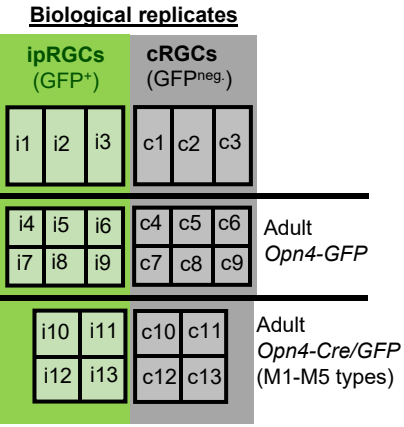

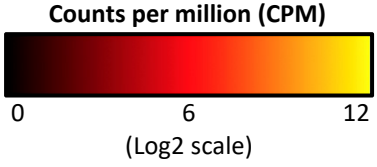

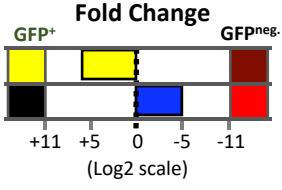

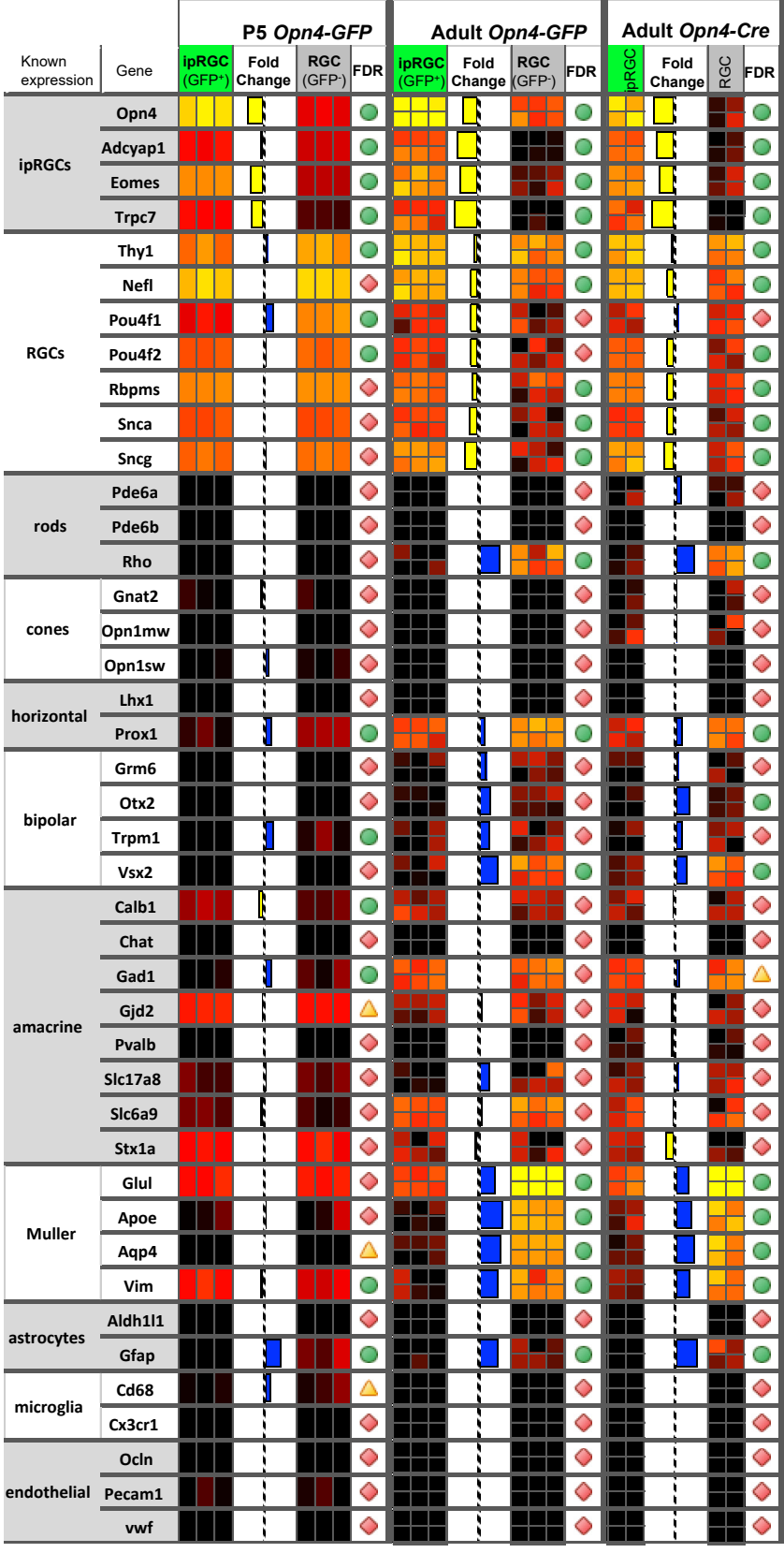

Figure 2.

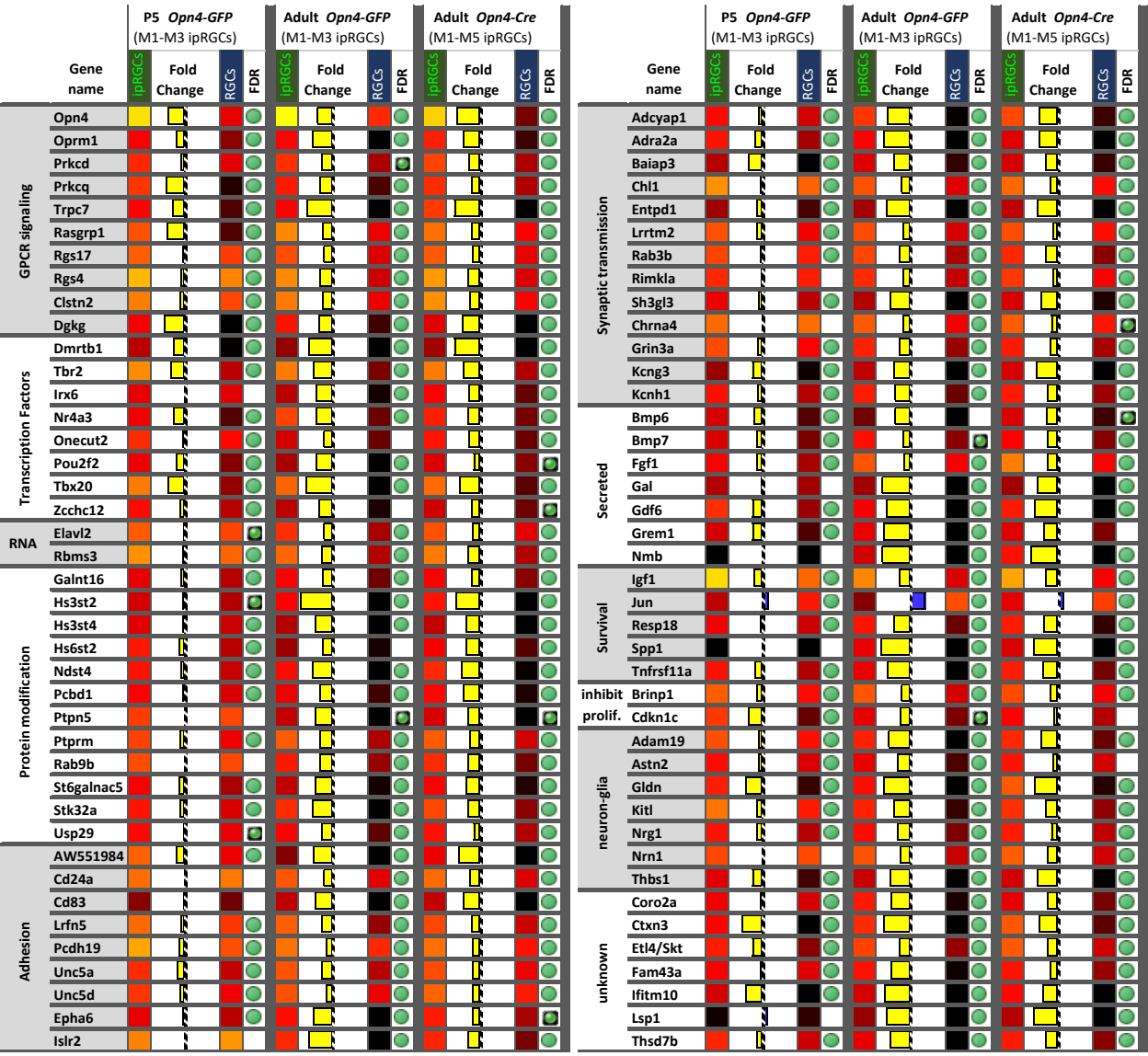

Counts per million (CPM)

0 6 12

(Log2 scale)

Fold Change

GFP+ GFPneg.

Median count values across samples

+11 +5 0 -5 -11

(Log2 scale)

False Discovery Rate (FDR)

< 0.05 < 0.1

Figure 2—figure supplement 1.

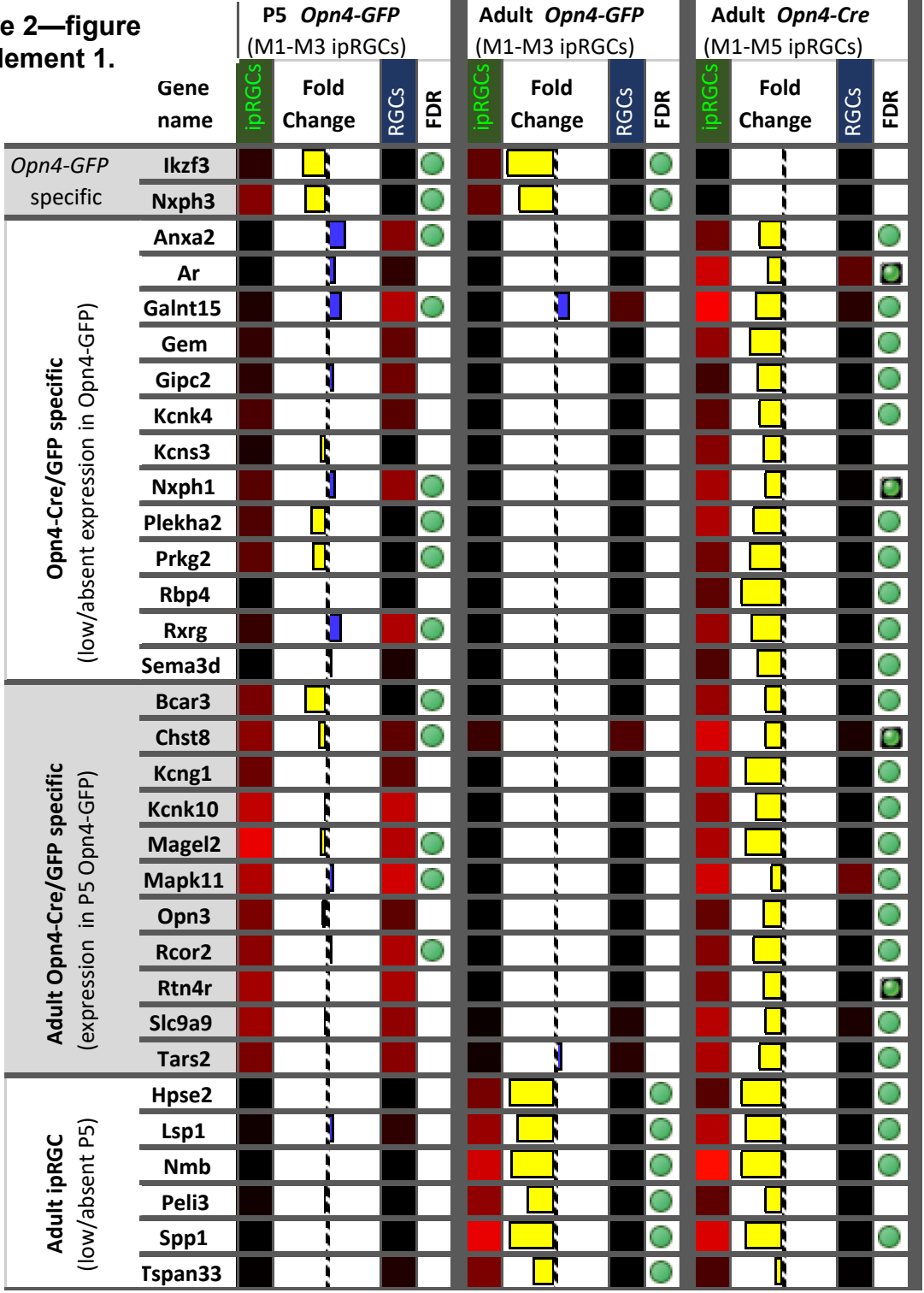

Figure 2—figure supplement 2.

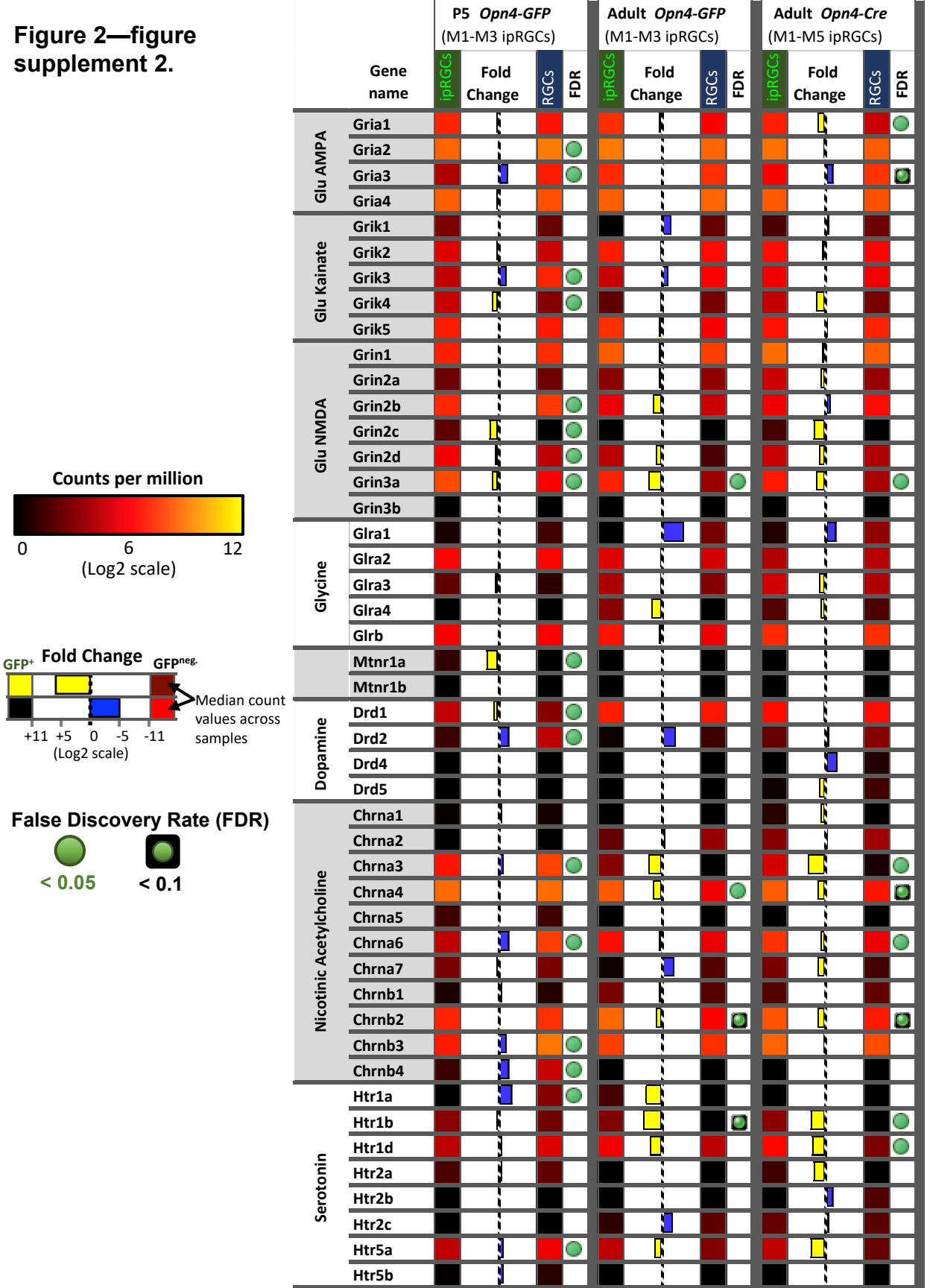

Figure 2—figure supplement 3

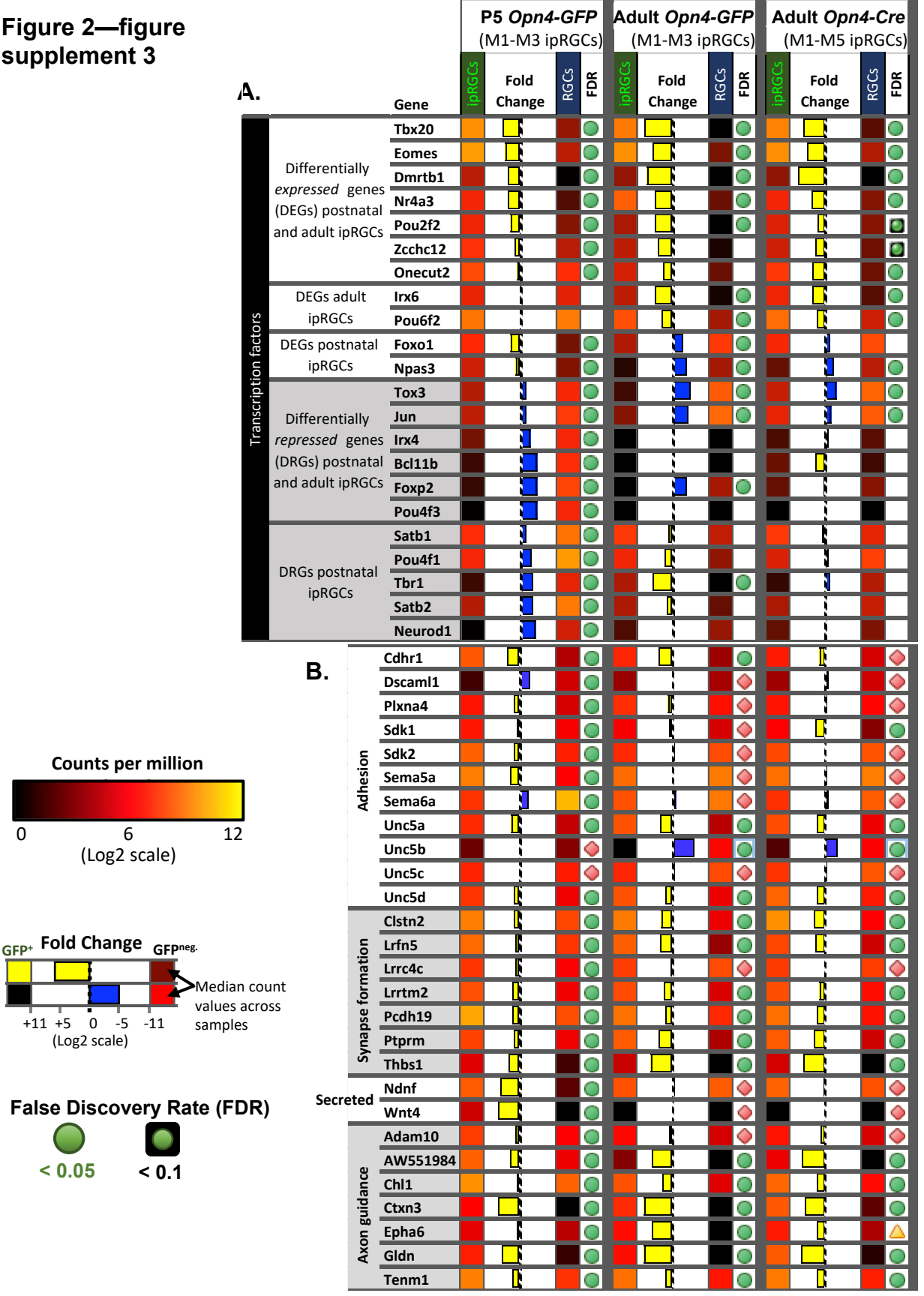

Figure 2—figure supplement 4.

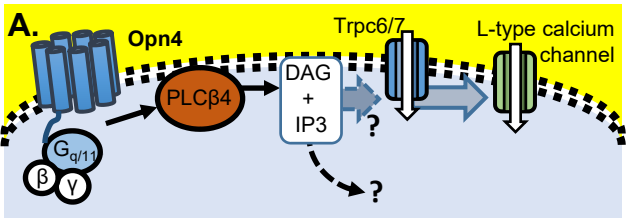

B.

C.

Gene name	P5 *Opn4-GFP* (M1-M3 ipRGCs) ipRGCs	P5 *Opn4-GFP* (M1-M3 ipRGCs) Fold Change	P5 *Opn4-GFP* (M1-M3 ipRGCs) RGCs	P5 *Opn4-GFP* (M1-M3 ipRGCs) FDR	Adult *Opn4-GFP* (M1-M3 ipRGCs) ipRGCs	Adult *Opn4-GFP* (M1-M3 ipRGCs) Fold Change	Adult *Opn4-GFP* (M1-M3 ipRGCs) RGCs	Adult *Opn4-GFP* (M1-M3 ipRGCs) FDR	Adult *Opn4-Cre* (M1-M5 ipRGCs) ipRGCs	Adult *Opn4-Cre* (M1-M5 ipRGCs) Fold Change	Adult *Opn4-Cre* (M1-M5 ipRGCs) RGCs	Adult *Opn4-Cre* (M1-M5 ipRGCs) FDR
ipRGC phototransduction (depolarization)												
Opn4												
Gna11												
Gna14												
Gna15												
Gnaq												
Gng4												
Plcb4												
Trpc6												
Trpc7												
Pirt												
Cacna1c												
Cacna1d												
Cacna1f												
Cacna1b												
Arrb1												
Arrb2												
Prkcd												
Prkcq												
Dgkg												
Rasgrp1												
Clstn2												
Oprm1												
Rgs17												
Rgs4												
Clvs2												
Light response (activation, hyperpolarization)												
Opn1lw												
Opn1mw												
Opn1sw												
Rho												
Gngt1												
Gngt2												
Gnat1												
Gnat2												
Gnb1												
Gnb3												
Pde6g												
Pde6h												
Pde6a												
Pde6b												
Pde6c												
Pde6d												
Cnga1												
Cnga3												
Cngb1												
Cngb3												
Gucy2d												
Gucy2f												
Rcvrn												
Dark (recovery, depolarization)												
Grk1												
Arr3												
Sag												
Guca1b												
Guca1c												
Guca1a												
Slc24a1												
Slc24a2												
Slc24a3												
Kcnh1												
Cdipt												
Cds1												
Cds2												
Gnb5												
Rgs9												
Rgs9bp												
Chromophore regeneration												
Rdh12												
Rdh8												
Rbp3												
Rbp1												
Lrat												
Rpe65												
Degs1												
Awat2												
Rdh10												
Rdh11												
Rdh5												
Rlbp1												

Counts per million

0 6 12

(Log2 scale)

Fold Change

GFP+ GFPneg.

+11 +5 0 -5 -11

(Log2 scale)

Median count values across samples

False Discovery Rate (FDR)

< 0.05 < 0.1

Figure 3.

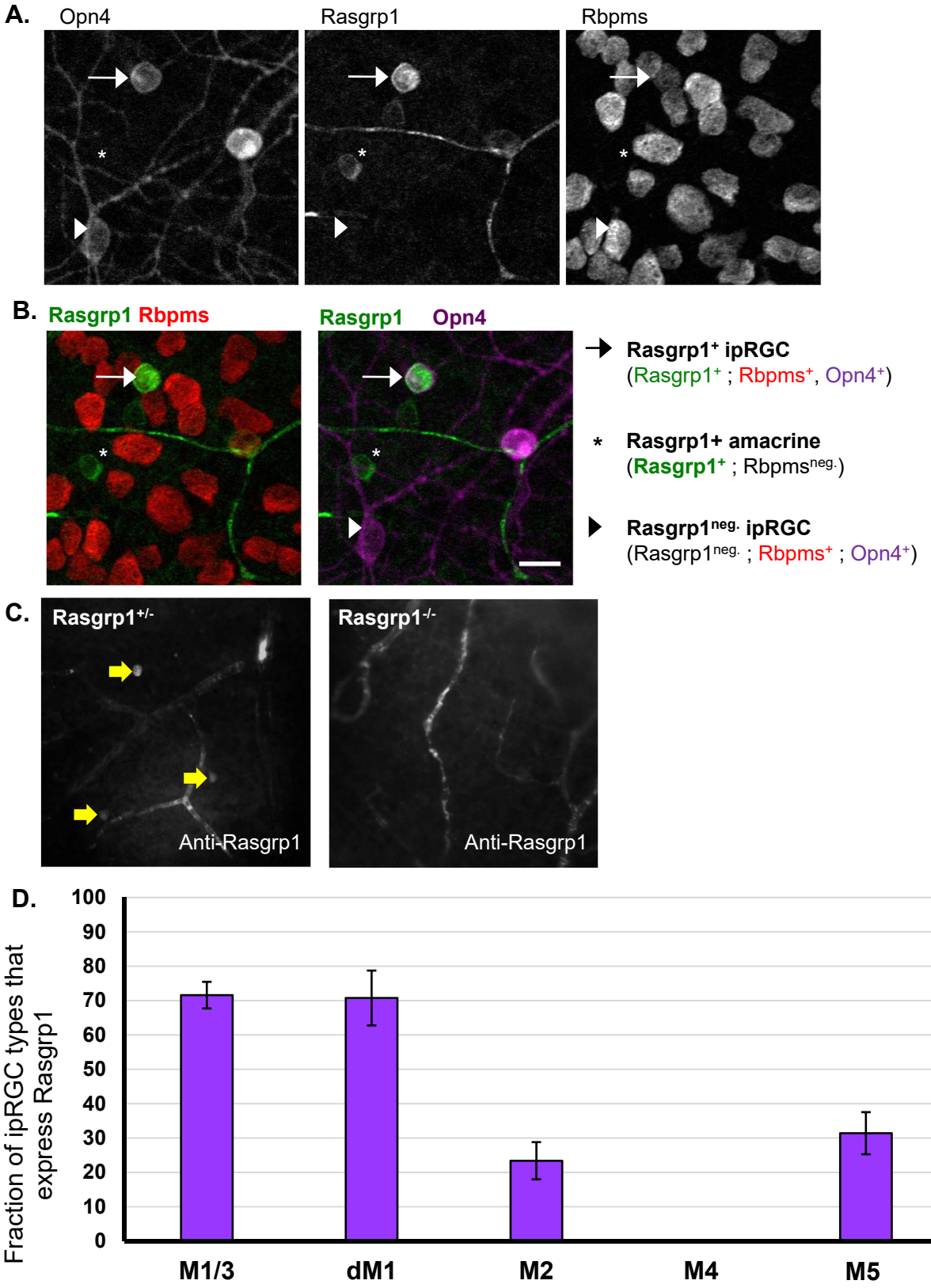
A.
Opn4
Rasgrp1
Rbpms
B.
Rasgrp1 Rbpms
Rasgrp1 Opn4
Rasgrp1+ ipRGC
(Rasgrp1+ ; Rbpms+, Opn4+)
Rasgrp1+ amacrine
(Rasgrp1+ ; Rbpmsneg.)
Rasgrp1neg. ipRGC
(Rasgrp1neg. ; Rbpms+ ; Opn4+)
C.
Rasgrp1+/-
Anti-Rasgrp1
Rasgrp1-/-
Anti-Rasgrp1
D.
Fraction of ipRGC types that express Rasgrp1
100
90
80
70
60
50
40
30
20
10
0
M1/3
dM1
M2
M4
M5

Figure 3—figure supplement 1.

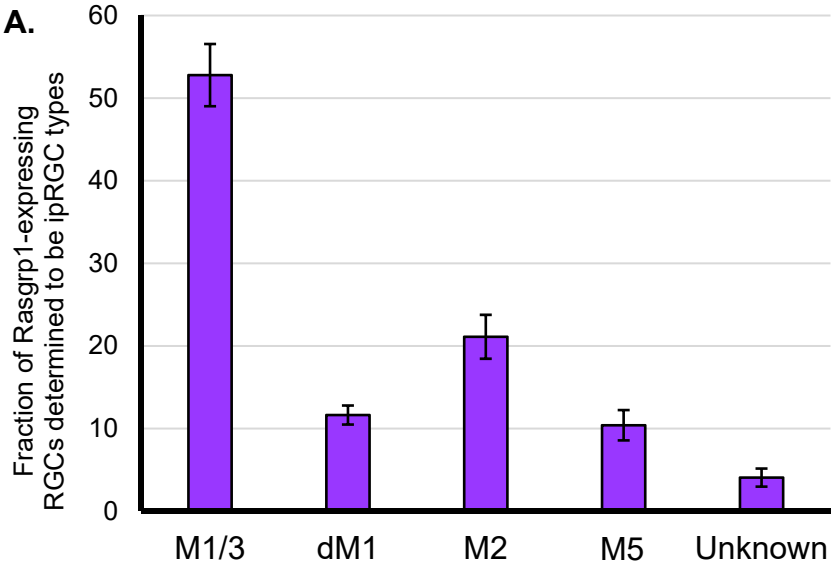

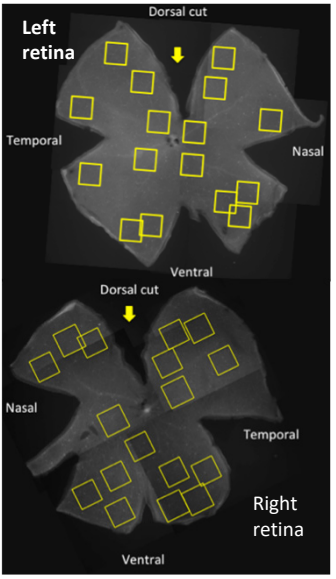

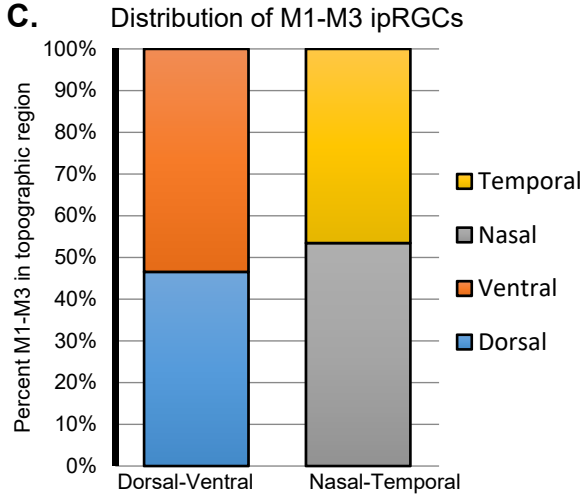

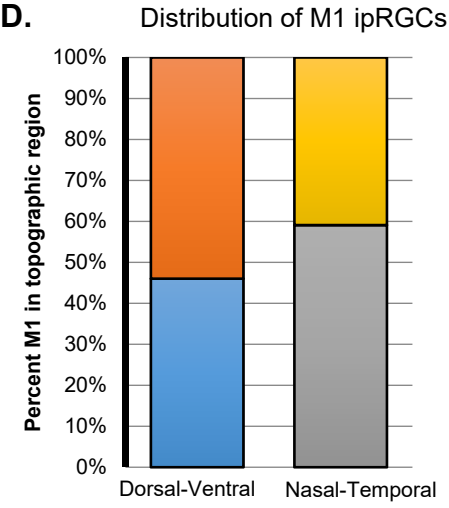

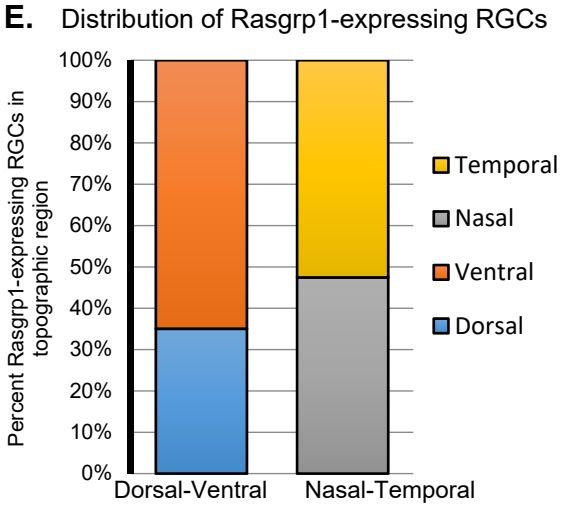

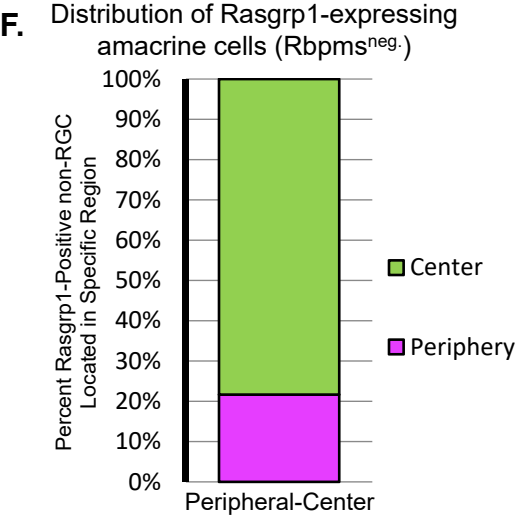

Figure 4.

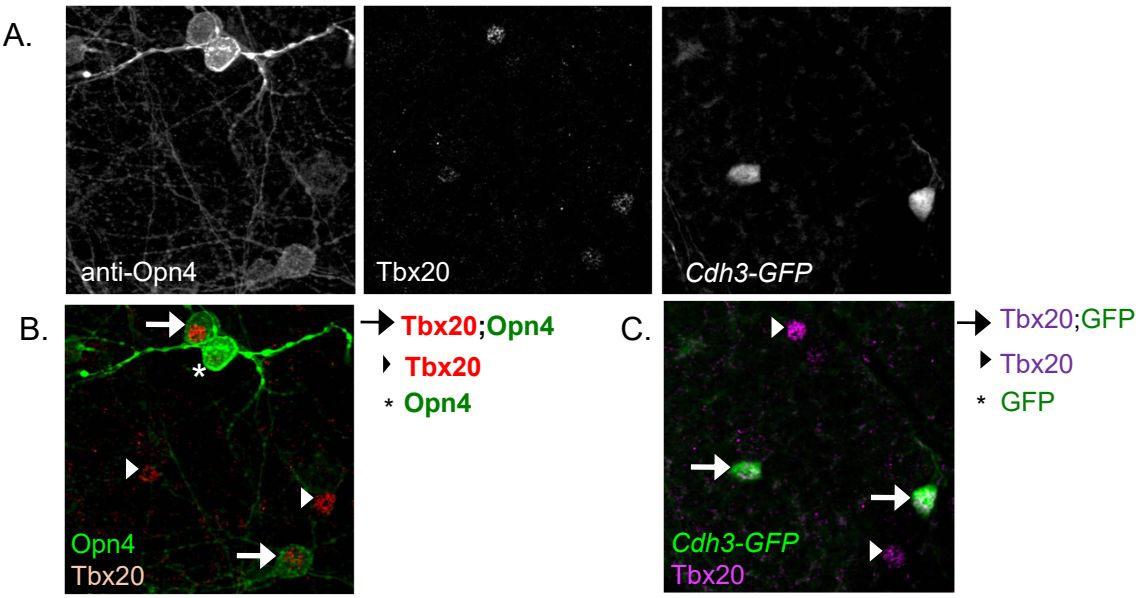
A.
anti-Opn4
Tbx20
Cdh3-GFP
B.
Tbx20;Opn4
Tbx20
Opn4
Opn4
Tbx20
C.
Tbx20;GFP
Tbx20
GFP
Cdh3-GFP
Tbx20

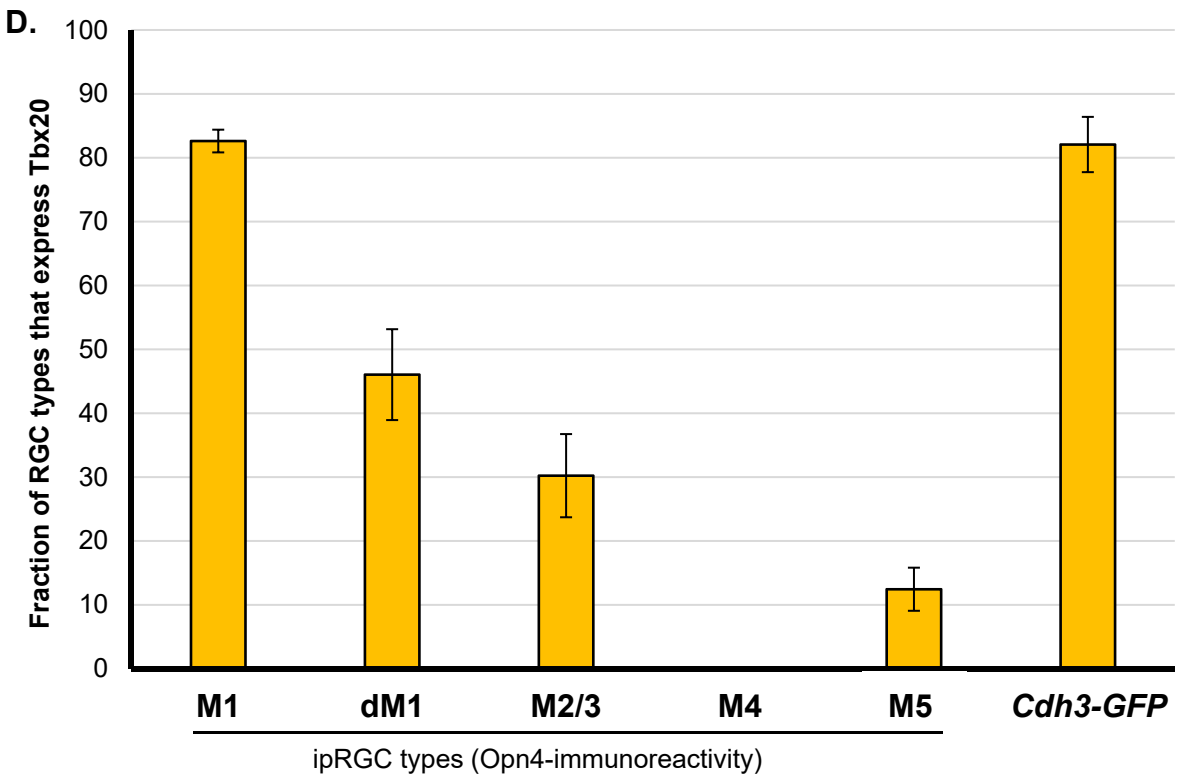
D.
Fraction of RGC types that express Tbx20
100
90
80
70
60
50
40
30
20
10
0
M1
dM1
M2/3
M4
M5
Cdh3-GFP
ipRGC types (Opn4-immunoreactivity)

Figure 4—figure supplement 1.

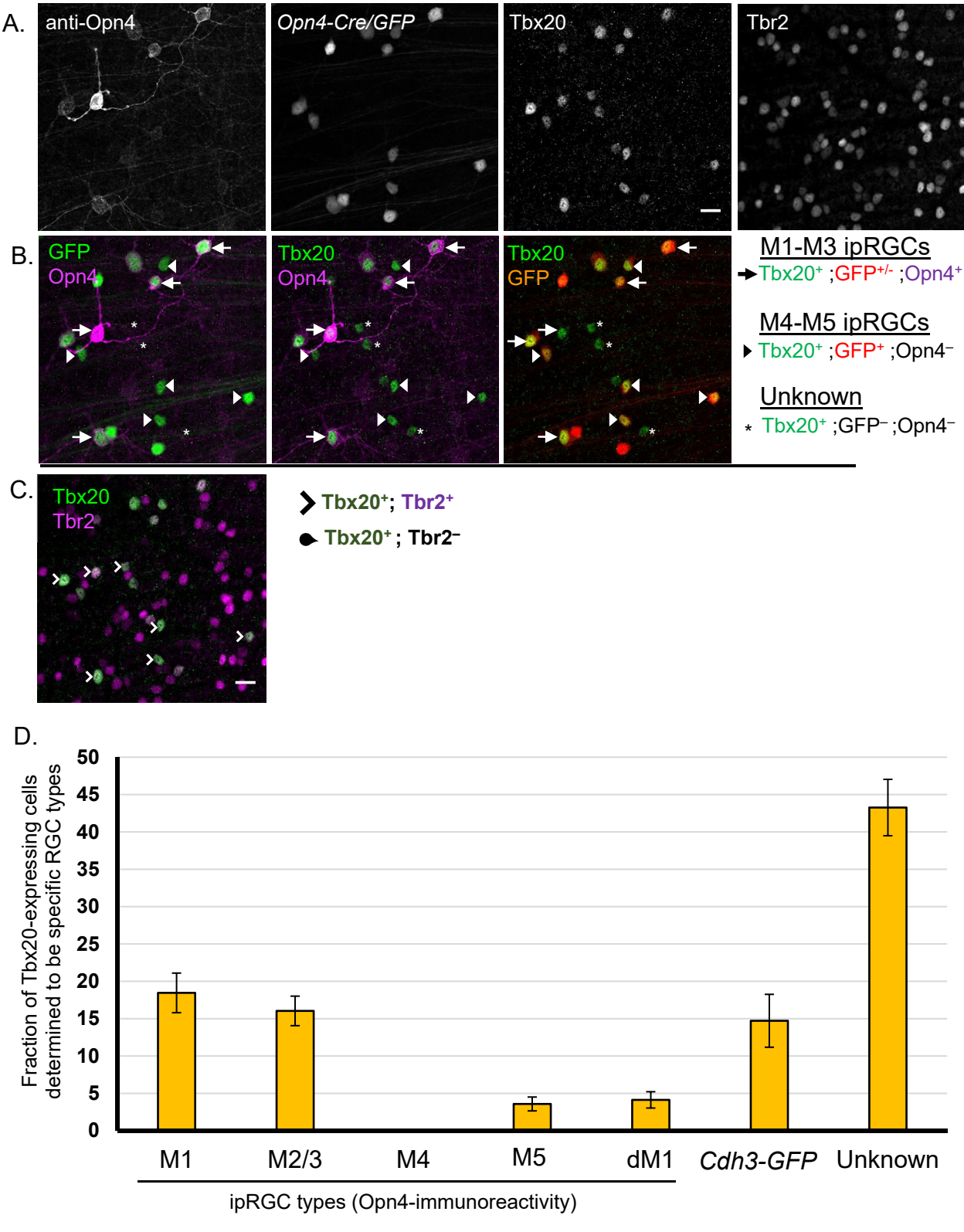

Figure 5. **A.**

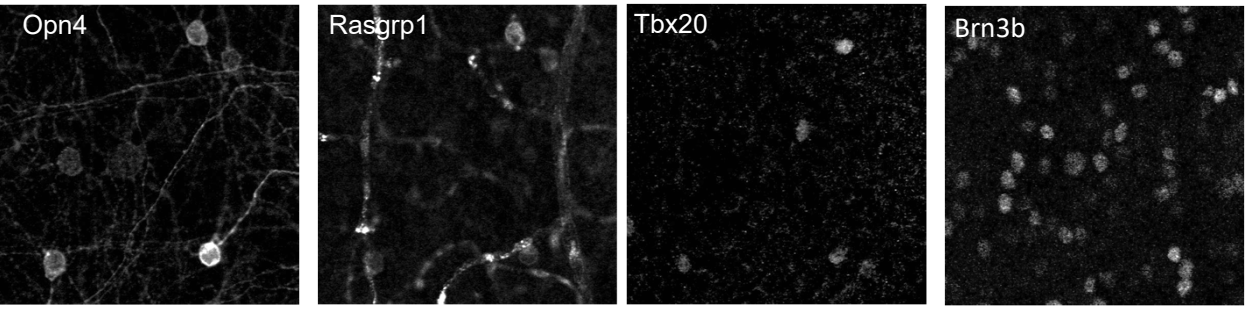

B.

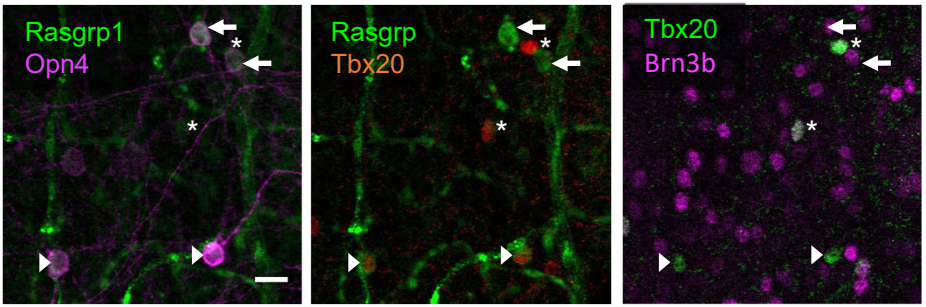

➔ Opn4⁺ ; Rasgrp1⁺ ; Tbx20⁻ ; Brn3b⁻

▶ Opn4⁺ ; Rasgrp1⁺ ; Tbx20 ; Brn3b⁻

* Opn4⁻ ; Rasgrp1⁻ ; Tbx20⁺ ; Brn3b⁺

C.

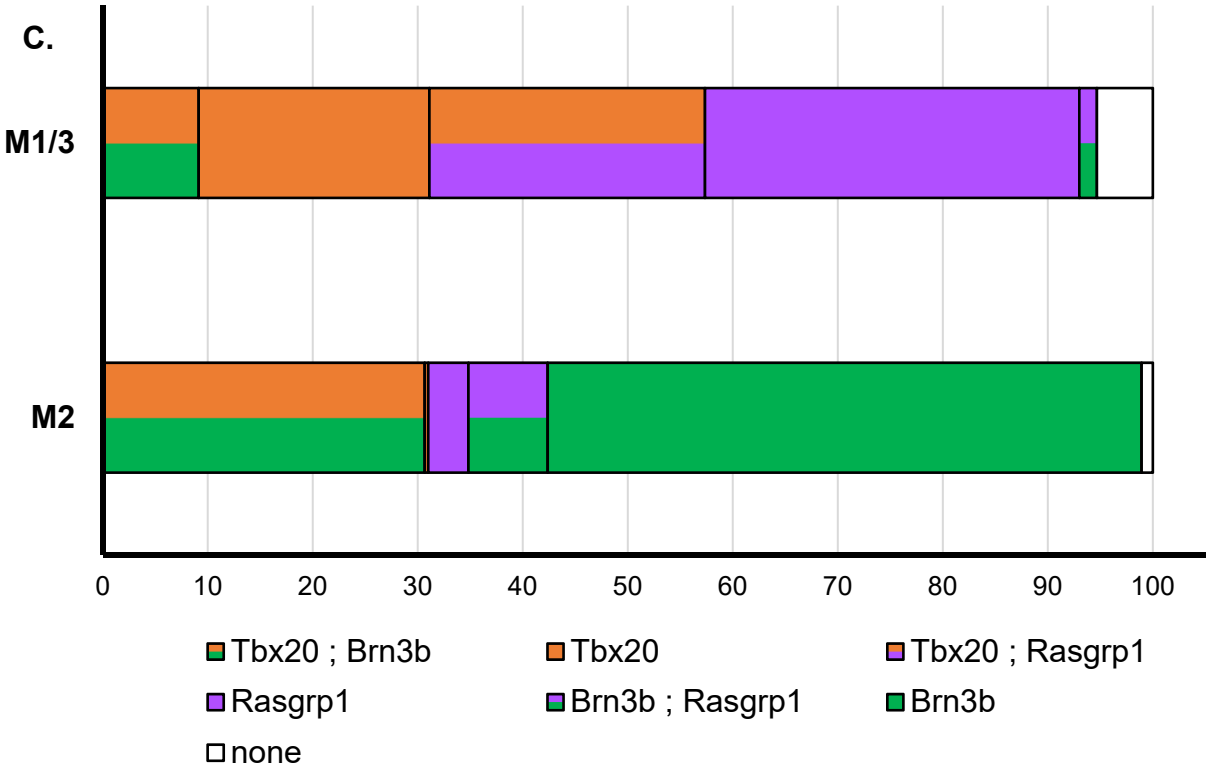

Figure 5—figure supplement 1.

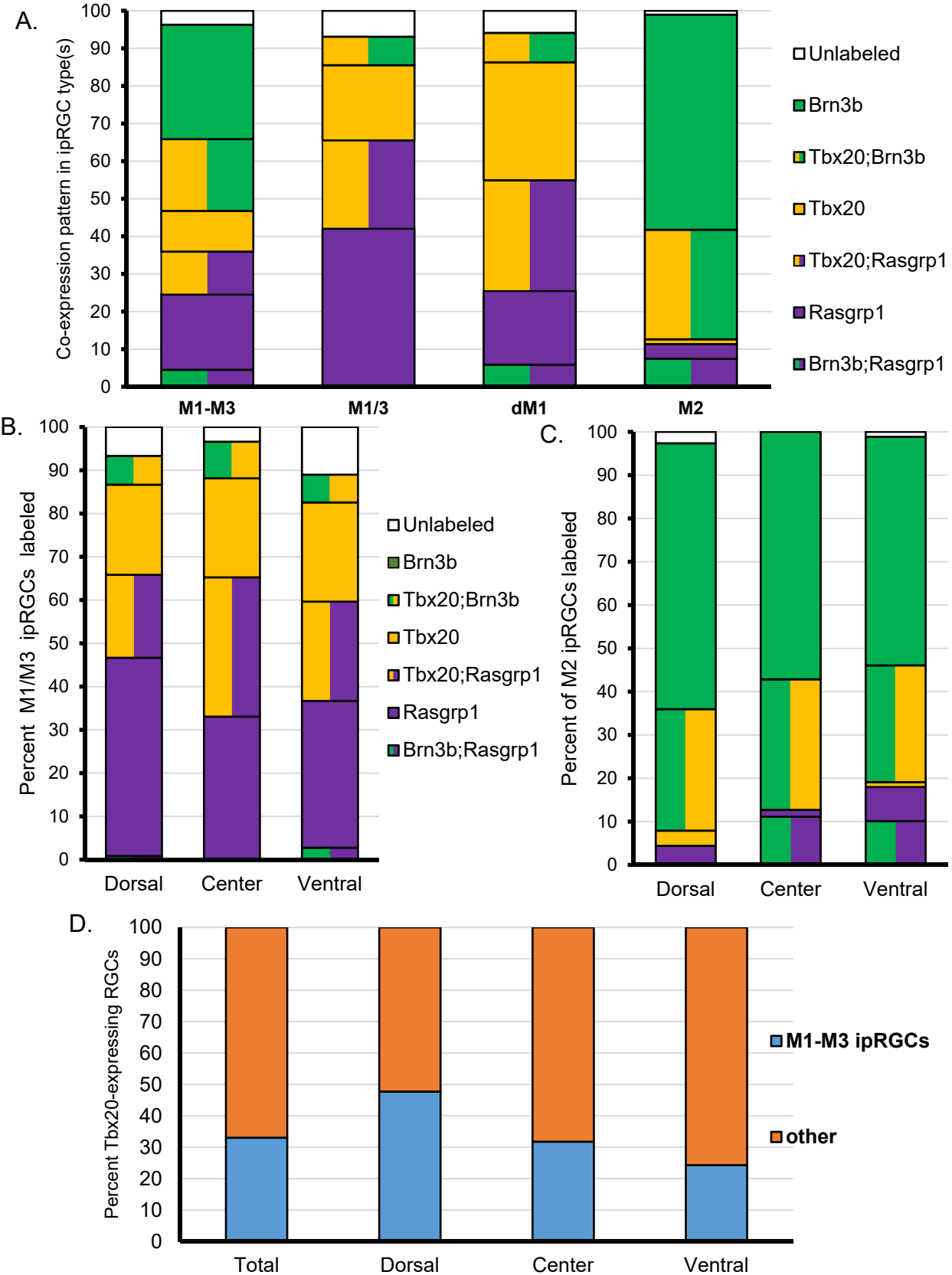

Figure 6.

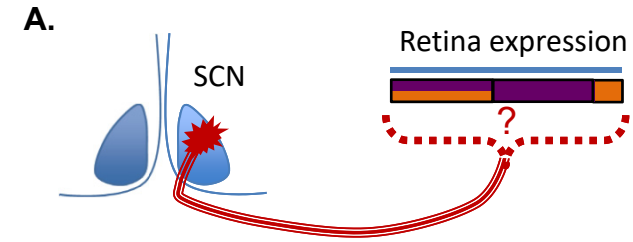
A.
SCN
Retina expression
?

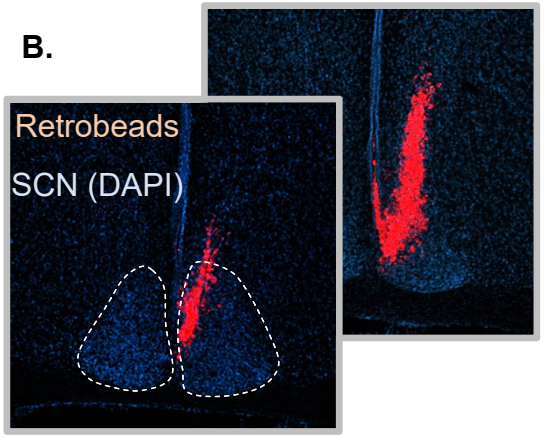
B.
Retrobeads
SCN (DAPI)

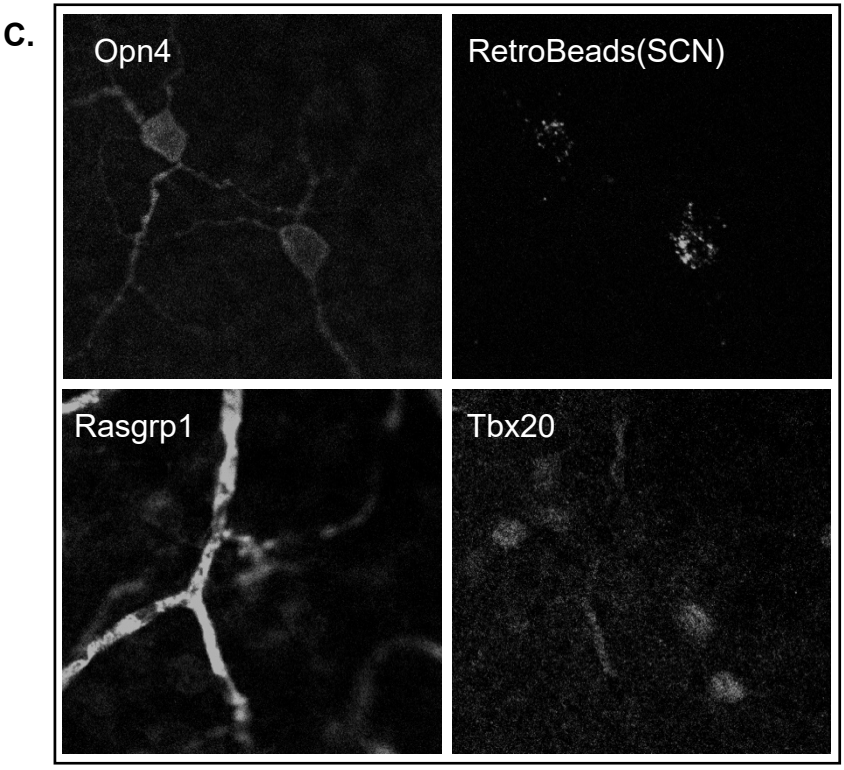
C.
Opn4
RetroBeads(SCN)
Rasgrp1
Tbx20

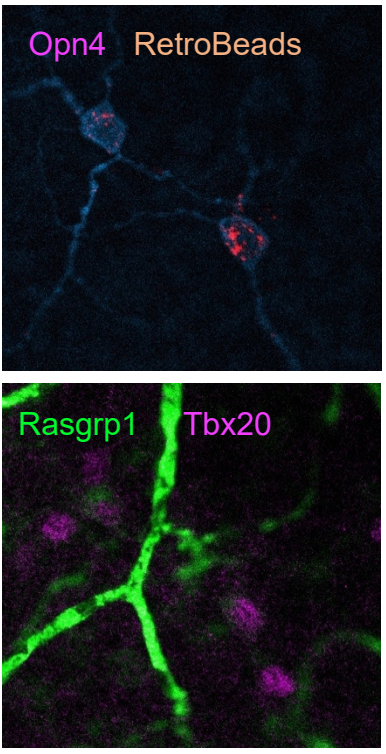
Opn4 RetroBeads
Rasgrp1 Tbx20

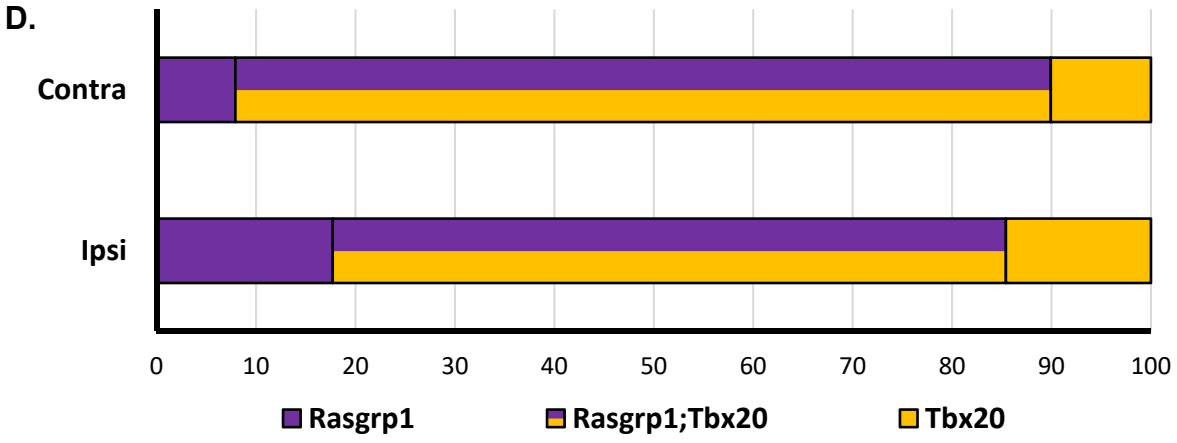
D.
Contra
Ipsi
0
10
20
30
40
50
60
70
80
90
100
Rasgrp1
Rasgrp1;Tbx20
Tbx20

Figure 7.

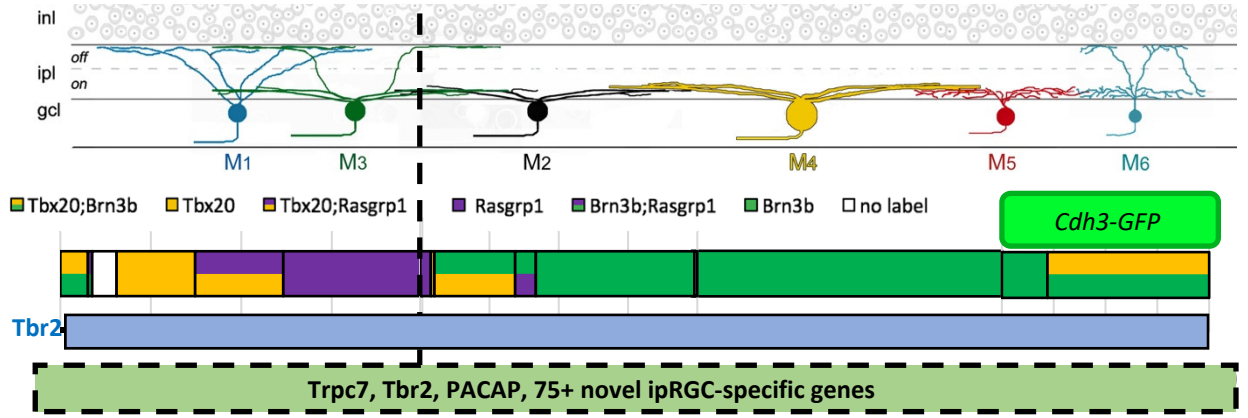

Circadian rhythm photoentrainment	
Morphology	Mostly M1, rare M2
Molecular	Brn3b^{-}
	Rasgrp1 +/- Tbx20
Brain targets	SCN

Figure 8. A.

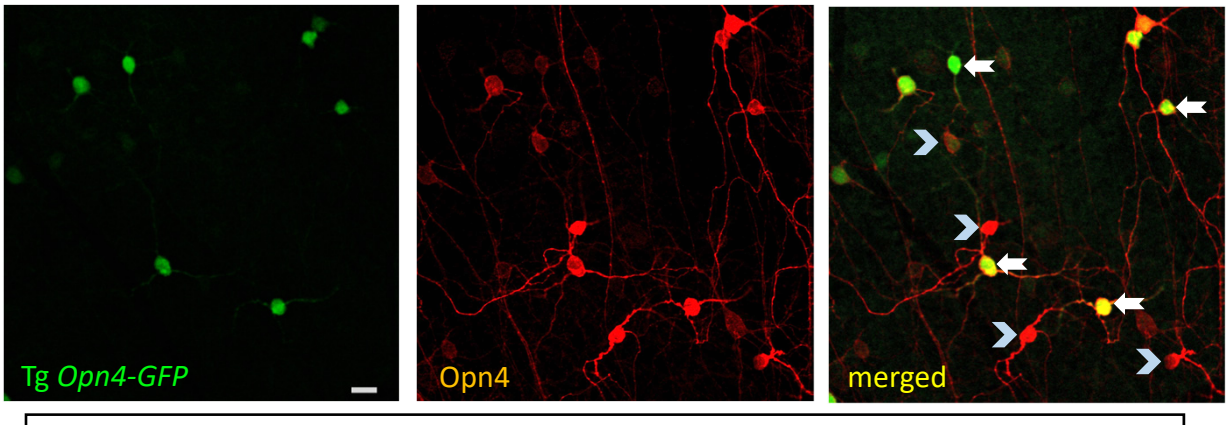
Tg Opn4-GFP
Opn4
merged
GFP ; anti-Opn4
GFP^neg. ; anti-Opn4
GFP+ ; anti-Opn4^neg.

B.

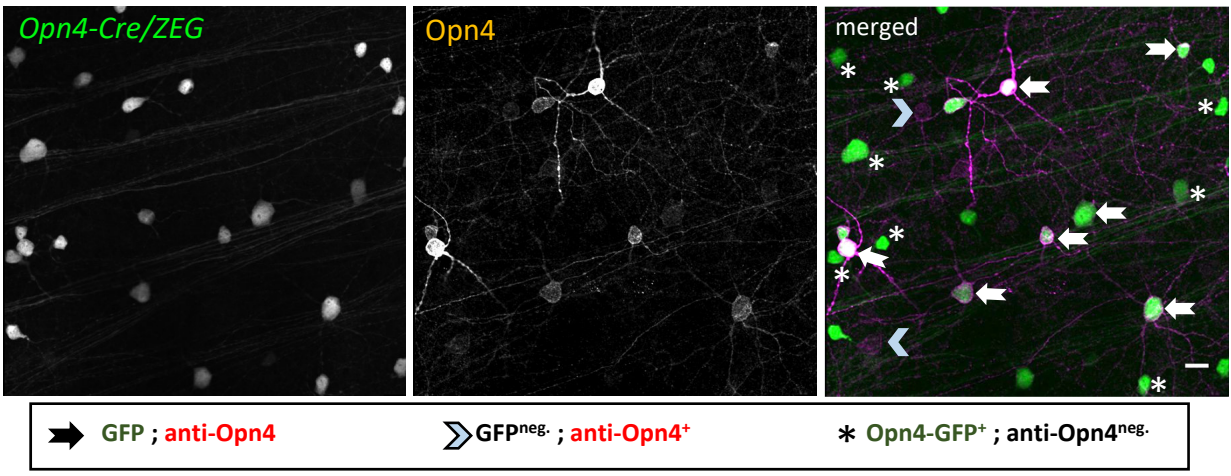
Opn4-Cre/ZEG
Opn4
merged
GFP ; anti-Opn4
GFP^neg. ; anti-Opn4+
Opn4-GFP+ ; anti-Opn4^neg.

C.

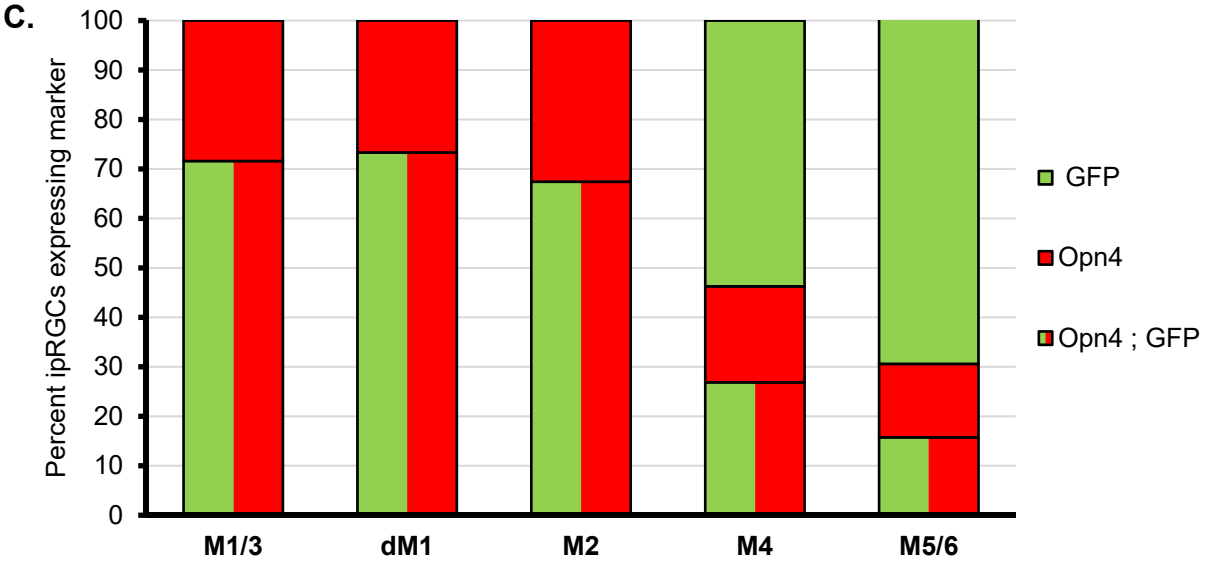
Percent ipRGCs expressing marker
100
90
80
70
60
50
40
30
20
10
0
M1/3
dM1
M2
M4
M5/6
GFP
Opn4
Opn4 ; GFP

Figure 9.

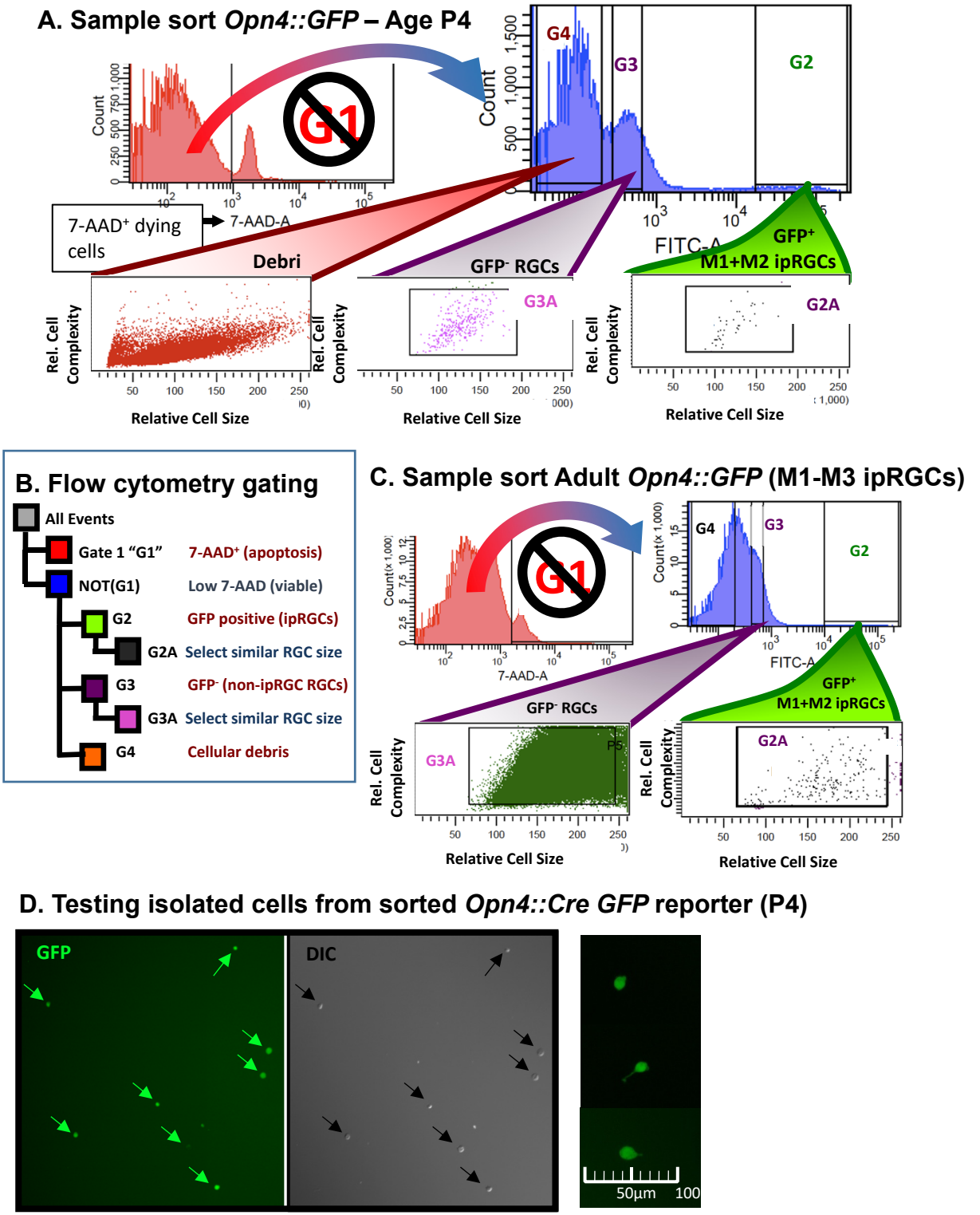
A. Sample sort Opn4::GFP – Age P4
G1
G4
G3
G2
Count
7-AAD⁺ dying cells
7-AAD-A
Debri
GFP⁻ RGCs
FITC-A
GFP⁺ M1+M2 ipRGCs
G3A
G2A
Rel. Cell Complexity
Relative Cell Size
B. Flow cytometry gating
All Events
Gate 1 "G1"
7-AAD⁺ (apoptosis)
NOT(G1)
Low 7-AAD (viable)
G2
GFP positive (ipRGCs)
G2A
Select similar RGC size
G3
GFP⁻ (non-ipRGC RGCs)
G3A
Select similar RGC size
G4
Cellular debris
C. Sample sort Adult Opn4::GFP (M1-M3 ipRGCs)
G1
G4
G3
G2
Count(x 1,000)
7-AAD-A
FITC-A
GFP⁻ RGCs
GFP⁺ M1+M2 ipRGCs
G3A
G2A
Rel. Cell Complexity
Relative Cell Size
D. Testing isolated cells from sorted Opn4::Cre GFP reporter (P4)
GFP
DIC
50µm
100

Figure 10.

A. RNA extraction and quality test for degradation

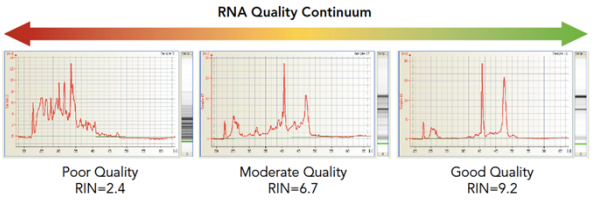

Nugen Ovation user manuel

Total RNA of P4 Opn4::GFP - high Quality RNA

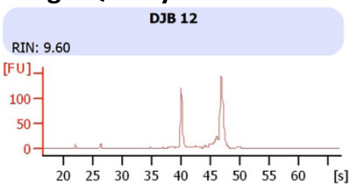

B. cDNA processing of extracted RNA

Total RNA input

Nugen Ovation system

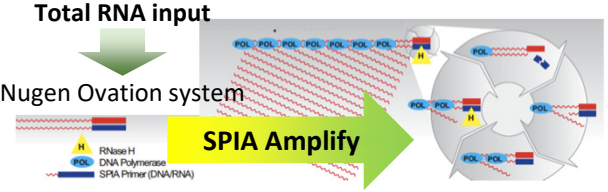

Adapted from Nugen Ovation user manuel

Nugen Output (cDNA)

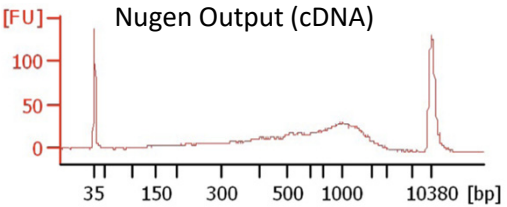

C. RNA-seq library preparation (Truseq)

cDNA shearing (Covaris)

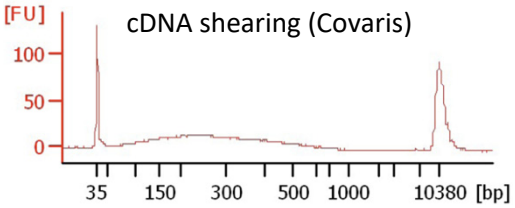

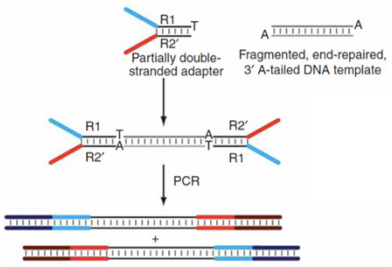

D. Test concentration and adapter length (qPCR & Bioanalyzer)

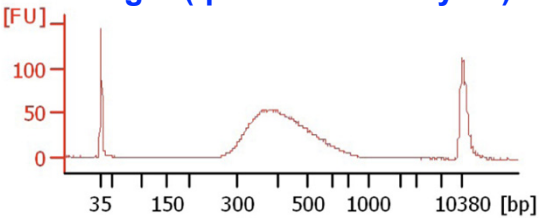

E. Multiplexed Illumina sequencing

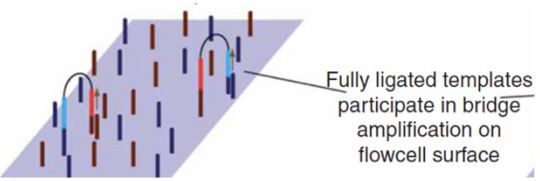

F.

Opn4-GFP

(M1-M3 ipRGCs)

raw reads	GFP+ sample	GFP- sample	raw reads
95016286	DJB0007*	DJB0008*	90897302
44201103	DJB0030*	DJB0031*	43690608
45578821	DJB0028*	DJB0029*	49110355
49661171	DJB0016*	DJB0021*	47265858
10724088	DJB0036	DJB0037	11294631
11377625	DJB0038	DJB0039	22789777

Opn4-Cre/ZEG

(M1-M6 ipRGCs)

raw reads	GFP+ sample	GFP- sample	raw reads
109774976	DJB0005*	DJB0006*	96032720
98636762	DJB0022*	DJB0023*	110267207
64188702	DJB0032*	DJB0035*	68930442
21602002	DJB0040	DJB0041	22028459

*** concatenated technical replicates**